EUROPEAN ORGANISATION FOR NUCLEAR RESEARCH

The **n_TOF** Collaboration

STATUS REPORT *[July 2001]*

Geneva
Switzerland

ABBONDANNO U.[20], ANDRIAMONJE S.[10], ANDRZEJEWSKI J.[24], ANGELOPOULOS A.[12], ASSIMAKOPOULOS P.[15], BACRI C-O.[8], BADUREK G.[1], BAUMANN P.[9], BEER H.[11], BERTHIER B.[8], BONDARENKO I.[26], BOS A.J.J.[36], BUSTREO N.[19], CALVINO F.[33], CANO-OTT D.[28], CAPOTE R.[31], CARLSON P.[34], CHARPAK G.[5], CHAUVIN N.[8], CENNINI P.[5], CHEPEL V.[25], COLONNA N.[20], CORTES G.[33], CORVI F.[23], DAMIANOGLOU D.[16], DAVID S.[8], DIMOVASILI E.[12], DOMINGO C.[29], DOROSHENKO A.[27], DURAN ESCRIBANO I.[32], ELEFTHERIADIS C.[16], EMBID M.[28], FERRANT L.[8], FERRARI A.[5], FERREIRA–MARQUES R.[25], FRAIS-KOELBL H.[3], FURMAN W.[26], FURSOV B.[27], GARZON J.-A.[32], GIOMATARIS I.[10], GLEDENOV Y.[26], GONZALEZ–ROMERO E.[28], GOVERDOVSKI A.[27], GRAMEGNA F.[19], GRIESMAYER E.[3], GUNSING F.[10], HAIGHT R.[37], HEIL M.[11], HOLLANDER P.[36], IOANNIDES K.G.[15], IOANNOU P.[12], ISAEV S.[27], JERICHA E.[1], KADI Y.[5], KAEPPELER F.[11], KARADIMOS D.[17], KARAMANIS D.[15], KAYUKOV A.[26], KAZAKOV L.[27], KELIC A.[9], KETLEROV V.[27], KITIS G.[16], KOEHLER P.E.[38]., KOPACH Y.[26], KOSSIONIDES E.[14], KROSHKINA I.[27], LACOSTE V.[5], LAMBOUDIS C.[16], LEEB H.[1], LEPRETRE A.[10], LOPES M.[25], LOZANO M.[31], MARRONE S.[20], MARTINEZ-VAL J. M.[30], MASTINU P.[19], MENGONI A.[18], MEUNIER R.[7], MEZENTSEVA J.[26], MILAZZO P.[21], MINGUEZ E.[30], MITROFANOV V.[27], NICOLIS N.[15], NIKOLENKO V.[26], OBERHUMMER H.[1], PAKOU A.[15], PANCIN J.[6], PAPADOPOULOS K.[13], PAPAEVANGELOU T.[16], PARADELA C.[32], PARADELIS T.[14], PAVLIK A.[2], PAVLOPOULOS P.[15,35,*], PEREZ-PARRA A.[28], PERRIALE L.[19], PERLADO J. M.[30], PESKOV V.[34], PIKSAIKIN V.[27], PLAG R.[11], PLOMPEN A.[23], POCH A.[33], POLICARPO A.[25], POPOV A.[26], POPOV Y.P.[26], PRETEL C.[33], QUESADA J.M.[31], RADERMACHER E.[5], RAUSCHER T.[35], REIFARTH R.[11], REJMUND F.[8], RUBBIA C.[22], RUDOLF G.[9], RULLHUSEN P.[23], SAKELLIOU L.[12], SALDANA F.[5], SAMYLIN B.[27], SAVVIDIS E.[16], SAVVIDIS S.[17], SEDYSHEV P.[26], STEPHAN C.[8], SZALANSKI P.[24], TAGLIENTE G.[20], TAIN J.L.[29], TAPIA C.[33], TASSAN–GOT L.[8], TERCHYCHNYI R.[27], TSABARIS C.[13], TSANGAS N.[17], van EIJK C.W.E.[36], VANNINI G.[20], VENTURA A.[18], VILLAMARIN A.[28], VLACHOUDIS V.[5], VLASTOU R.[13], VOINOV A.[26], VOSS F.[11], WENDLER H.[4,**], WIESCHER M.[39], WISSHAK K.[11], ZEINALOV S.[27], ZHURAVLEV B.[27]

---

* *Spokesperson*
** *Technical Coordinator*

1. Atominstitut der Österreichischen Universitäten, Technische Universität Wien, Austria
2. Institut für Isotopenforschung und Kernphysik, Universität Wien, Austria
3. Fachhochschule Wr. Neustadt, Wien, Austria
4. CERN, EP Division, Geneva, Switzerland
5. CERN, SL Division, Geneva, Switzerland
6. Centre National de la Recherche Scientifique/IN2P3, CENBG, Bordeaux, France
7. Centre National de la Recherche Scientifique/IN2P3, CSNSM, Orsay, France
8. Centre National de la Recherche Scientifique/IN2P3, IPN, Orsay, France
9. Centre National de la Recherche Scientifique/IN2P3, IreS, Strasbourg, France
10. Commissariat à l'Energie Atomique/DSM, Gif-sur-Yvette, France
11. Forschungszentrum Karlsruhe GmbH (FZK), Institut für Kernphysik, Germany
12. Astro-Particle Consortium, Nuclear Physics Lab., University of Athens, Greece
13. Astro-Particle Consortium, Nuclear Physics Dep., Technical University of Athens, Greece
14. Astro-Particle Consortium, Nuclear Physics Institute, NCSR "Demokritos", Athens, Greece
15. Astro-Particle Consortium, Nuclear Physics Lab., University of Ioannina, Greece
16. Astro-Particle Consortium, Nuclear Physics Lab., University of Thessaloniki, Greece
17. Astro-Particle Consortium, Nuclear Physics Dep., University of Thrace, Greece
18. ENEA, Applied Physics Division, Bologna, Italy
19. Laboratori Nazionali di Legnaro, Italy
20. Instituto Nazionale di Fisica Nuclear-Bari, Italy
21. Instituto Nazionale di Fisica Nuclear-Trieste, Italy
22. Universita degli Studi Pavia, Pavia, Italy
23. JRC-EC, IRMM, Geel, Belgium
24. University of Lodz, Lodz, Poland
25. Laboratorio de Instrumentacao e Phisica Experimental de Particulas,LIP-Coimbra & Departamento de Fisica da Universidade de Coimbra, Portugal
26. Joint Institute for Nuclear Research, Frank Laboratory of Neutron Physics, Dubna, Russia
27. Institute of Physics and Power Engineering, Kaluga region, Obninsk, Russia
28. Centro de Investigaciones Energeticas Medioambientales y Technologicas, Madrid, Spain
29. Consejo Superior de Investigaciones Cientificas – University of Valencia, Spain
30. Universidad Politecnica de Madrid, Spain
31. Universidad de Sevilla, Spain
32. Universidade de Santiago de Compostela, Spain
33. Universitat Politecnica de Catalunya, Barcelona, Spain
34. Kungliga Tekniska Hogskolan, Physics Department, Stockholm, Sweden
35. Department of Physics and Astronomy, University of Basel, Basel, Switzerland
36. Delft University of Technology, Interfaculty Reactor Institute, Delft, The Netherlands
37. Los Alamos National Laboratory, New Mexico, USA
38. Oak Ridge National Laboratory, Physics Division, Oak Ridge, USA
39. University of Notre Dame, Notre Dame, USA

EXECUTIVE SUMMARY

The CERN Research Board approved the n_TOF project on April 15, 1999 as experiment PS213. Following the Research Board recommendation that each measurement at this neutron facility should be reviewed, a proposal "*Determination of the neutron fluence, the beam characteristics, and the backgrounds at the CERN-PS TOF facility*" was submitted to the newly formed INTC Committee on February 28, 2000, and approved as experiment nTOF-02 by the Research Board on April 13, 2000.

The construction and commissioning of the neutron beam line has been completed in April 2001. After two touch-and-go periods of 24 hours each on April 13 and 21, the n_TOF Collaboration started on Saturday, 28th April 2001, with the first in-beam operation of the Data Acquisition system and the commissioning of the monitor, capture and fission detectors foreseen in the nTOF-02 programme. All detectors and the data acquisition system were properly working and reached the designed performance. The DAQ system, developed jointly between the Collaboration and industry, was performing without dead time even at a peak data rate of 18 MBytes/s. Data have been collected from all detectors according to the objectives of the nTOF-02 experimental campaign. Simultaneously, an off-line group started to analyse the acquired data and alarmed soon the n_TOF Collaboration on the existence of a high ambient background in the experimental area jeopardising the quality of the capture measurements and even preventing the operation of the BaF_2 calorimeter. Under these conditions part of the nTOF-02 programme has been compromised and the n_TOF Collaboration defined on May 8, 2001 a series of additional measurements in order to understand the nature and the origin of this background. Finally, the presence of this background has forced us to interrupt the data taking runs on June 11, 2001 and to request on June 1 – in agreement with the group responsible for the construction of the neutron beam – the modification of the shielding in the vicinity of the spallation target.

The data collected in the period from April 28 to June 11 exceeded 800 GBytes and have been analysed within a month for all studied neutron induced reactions, i.e. fission, capture and $^6Li(n,\alpha)$. The results of the analysis provided the determination of the neutron flux in a range of neutron energies spanning over eight orders of magnitude, i.e. from 1 eV to over 250 MeV. The achieved energy resolution is excellent, but needs to be confirmed at higher energies where the influence of Doppler broadening is less important. Despite the high background level the recorded data has allowed to obtain very promising results for the neutron beam intensity and profile as well as a first evaluation of the weighting functions required for the analysis of the capture measurements with the C_6D_6 detectors.

At present, the unexpected backgrounds are the most crucial problem. The information collected in a series of measurements indicates that backgrounds are about 50 times larger than anticipated from simulations. Although n_TOF should have a clear advantage with respect to the background due to its unique combination of a 4 times longer flight path and a 50 times lower duty cycle, comparison with existing facilities yields in fact only similar conditions.

There are three distinct background components, one contained within 400 ns after the "flash" induced by the proton beam with contributions from charged particles, high energy neutrons and photons, the second arriving within 20 μs including mainly high energy neutrons and a third component related to longer times, exceeding even 16 ms.

The main feature of the first and second background components is their strong

dependence on the position inside the experimental area with the right-hand side in the neutron beam direction being significantly more enhanced. A special simulation was performed to find possible weak points in the shielding of the TOF tunnel, showing a minimum density of 1400 g/cm^2 at the right-hand side corresponding to only 5.2 m of concrete. Although the Pb spallation target itself seems to be appropriately shielded, the actual size of the neutron source is considerably extended because more than 50% of the protons are not completely stopped in the lead. The inhomogeneous shielding of the tunnel, in particular the weak areas at the right side of the beam, allows fast neutrons, charged particles and possibly photons, which are created outside the lead target, to invade the experimental area. For example, extensive Monte Carlo calculations revealed the presence of a huge muon fluence of 10–100 μ/cm^2/7×10^{12} protons entering the experimental area with an average energy of ~1 GeV. These muons are prohibitive for the operation of a crystal calorimeter of BaF$_2$.

The third background component, which is obscuring the capture measurements, can be characterised by the following observations:

- This component extends from several tens of microseconds to above 16 ms after the arrival of the proton beam, corresponding to the neutron energy range from thermal to ~100 keV.
- It exhibits a time distribution composed of two exponentials with decay times of approximately 160 μs and 1.8 ms.
- It depends strongly on the position inside the experimental area with the right-hand side in the neutron beam direction being more enhanced.
- The spectra obtained with various samples having negligible capture cross sections show hardly a difference to the spectrum taken without sample, providing evidence that the present background does not originate from the material inside the neutron beam.
- It is difficult to accommodate this background to interactions of the beam with the second collimator, the vacuum TOF tube, and the neutron escape line.

These points strongly indicate the ambient nature of this background component. According to a series of Monte Carlo simulations it could be attributed to high-energy neutrons leaking through the concrete shielding and colliding with the walls of the experimental area, where they are quickly thermalised and either captured within a few 100 μs or scattered across the experimental area and captured after several ms in the opposite walls. These capture events generate a photon flux with an energy spectrum up to ~10 MeV and features of the predominant capture reactions on H, Si, K, Ca and Fe.

The presence of this background handicaps the scientific programme based on the capture measurements by introducing a significant delay to the execution of the n_TOF project, and actions must be urgently taken to mitigate the observed sources of background. In order to minimise conflicts with the work plan of the EC contract we suggest to start immediately with the improvement of the shielding near the spallation target and at all critical points of the n_TOF tunnel, so that meaningful experiments can be resumed as soon as possible. The detailed design of this shielding must be urgently agreed between CERN and the n_TOF collaboration.

The developments of the data acquisition system and of various detectors show promising potentials for future spin-off applications.

The activities related to the evaluation and dissemination of the experimental data are progressing in full cooperation with international organisations. A first cross section evaluation has been performed by n_TOF for the neutron capture cross section of ^{233}Pa(n,γ).

CONTENTS

1. INTRODUCTION.

After two touch-and-go periods of 24 hours each on April 13 and 21, the n_TOF Collaboration started on Saturday 28th April 2001, the first in-beam operation of the monitor, capture and fission detectors [1,2]. After the first and second commissioning of the neutron beam by the EET group and the completion of the beam infrastructure during the 2000-2001 accelerator shutdown, the experimental area constructed according to the planned design [2] under CERN's safety and radioprotection authorisation was fully equipped with detectors (Figure 1-1). We focused on the commissioning of those detectors necessary in the determination of the characteristics [1] of this newly installed 185 m long TOF neutron beam, i.e.

- The Silicon detectors facing a ^{6}Li target and covering the neutron energy range from thermal to 1 MeV;

- The Micromegas detectors equipped with a ^{6}Li sample for the determination of the profile and the homogeneity of the neutron beam spot at the experimental area. The detectors operated also with hydrogen rich gas in order to increase its sensitivity to higher energies;

- The set of C_6D_6 gamma detectors for the determination of the neutron fluence from the ^{197}Au data, being a "standard" in the range from 200 keV to 2.5 MeV, and for the experimental confirmation of their weighting functions from the ^{56}Fe data [1,2]. The associated sample exchanger allows to study, quasi-simultaneously with the sample under investigation, both background components, the general ambient background and the background due to neutrons elastically scattered on the sample;

Figure 1-1: General view of the experimental area and the installed detectors.

- The PPAC fission fragment detectors utilising the fission reaction on ^{235}U, ^{238}U and ^{209}Bi and covering the neutron energy range from thermal up to 200 MeV;

- Monitor detectors such as ^{6}Li/^{7}Li scintillation counters, integral thermoluminescence (TLD) and track etch plastic (TED) detectors, activation foils, and in-beam BF_3 long counters;

- An array consisting of ten modules of the Karlsruhe 4π BaF_2 calorimeter verifying the possibility to operate such a total absorption detector at the n_TOF experimental area. These tests were foreseen for the ^{197}Au samples, for which the simulations are based on well-established experimental information for the capture cascades;

- HPGe detectors for appreciating the possibility in detecting the prompt γ's from the transitions of the excited nucleus formed after (n,xn) or even neutron capture reactions.

The magnitude of the different background components as well as their time structure, the intensity and shape of the neutron beam and the homogeneity of the neutron spot plays a predominant role in the quality of the planned measurements and in the operation of the above detectors. For achieving the required high precision in the results of the proposed measurements, the following quantities should be experimentally determined:

(a) DETERMINATION OF THE BEAM SIZE: The Micromegas detectors have taken advantage of both the "standard" ^{6}Li(n,α)^{3}H reaction and the (n,p) elastic scattering. Since the neutron energy is not determined from the energy of the alpha and tritium, the ^{6}Li method can be quite sensitive even above 2.5 MeV through the reactions, ^{6}Li(n,n'α)p and ^{6}Li(n,p). The utilisation of hydrogen-rich gases provides sufficient sensitivity even at higher neutron energies through the (n,p) elastic reaction. Their excellent spatial resolution enabled us to determine the size and homogeneity of the beam spot at several energy intervals.

(b) DETERMINATION OF THE GAMMA BACKGROUND: The gamma background in the experimental area can originate either from the "γ-flash" and the in-beam photons, or from neutrons reaching the experimental area or produced therein. Neutron background can induce a significantly high γ-background due to capture and inelastic interactions with the different materials in the experimental area including the shielding.

For the determination of this background we applied a method based on the use of a "sample changer" [1,2]. It allows studying, in parallel with the measurement both the background related to the interaction of in-beam photons and neutrons with the sample and the ambient photon background inside the experimental area. The first component can be experimentally simulated with a carbon and/or a ^{208}Pb sample, which have negligible (n,γ) cross sections. The second component can be determined by means of an empty position or by using an empty sample container. A high level of background without a sample in the beam would indicate insufficient shielding of the experimental area either upstream from the spallation target and/or downstream from the neutron escape line. The difference of the two spectra, i.e. ^{12}C/^{208}Pb sample and no sample, would provide the amount and the time structure of the γ-background related to the beam photons and neutrons interacting with the sample.

We recall that our "sample changer" [2] is made from carbon fibre and is connected directly to the vacuum neutron guide, also made of carbon fibre at the position of the C$_6$D$_6$ detectors (see Figure 1-1, left). Its construction was based on Monte Carlo simulations minimising possible backgrounds from the interaction of scattered neutrons with the various parts of the "sample changer".

The design of the experimental area [2] was guided by two criteria, the fluence of neutrons scattered by the sample should dominate the ambient neutron background and the ambient γ-background should be small compared to the number of γ's produced by capture in the sample under study.

(c) DETERMINATION OF THE NEUTRON BACKGROUND: These backgrounds consist of neutrons that do not have a clear relation between their kinetic energy and their time-of-flight. They are usually low energy neutrons originating from the interaction and thermalisation of high-energy neutrons. They can originate also from charged particles penetrating the shielding of the experimental area, from the backscattering of beam neutrons at the "Neutron Escape

Line" or from neutrons rescattering at the materials surrounding the detectors. The only way to determine the amount of this background is to put in the neutron beam filters containing isotopes with so-called "black" resonances, removing selectively neutrons from the beam. Large resonances at specific energies impose that all neutrons undergo an interaction at the resonance energy and have a transmission coefficient close to zero. The designed [2] "filter changer", which has several positions of large diameter (15×15 cm^2) filters, is under construction and will be installed into the beam in front of the second collimator.

(d) MEASUREMENT OF THE NEUTRON FLUENCE: The determination of the neutron fluence as function of the neutron energy has been performed by the Silicon detectors through ^{6}Li reactions, by the PPAC's through fission reactions, and by the C$_6$D$_6$ detectors through neutron capture on ^{197}Au, covering redundantly the neutron energy range from thermal to above 200 MeV.

(e) DETERMINATION OF THE RESOLUTION FUNCTION: Isotopes that are well suited to determine the resolution over a large energy range are ^{238}U and ^{56}Fe. Several narrow resonances of ^{238}U are commonly used as neutron energy "standard" in the resolved energy range where the cross section is described in terms of resonance parameters. At low energies (below 1 or 2 keV) these resonances are used to determine the resolution. The large level spacing of ^{56}Fe makes it possible to measure resolved resonances up to at least 200 keV. The resolution parameters should be fitted from the measured capture yield by an R-matrix analysis including an adequate modelling of the resolution function.

All detectors and the data acquisition system have shown a satisfactorily behaviour and reached their designed performances, as described in chapters 2 and 3 together with first results from our preliminary data analysis, presented in chapter 5. These experimental results supported by the results from extensive Monte Carlo simulations, presented in chapter 4, indicate the presence of an unreasonably high background in the experimental area, preventing high quality capture cross sections measurements [3,4]. The presence of this background has forced us to interrupt our data taking runs on 11th June 2001 and to request on June 1 modification of the shielding in the vicinity of the spallation target.

In chapter 6 we present the progress, achieved since the "n_TOF Technical Report" [2] in November 2000, in developing successfully novel detector techniques in the field of liquid noble gas calorimetry.

The progress and networking between the n_TOF Institutes collaborating in the evaluation and modelling of Nuclear Data (ND) is presented in chapter 7.

2. THE DATA ACQUISITION SYSTEM

2.1. INTRODUCTION

An innovative, general purpose Data Acquisition System (DAQ) has been developed [2] by considering the CERN TOF beam repetition rates[1], the expected number of event rates and the characteristics of the detector signals. We achieved a highly flexible and adaptable DAQ that accommodates the various detector requirements without any loss of efficiency or dead time, in a user-friendly software environment. Without compromising the possibility to record all information, the present system has the novel and unique feature to sample and store exclusively the full analogue waveform of the detector signals for each channel and beam burst by using on–line zero-suppression [2]. Additional data reduction is achieved by recording the data in compressed "tar"[2] file format, providing typically a reduction of a factor of two. This on–line zero-suppression yields respectable data reduction factors shown in Figure 2-1 for the C_6D_6 and the silicon detector and for different samples in the beam having different reaction rates.
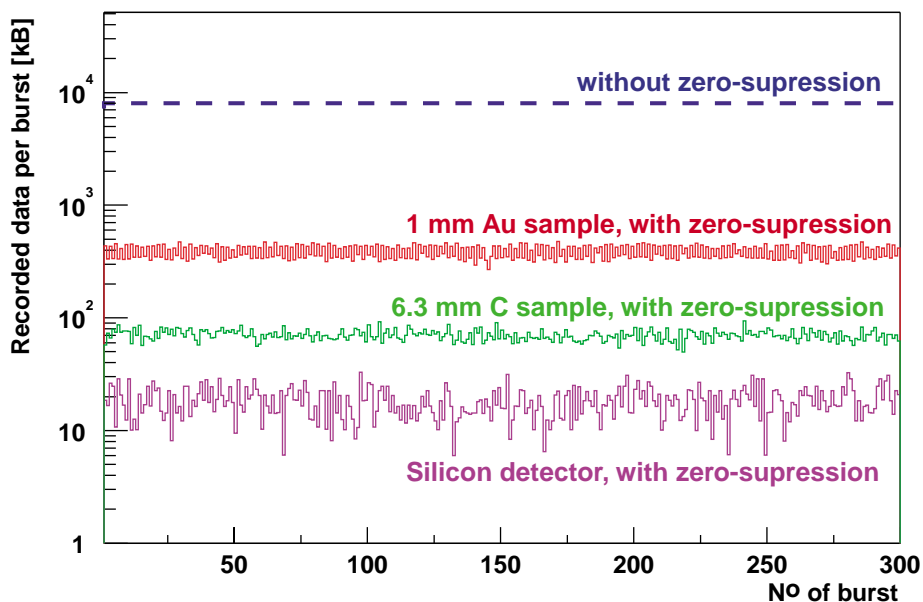

Figure 2-1: The data reduction due to the zero-suppression is presented for the C_6D_6 detectors in the case of the 1 mm ^{197}Au sample with ~350 signals per burst and in the case of the 6.3 mm C sample with ~70 signals per burst. The reduction of the Silicon data with ~10 signals per burst is also shown.

The sampling is performed by Flash ADC[3] (FADC) modules that provide for a time-tag and which allow full pipelining (digital conversion not blocked by data readout). This DAQ architecture [2] permits the complete reconstruction of the detector response in off-line analysis with the advantage of the possibility to resolve pile-up or background events. The n_TOF DAQ system is able to synchronously collect the data of all detectors and transfer them after each

---

[1] At the TOF neutron facility the detectors are active for 16 ms during a PS burst, i.e. at the maximum repetition of 2.4 s, covering neutron energies down to below 1 eV.

[2] **T**ape **AR**chive files.

[3] ADC: **A**nalogue to **D**igital **C**onverter.

burst through a Gigabit switch to the CERN CDR[4] facility for fast data storage.

2.2. THE FRONT-END ELECTRONICS

The n_TOF Data Acquisition System consists of Digitiser modules based on FADCs with a repetition rate up to 2 Gsamples per second (Gs/s). The detector signal characteristics define the sampling rate and the dynamic range to be used. The various detector requirements imposed the use of two types of FADCs.
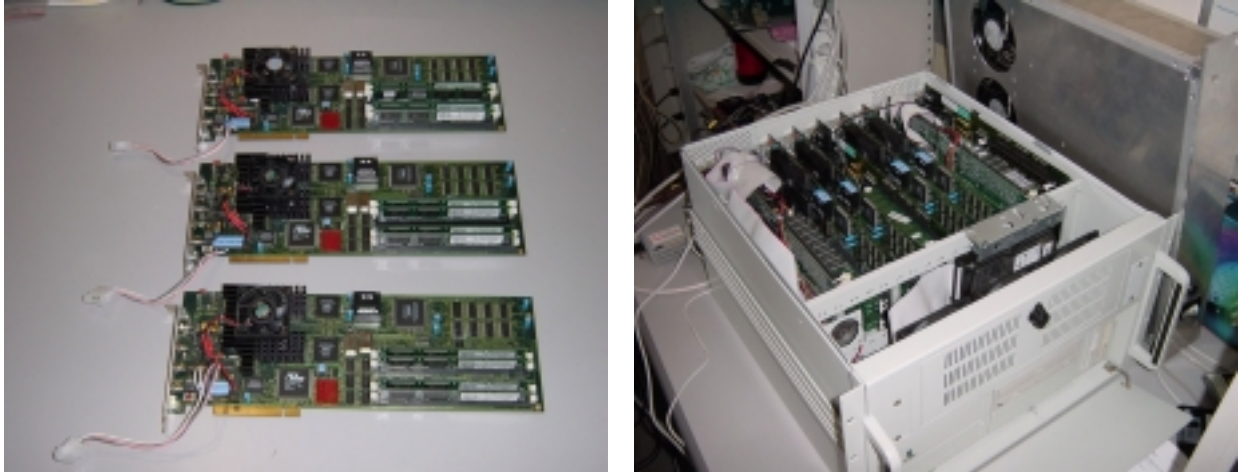

Figure 2-2: The ETEP digitiser modules (*left*) and the chassis (*right*).

One type (ETEP[5]) has a single dynamic range from 0 to –500 mV and sample rates of 1 Gs/s down to 62.5 Ms/s (binary division), with memory depth up to 512 Mbytes and with zero-suppression applied prior of writing to memory. We apply this first type on all standard n_TOF detectors [2] and due to its unique memory depth it can be also used in our experiments at other neutron sources, providing for a very long recording time.

Figure 2-3: The ACQIRIS digitiser modules and the chassis.

---

[4] **C**entral **D**ata **R**ecording facility in CERN's IT Division.
[5] ETEP S.A. (**E**tudes **T**echniques de l'**E**lectronique **P**rofessionnelle), Toulon, France.

The other type (ACQIRIS)[6] has several dynamic ranges between ±5 V down to ±5 mV and sample rates from 2 Gs/s down to 1 Ms/s (steps of 1,2,5), with memory depth up to 16 Mbytes and with zero-suppression applied by software after writing to memory. This second type, due to its flexibility is used for detector commissioning and for multipurpose applications requiring the features of a multichannel digital oscilloscope combined with large memory.

The hardware specifications for both types of digitiser modules, the "slow control" and the networking features are presented in references [2] and [5].

Both types of digitisers modules have been commonly developed between the n_TOF Collaboration and industry. The conceptual design of a digitiser in PCI format, the on-line zero–suppression mechanism, the large memory feature, the horizontal data path for event monitoring (SPY[2]), the clock generator and its fan-out and the 200 MHz FADC front-end design have been the n_TOF contribution to the first type. The software zero-suppression mechanism and its driver have been the n_TOF contribution to the second type.

Our DAQ system was operational with 16 channels since November 2000. The data presented in this report have been obtained using 36 channels of the second digitiser type. The application of the first type of digitisers has shown that they can operate according to the specifications with the exception of the presence of excessive noise on the input channel and of an uncertainty of 8 sampling clock periods in the inter-module synchronisation. The offset circuitry in front of the digitiser inputs combined with the input protection circuitry have been developed by the n_TOF Collaboration and will be incorporated in the DAQ system by end of August 2001 in order to eliminate the input noise. Our industrial partner has localised the synchronisation problem at the clock multiplexing integrated circuit and will provide an upgrade to the digitiser modules by mid September 2001.

2.3. THE DAQ ARCHITECTURE

The architecture of our DAQ system has been extensively described elsewhere [2],[5],[6],[7] and only a brief overview with the upgrades and the present status will be presented for completeness.

The DAQ system during the April 28 to June 11 2001 run period consisted of 4 data streams equipped with 36 digitiser channels employing 4 PCs and a fifth stream containing the "slow control" information and the beam information relevant to n_TOF provided by the PS control room (CR), employing 2 PCs. All this equipment was situated in the experimental area and the data transfer to the n_TOF CR was performed via an optical Gigabit switch. The PC server in the CR has been upgraded to a 500 GB disk server in March 2001. At the same time the 200 GB disk server situated in the CDR area has been also replaced by a 500 GB disk server. Additionally we had a 100 Mb Ethernet switch installed in the CR to improve the access to the 500 GB disk server. For the run control, the event monitoring and the on-line analysis we employed three PC Workstations in the CR and for the data analysis ten PCs in offices and the LXPLUS cluster.

In collaboration with the IT-CS group we will upgrade the network infrastructure in the following way:
- Replacement of the optical Gigabit switch in the experimental area by a copper Gigabit switch; the optical Gigabit links to the CR remains as well as the local 10 Mb

---

[6] ACQIRIS S.A., Geneva, Switzerland.

Ethernet connections.
- Replacement of the optical Gigabit Interface cards in the five data streams in the experimental area by Copper Gigabit Interface cards and replacing optical cables by inexpensive copper cables (RJ45).
- The optical Gigabit switch from the experimental area, the optical Gigabit Interface cards and optical cables will be employed in the CR, in order to speed up the access to the PC workstations.
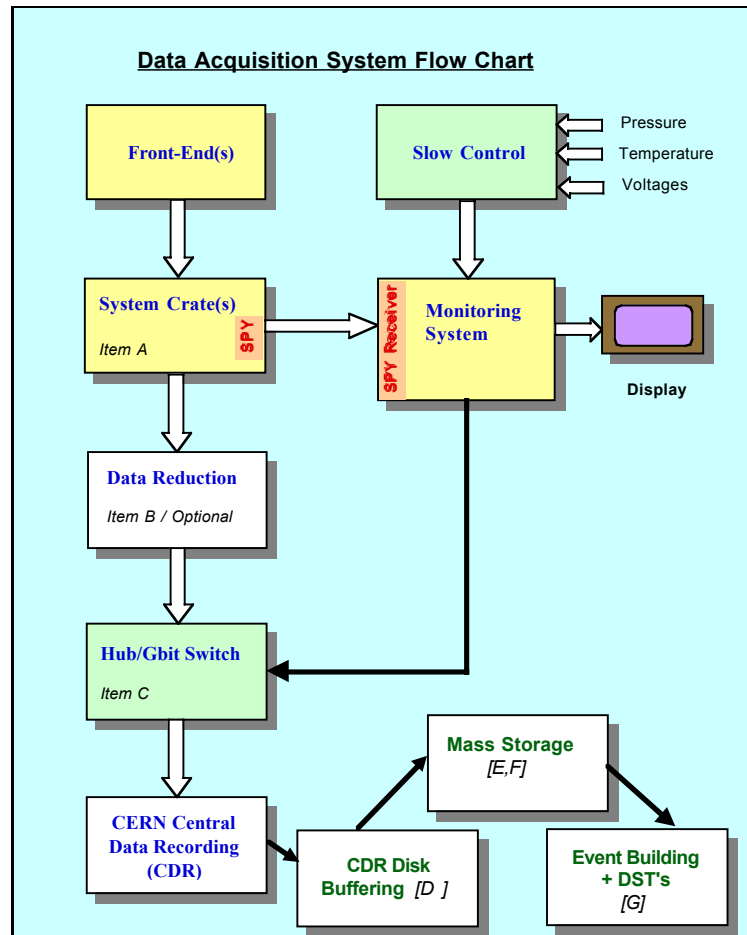

Figure 2-4: *The block diagram of the n_TOF DAQ.*

2.3.1. Monitoring and synchronisation across multiple data streams (SPY).

The monitoring and synchronisation across the various data streams has been extensively described elsewhere [2]; therefore only an overview and the status are presented here.

The SPY[2] and SPY RECEIVER[2] modules together with their drivers have been delivered by ETEP on July 11 2001 with a delay of four months. The modules and drivers have been successfully tested since then and the implementation of the drivers and associated software is under progress.

Despite the four months delay, the n_TOF Collaboration elaborated after intensive software optimisation an alternative software solution replacing the horizontal hardware path for the on-line event building and monitoring. The penalty of this solution was the difficulty to meet the appropriate speed for running with the repetition rate of 2.4 s per burst.

2.3.2. Trigger (GATE) Fan-out.

The prompt beam pulse from the PS, suitably attenuated and delayed generated the trigger signal at the CR. It was used to make the GATE signal, which was kept active during the whole acquisition period of 16 ms and was interlocked with the busy signals of the processor and the monitoring chassis via a PC parallel port to NIM converter module[7]. A single coaxial cable of high quality conveyed the GATE signal to the experimental area where our special fan-out unit distributed it to the individual digitiser modules via equal length cables. The skew of each output is < 200 ps in respect to all other outputs.

2.3.3. Slow Control and Beam Data.

During this data-taking period the "Slow Control" system was comprised of the setting and monitoring of the CAEN high voltage system crate. The data stream from the "Slow Control" contains apart from the high voltage data also the beam information acquired via a different PC communicating via Ethernet with the PS beam monitors. The utilisation for a dedicated PC for the beam information was imposed by synchronisation constraints, since this beam information is available at the PS beam monitor module only during a short time interval within the PS bursts.

The *"Monitoring Processor Chassis"* [2] can acquire upon request the "Slow Control" data via a LABVIEW interface including further data on low voltages, currents, temperature, pressures etc.

2.3.4. Performance of DAQ and the data rates.

The digitisers are acquiring data during 16 ms for each proton burst. The stored data amounts to 8 MB per channel and proton pulse, due to the 500 Ms/s sampling rate of the digitisers. With a 8 Ms acquisition memory per channel and a repetition rate of the proton beam pulse of 2.4 s the designed system had no dead time. The transfer of these 8 MB to the PC memory took ~0.7 s on the PCI bus. The data of the five data streams amounting to 10 MB on average have been transferred via the Gigabit Switch to the disk buffer in the CR in 0.1 s; the transfer from the CR to the CDR took another 0.1 s. We like to emphasise that the system was performing without dead-time also at a peak data rate of 18 MB/s. The data storage at the CDR was transparent for us, since the system is using CASTOR software.

2.4. THE DAQ SOFTWARE

The software was extensively presented in reference [2] and has been operational since November 2000. A major improvement [6] was required since then by the introduction of the CASTOR software for data recording in the CDR. The additional disk server in the control room required also some adjustments. After the first experience with the data visualisation and monitoring programme it was found necessary to proceed to a major re-write of this software [6,7], in order to permit direct and user-friendly on-line information on the quality of the data.

---

[7] Designed and constructed by the n_TOF Collaboration.

3. COMMISSIONING OF THE DETECTORS AND FIRST RESULTS.

The measurement of the ^{6}Li(n,α)^{3}H reactions has been performed with four Silicon detectors viewing a ^{6}LiF sample of 500 µg/cm^2 thickness and 3 cm diameter on a substrate of 1.5 µm mylar. They are placed inside the carbon fibre vacuum chamber shown in Figure 3-1. The Silicon detectors and the associated electronics achieved the expected time and energy resolution as shown in Figure 3-2 (*left*) and in agreement with our results from Monte Carlo simulations.
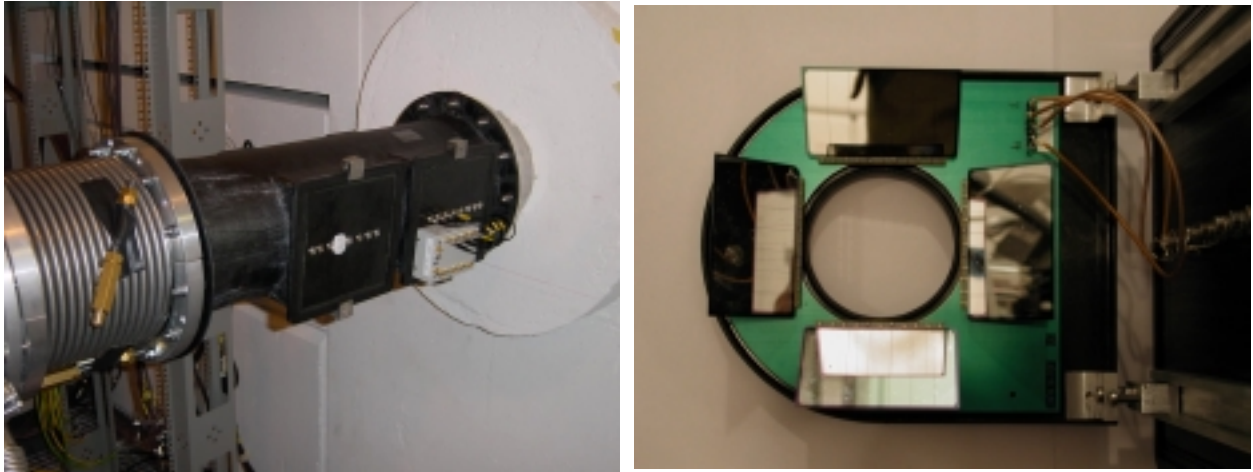

Figure 3-1: The Silicon detectors (*right*) and the ^{6}Li sample are placed inside the carbon fibre vacuum chamber (*left*).

The measured event rates are shown in Figure 3-2 (*right*) as function of the incident neutron energy for hundred bins per energy decade. The Monte Carlo calculated geometrical acceptance and the well-known ^{6}Li(n,α)^{3}H reaction cross section allowed a first, preliminary estimation of the neutron fluence, presented in Figure 3-3 (*left*).
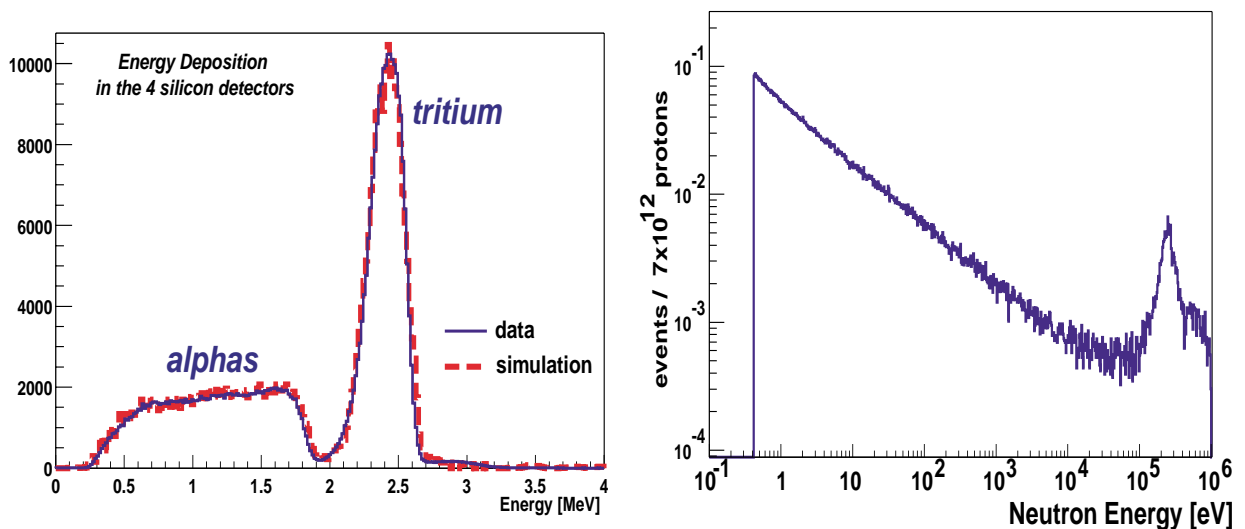

Figure 3-2: The energy spectrum of the detected reaction products is shown at the left side. The rate of triton events in the Si detectors as function of the neutron energy is plotted in the right panel.

This set of four Silicon detectors is providing the neutron flux integrated over the beam

surface with a precision mainly depending on the knowledge of the thickness and homogeneity of the ^{6}LiF sample. The exact comparison of the measured energy deposition of the reaction products with Monte Carlo simulations allows us to estimate the sample thickness with a precision of 10%. Future dedicated calibration measurements of the sample at a Van de Graaff would provide a precision of a few percent in the neutron flux determination by the silicon detectors. However, the main objective for the operation of these silicon detectors is only the monitoring of the flux and stability of the neutron beam in the n_TOF experimental area. The counting rate of the silicon detectors is proportional to the neutron flux and the stability of these counting rates allows to monitor the stability of the neutron beam without requiring the knowledge of the absolute neutron flux. The typical stability of the n_TOF beam is shown in Figure 3-3 (*right*) for several runs.
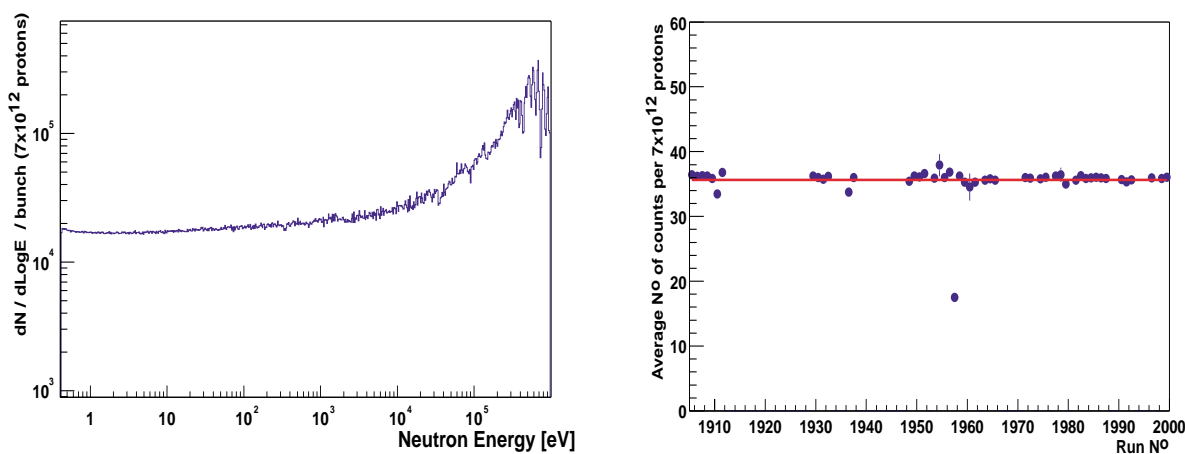

Figure 3-3: The measured neutron fluence integrated over the beam surface (~600'000 neutrons per bunch) via the "standard" cross section of the ^{6}Li(n,α) reaction (*left*). It is experimentally determined via the tritium events recorded by the silicon detectors. The stability of the n_TOF beam normalised to the proton intensity is monitored by the counting rates of the silicon detectors (*right*).

The Parallel Plate Avalanche Counters (PPAC) for the measurement of the fission cross sections has been also used for the determination of the neutron flux in the n_TOF beam for a range extending from thermal to over 200 MeV neutron energies. The in-beam initial measurements with these detectors have proven that they indeed satisfy the following three main features:

- Low level of background from scattered neutrons related to their low mass;
- Fast response and timing even during the high intensity runs;
- Sensitivity only to highly ionising particles. This particular feature makes these detectors insensitive to the "gamma" flash, allowing thus to measure fission events as high as 250 MeV neutron energy.

A set of five PPAC fission detectors equipped with the "standard" fission samples, ^{235}U, ^{238}U and ^{209}Bi, have been installed immediately after the vacuum chamber of the Silicon detectors (Figure 1-1). The vacuum chamber housing these detectors is shown in Figure 3-4, together with the associated control unit. The events corresponding to the fission process are obtained from the raw on-line data by requiring a time coincidence of two highly ionising particles between two adjacent counters. The quality of the fission measurements can be seen in

Figure 3-5 for all three targets, together with the excellent on-line separation of the ^{235}U low energy resonances. We would like to emphasise that these spectra exceeding a range of over eight orders of magnitude in neutron energy have been collected simultaneously during the same runs, proofing thus the power of our method in measuring Fission Nuclear Data using spallation neutrons produced by a high-energy proton beam.

Figure 3-4: The vacuum chamber of the PPAC detectors (*left*) and the associated gas and safety control unit (*right*).
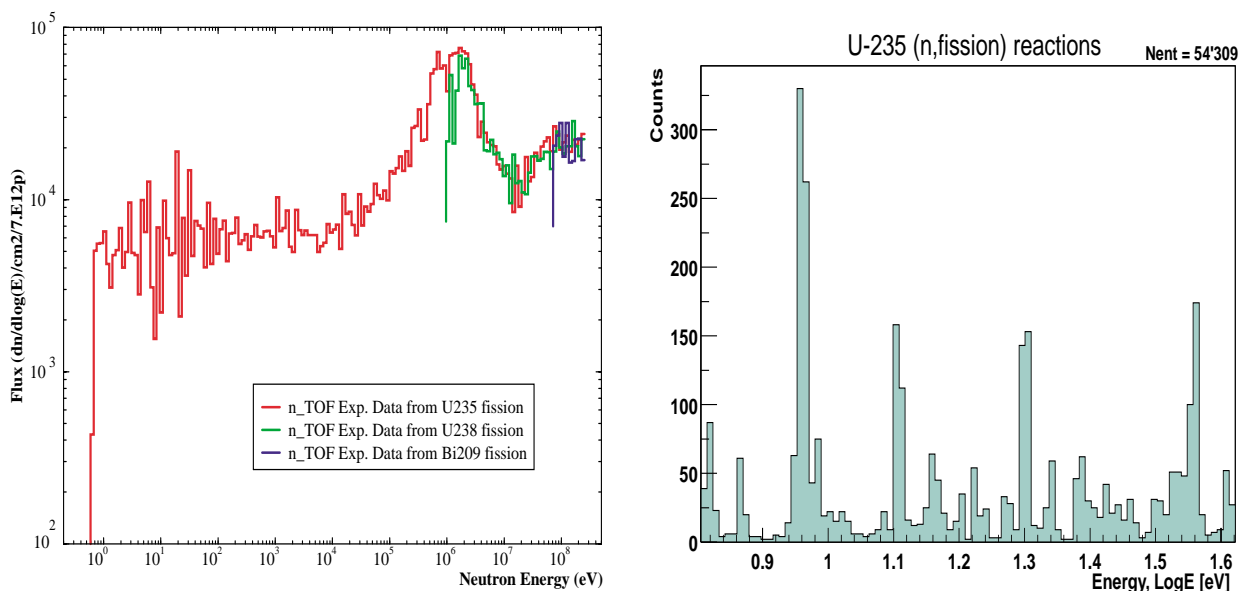

Figure 3-5: On-line fission data with the PPAC detectors for three different samples (*left*) and the ^{235}U fission data zoomed in the resonance region around 1 eV (*right*).

In the framework of the TOF-02 experiment we planned to measure the neutron fluence also through the ^{197}Au(n,γ)^{198}Au reaction, considered as "standard" between 0.2 and 3.5 MeV.

Typical measured spectra of the gold capture reaction are shown in Figure 3-6 and Figure 3-9 for the 1 mm thick and the 100 μm thin sample respectively [8].
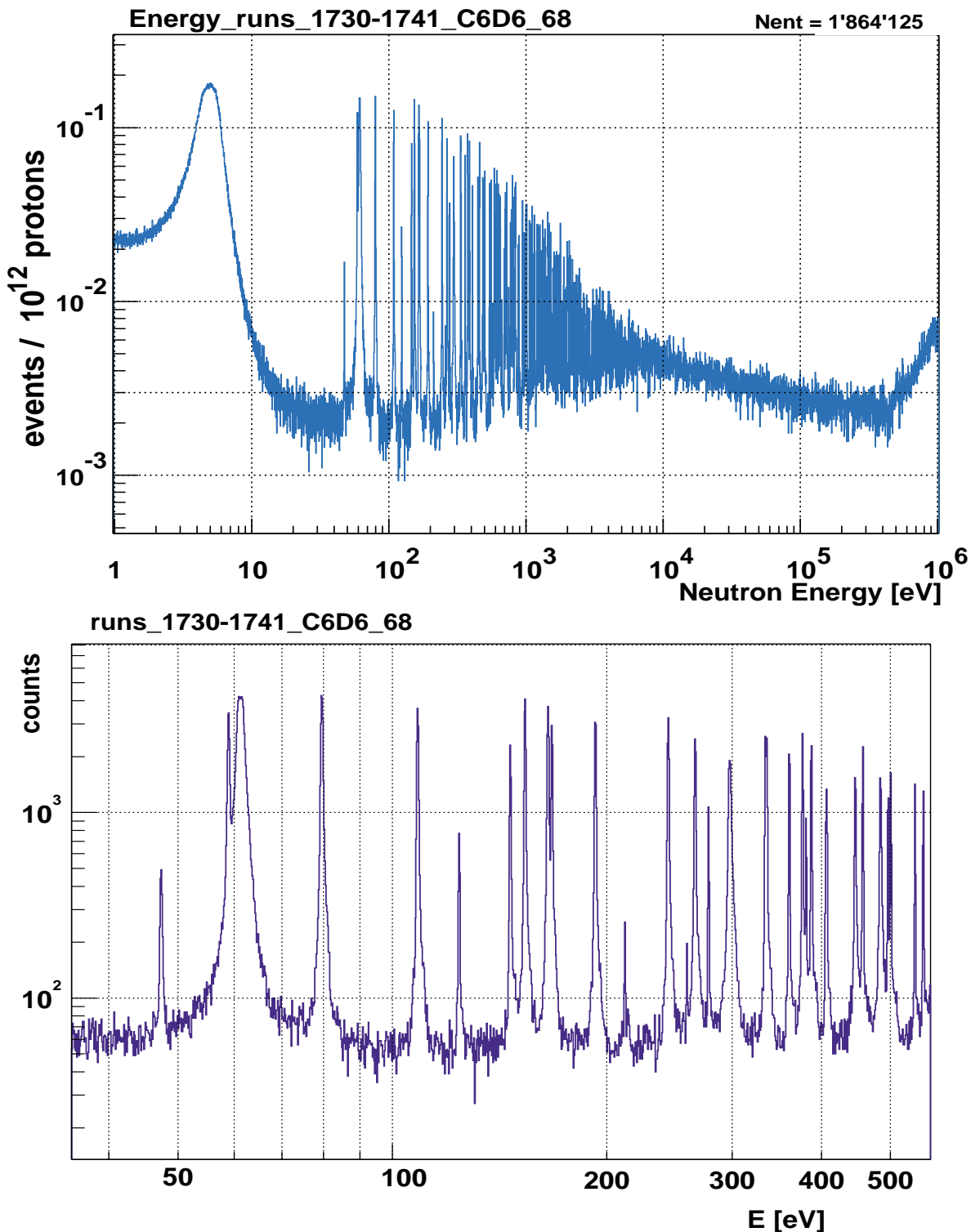

Figure 3-6: Raw neutron capture spectra from a typical run with a 1 mm thick ^{197}Au sample measured by the C_6D_6 detectors (*top*) and the zoomed region around 200 eV (*bottom*).

The structure at neutron energies above a few 100 keV can be understood in terms of neutron or photon interactions in the C_6D_6 detectors related to neutrons initially scattered by the sample and subsequently re-scattered or captured by various materials and the shielding in the

experimental area. The equivalent structure can also be seen with the 6.3 mm Carbon sample presented together with the MC simulated C_6D_6 rates [9] in Figure 3-7.
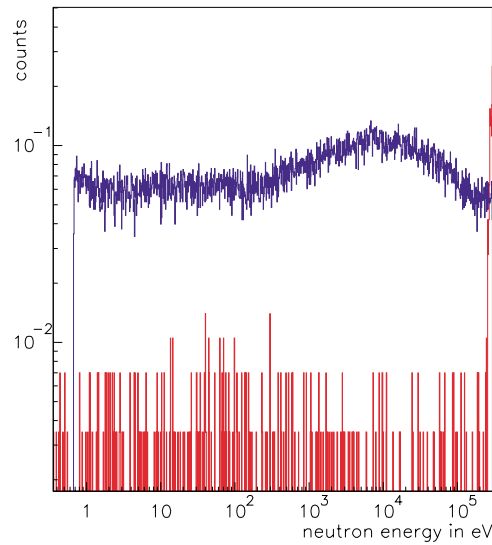

Figure 3-7: The measured (*blue*) and simulated (*red*) rates of the C_6D_6 detector viewing the 6.3 mm Carbon sample.

This unexpected background level is also obvious in our measurement with a 100 μm thin ^{197}Au sample (Figure 3-8 and Figure 3-9). In particular, Figure 3-8 compares the observed yield (red) with the result of the simulation (blue), showing the measured background to be about 50 times larger than simulated. The black spectrum was obtained by neglecting any background contribution.
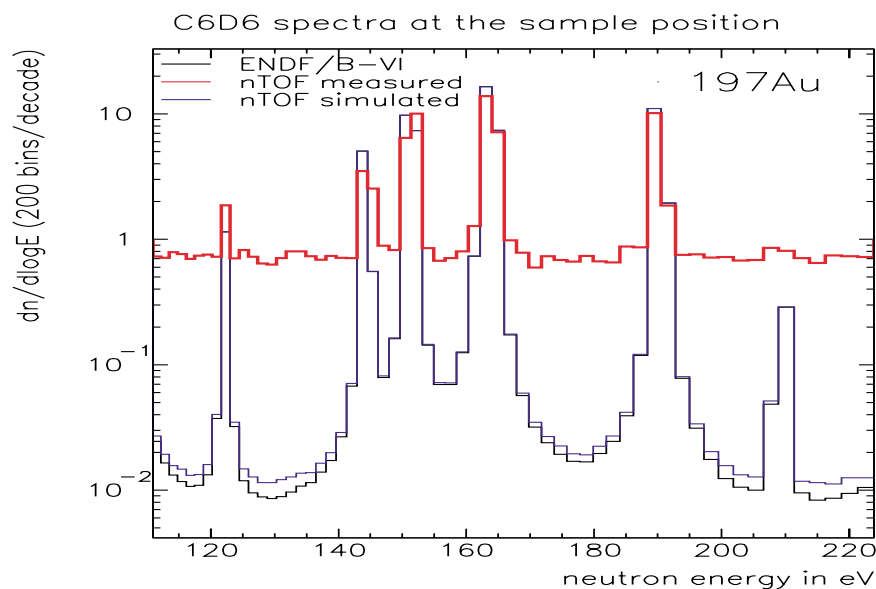
Figure 3-8: The measured (n,γ) rate for the 100 μm thin ^{197}Au sample. The simulated spectra of ^{197}Au [8] using the END/B-VI database are shown for comparison.

The problem with the high background level becomes also evident by comparison with corresponding spectra taken at the existing electron linear accelerators GELINA[10] and ORELA[11] , which leads to the conclusion that n_TOF shows similar or even higher ambient background despite the superior features of four times larger flight path and fifty times smaller duty cycle (see also chapter 5.2.3).

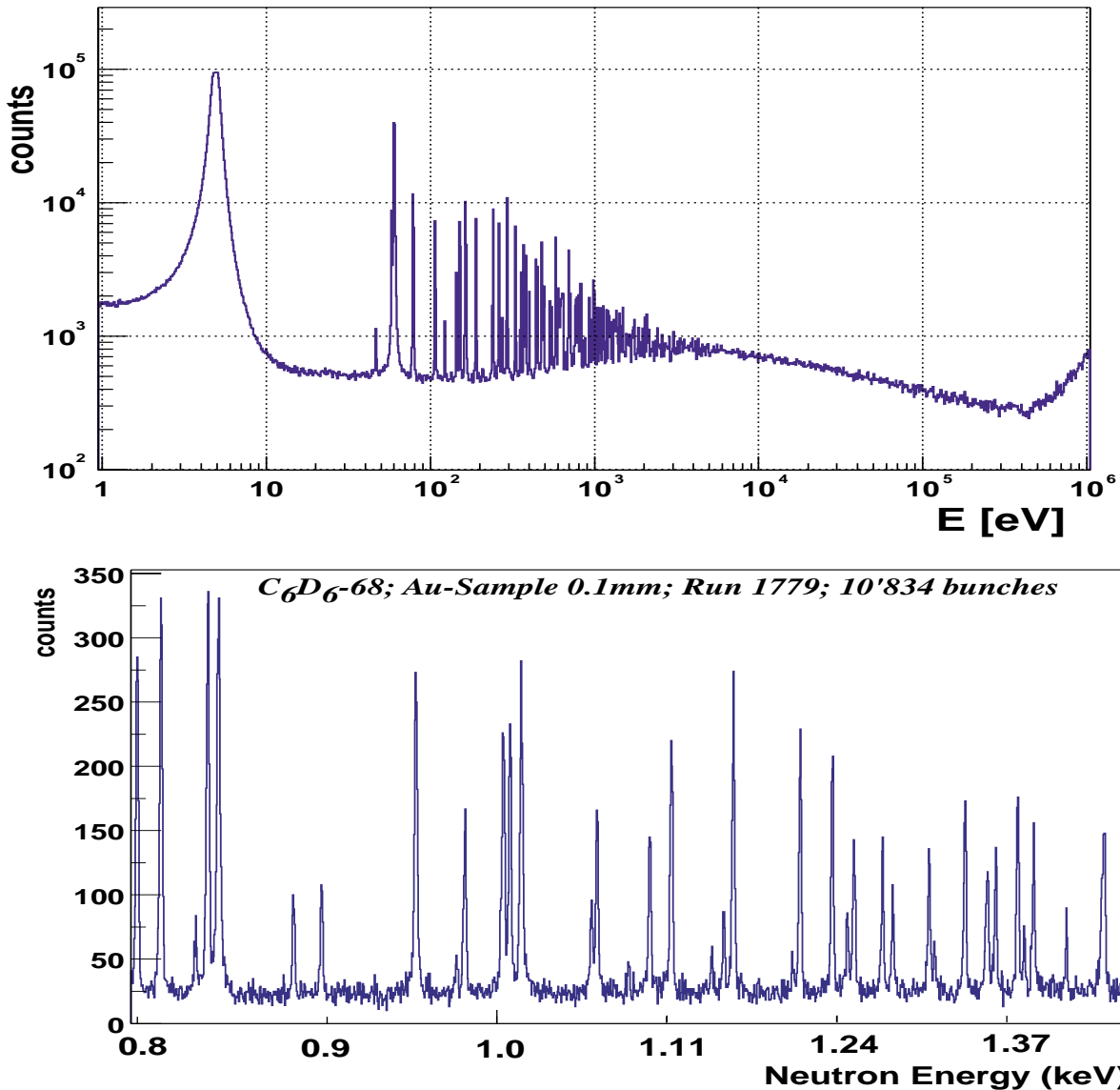**Figure 3-9:** Raw neutron capture spectra from a typical run with a 100 µm thin ^{197}Au sample measured by the C_6D_6 detectors (*top*) and the zoomed region around 1 keV (*bottom*).

The accuracy in the determination of the capture cross sections with the C_6D_6 detectors depends on the accuracy of the weighting function, which are derived from the response distributions in the energy range up to 10 MeV. As planned in the TOF-02 experimental programme we have determined such experimental weighting functions from measurements of the known ^{56}Fe(n,γ) capture cross section (Figure 3-10 *left*) and its validation with the measurement of the "standard" ^{197}Au isotope (Figure 3-9 *top*). We have verified that presently the peak to background ratio of the 1.15 keV ^{56}Fe resonance amounts to 4.3 in area or 21 in height (for 5'000 bins per energy decade). We also note that the high background level did not allow seeing the other resonances of ^{56}Fe at higher energies. Indeed, the ^{197}Au capture spectra also suffer from a high background, as can be seen in Figure 3-8. The high background level for these measurements implies higher statistics for a proper determination of the resolution function, firstly, and of the resonance parameters, secondly. Our data analysis and the applied pulse height weighting technique together with our results are described in chapter 5.

The prominent resonance in ^{56}Fe at 1.1 keV (Figure 3-10 *left*) may also provide a possibility to verify the theoretically calculated resolution function of the n_TOF facility. This possibility is indicated in Figure 3-10, which exhibits the various components contributing to the observed resonance width. However, the asymmetry of the resonance caused by the resolution function can only be verified reliably if the background in the n_TOF experimental area can be significantly reduced.
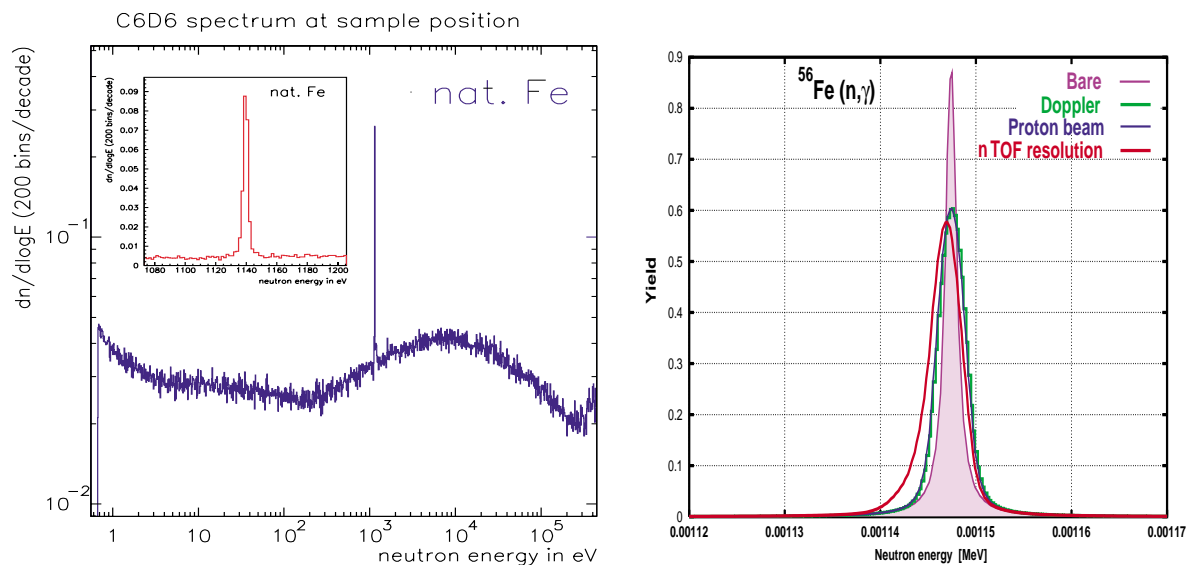

Figure 3-10: The ^{nat}Fe with the 1.15 keV resonance (*left*) and the broadening of the 1.1 keV ^{56}Fe resonance due to various effects (*right*). This resonance would allow testing the calculated resolution function of n_TOF. However, this requires significant background reduction to verify the characteristic tail indicated by the red shape.

The neutron capture experiments TOF-03 [3] and TOF-04[4] will be performed by using the same C_6D_6 γ-ray detectors and the pulse height weighting technique. The high background detected in the capture data would clearly prevent these planned experiments to attain their goals. In order to extract a maximum information on the possible background components, we performed the detailed analysis presented in chapter 5 for the capture data, which have been collected in May and June 2001.

3.1. THE BEAM-PIPE AND DETECTOR ALIGNMENT.

The presence of the unreasonably high background inside the n_TOF experimental area measured by the C_6D_6 detectors is in direct contradiction with extensive Monte Carlo calculations [2,12,13] performed by different groups with different methods and tools. We recall that these calculations considered all the beam elements, including both collimators and the shielding surrounding the vicinity of the neutron tube, and predicted a background flux level six to seven orders of magnitude lower than the flux in the beam. A possible source, not included in these Monte Carlo simulations, could result from misaligned beam and/or detector elements via elastic and inelastic interactions of the beam neutrons.

We have re-confirmed the correct alignment of the neutron beam relative to the beam-pipe, the detectors, the "sample exchanger" and the "Neutron Escape Line" (NEL) with the following measurements:

- More precise survey (better than 1 mm) of the position of the various elements in the experimental area by the CERN survey team.

- Determination of the beam position and size (Figure 3-12) using the ^{6}Li(n,t)α reaction, the reaction products being detected by our Micromegas chambers.
- Determination of the beam position and profile at the exit of the "sample exchanger" (Figure 3-12) using the ^{10}B(n, α)^{7}Li reaction, the reaction products being detected by CR-39 plastic track-etch detectors [14]. The CR-39 detectors have been covered with Cadmium foils with a thickness of 1 mm, eliminating thus their efficiency for neutron energies below 0.5 eV. This configurations provides the spatial distribution of the neutron beam in the range of ~ few eV neutron energies.
- Absence of ^{197}Au(n,γ)^{198}Au reaction events around the beam-pipe and at the reduction rings from 20 cm to 5 cm diameter tube before the "sample exchanger". A C_6D_6 detector was viewing the four gold samples covering the radii from 2 to 3 cm around the beam axis. A typical capture spectrum is shown in Figure 3-13 with the evident absence of the main gold resonance at 4.9 eV.
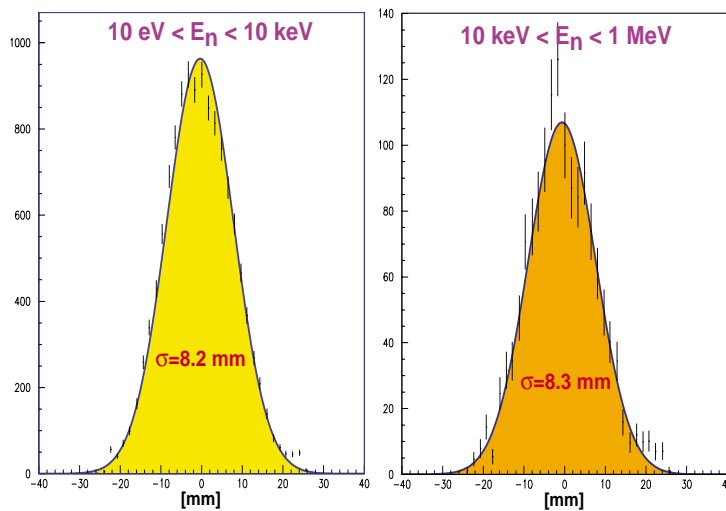

Figure 3-11: The vertical projections of the neutron fluence at the exit of the "sample exchanger" for two neutron energy ranges measured with the Micromegas.

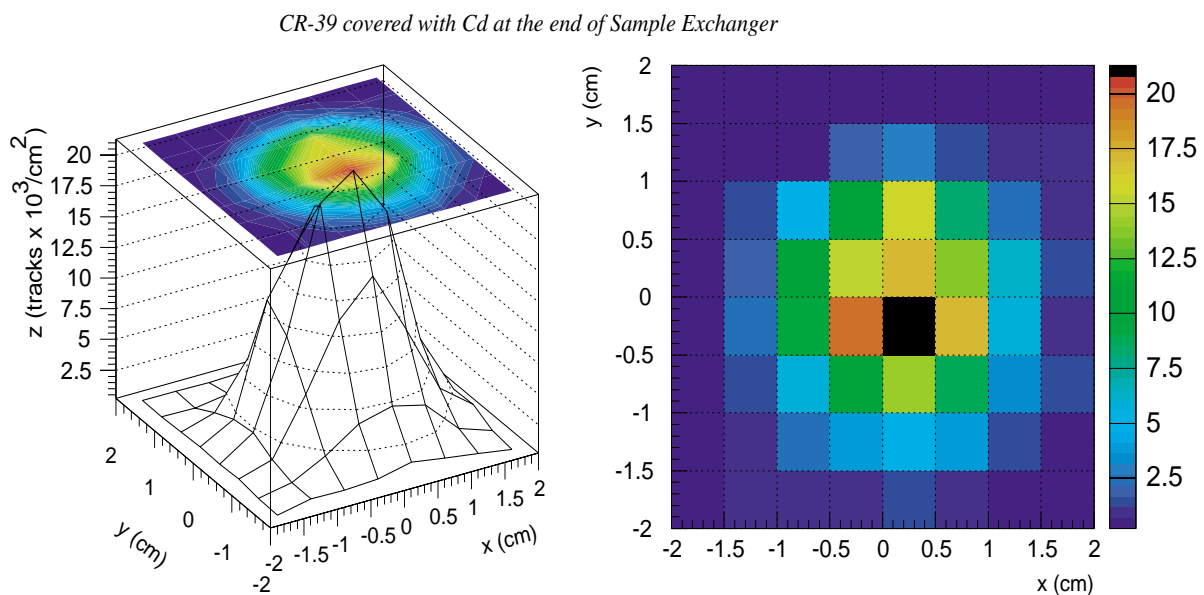*CR-39 covered with Cd at the end of Sample Exchanger*

Figure 3-12: Spatial distribution of the neutron beam in the range of a few eV neutron energies deduced from the CR-39 detectors [14].
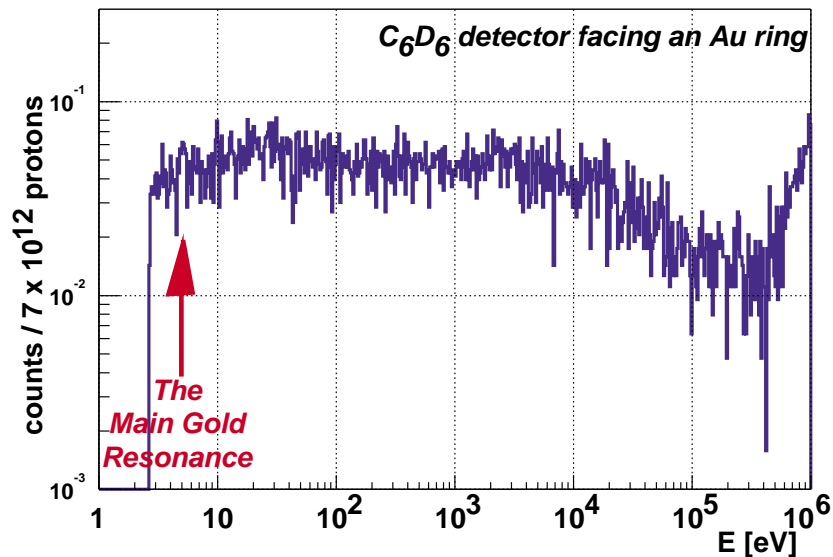
Figure 3-13: Typical capture spectrum measured with a C_6D_6 detector and the Au samples positioned at radii between 2 and 3 cm around the neutron beam axis, showing no evidence for (n,γ) reactions. Note in particular the absence of the strong resonance at 4.9 eV.

3.2. BACKGROUND EMANATING NEAR THE SECOND COLLIMATOR.

In the present configuration the shutter in front of the second collimator offered another possibility to study beam-related background contributions. The measured spectra corresponding to the "empty sample" position and with the 5 mm thick stainless steel shutter opened and closed exhibit different background levels as shown in the left image of Figure 3-14. Similar to the spectra taken with the Pb and C scattering samples (chapter 3.4) the application of the pulse height weighting operation (Figure 3-14 *right*) practically eliminates this difference, thus indicating that the related difference in the weighted spectra was due to low-energy γ-rays.
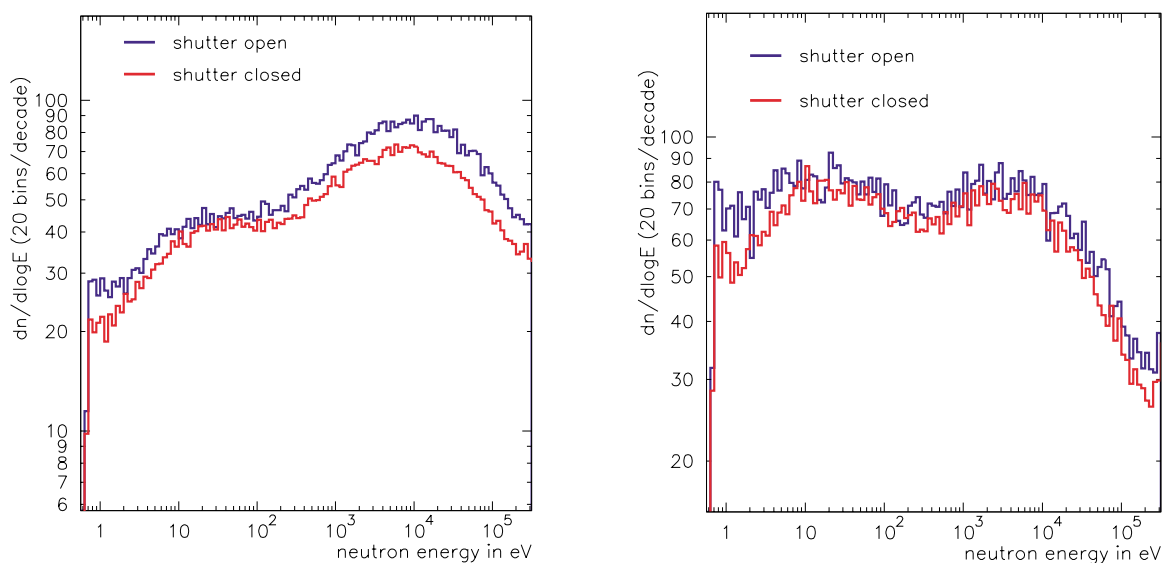

Figure 3-14: The effect of the vacuum shutter behind the second collimator introducing a scattering centre close to the experimental area. The spectra are shown at the right side after the application of pulse height weighting.

There are several potential sources for such low-energy γ-rays, which need to be investigated further by MC calculations.

3.3. BACKGROUND LEAKING FROM THE NEUTRON ESCAPE LINE.

At the beginning of the data-taking period, the Neutron Escape Line (NEL) was still in its preliminary shape. Nevertheless, various Monte Carlo simulations [2,13,15] had predicted that even under this condition, the neutron escape line should have an acceptably small effect on the overall background in the experimental area. This result was checked by comparing the C_6D_6 spectra obtained at two positions, immediately in front of the chicane to the neutron escape line and about 80 cm to the side, well behind the concrete shielding wall, which separates the experimental area from the NEL.
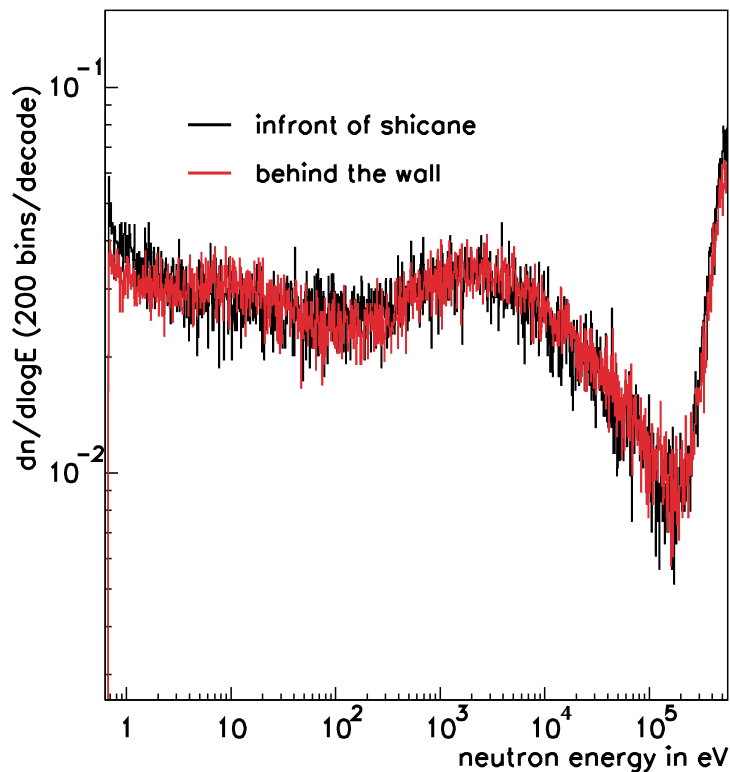

Figure 3-15: Spectra taken in front of the chicane to the neutron escape line and behind the shielding wall confirm that the enhanced background can not originate from the neutron escape line.

Both spectra are compared in Figure 3-15; their good agreement implies that the enhanced ambient background is NOT originating from the neutron escape line. At most, it could only be a small fraction as predicted by our simulations.

In addition, measurements with TLD-^{7}Li [16] and CR-39 TED [17] detectors have been performed at the entrance of the NEL on the neutron tube and at the wall of the chicane facing the beam dump. The TLD-^{7}Li detectors were sensitive only to photons and charged particles (prompt background) and the measurements revealed levels of radiation well below the corresponding level in the experimental area. These measurements in the area of the NEL showed that the radiation level is on the right side following the beam direction twice as high as in the middle of the area. The CR-39 TED detectors were sensitive only to neutrons with energy above 1 MeV and they showed neutron radiation levels below their detection limit.

3.4. THE BACKGROUND LEVEL FROM DIFFERENT SAMPLES.

For the determination of this background we have applied the method based on the use of a "sample changer", which allows to study, quasi-simultaneously with the sample under investigation, both background components. The first background component is related to beam photons and neutrons interacting with or scattered on the sample, which can be experimentally simulated with a carbon and/or a ^{208}Pb sample, both having negligible (n,γ) cross sections. The second component represents the ambient photon and neutron background inside the experimental area and can be determined by means of an empty position or by using an empty sample container. High level of background without a sample in the beam would indicate insufficient shielding of the experimental area either upstream from the spallation target and/or downstream from the neutron escape line. The difference of the two spectra, i.e. ^{12}C/^{208}Pb sample and no sample, would provide the amount and the time structure of the γ-background related to the beam photons and neutrons interacting with the sample. The background spectrum versus time of flight measured without sample in the beam is shown in Figure 3-16 (left) and on a neutron energy scale after rebinning and normalisation to the intensity of a single proton pulse (right).
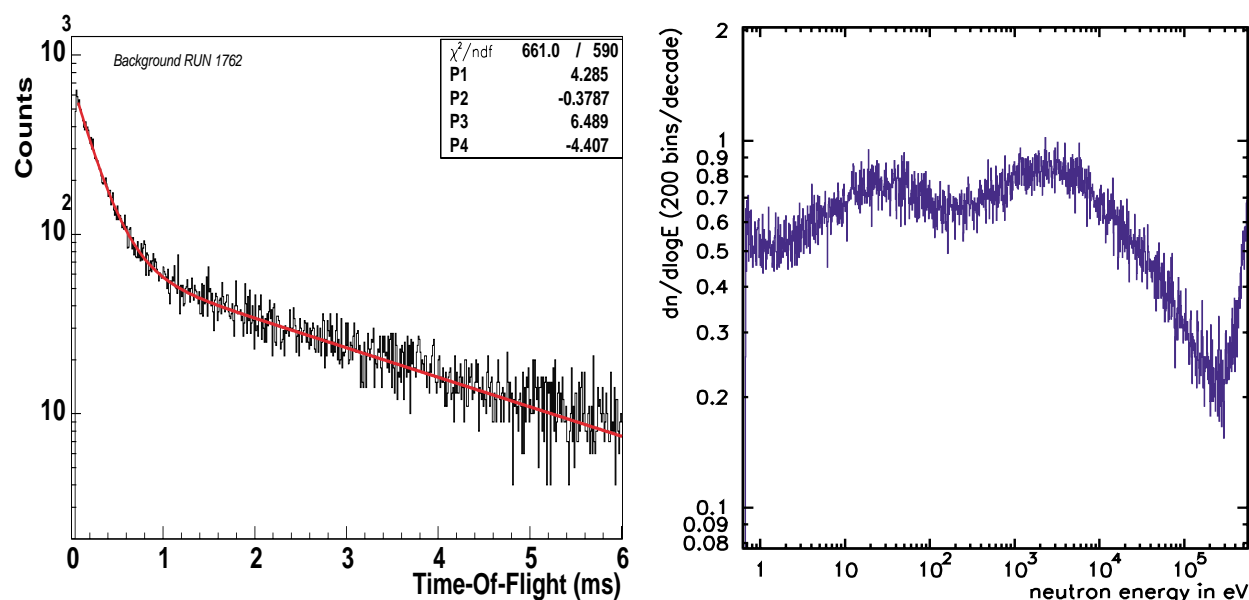

Figure 3-16: The background versus time of flight measured without sample in the beam (*left*). The same spectrum plotted versus neutron energy (*right*).

The decay of isotopes activated by the neutron beam in the experimental area could be the origin of the double exponential time distribution of the background events, but no isotope could be identified with the half life and concentration in the experimental area that could explain the observed background. Moreover, the energy spectrum of the photons in the background events extends to energies larger than 7 MeV, more typical for capture photons than for decay photons.

In contrast to the expected effect, the spectra obtained with the thick carbon and Pb samples and after application of a linear weighting function[8], show no significant difference compared to the spectra taken without any sample or with only a very thin Kapton foil in the

---

[8] To approximate the situation expected in later measurements of (n,γ) cross sections.

beam, the ambient background rendering this contribution negligible (see Figure 3-17). This provides additional strong evidence that the present background is much too high (see also chapter 5.2).
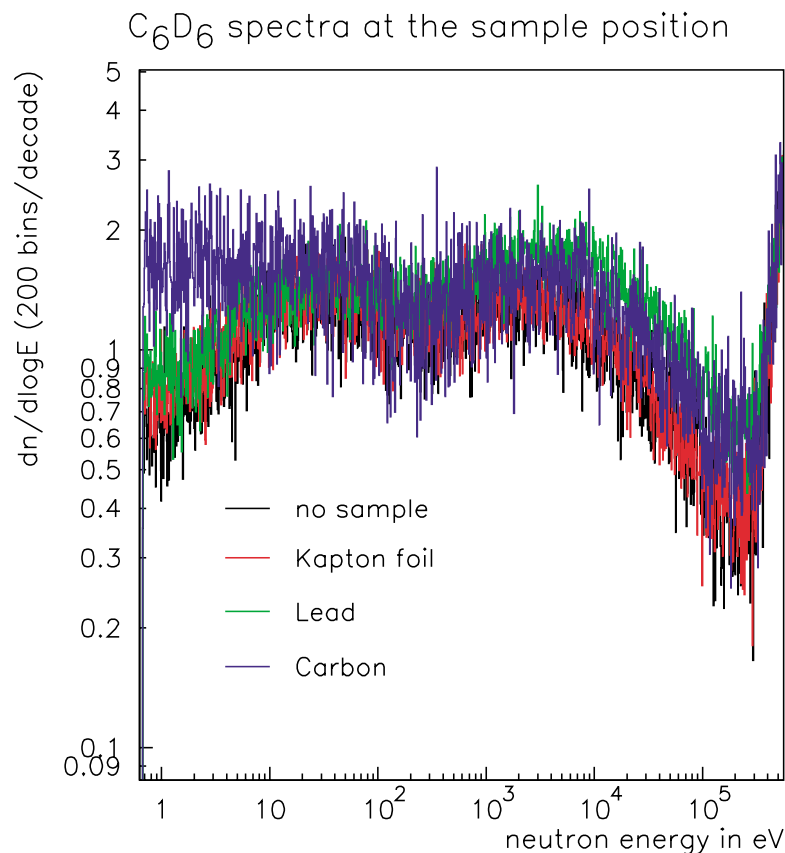

Figure 3-17: Comparison of measured background spectra with and without scattering samples after application of pulse height weighting. Even for the massive scattering samples used (6.3 mm C and 1 mm Pb), the ambient background is by far dominant.

3.5. SPATIALLY ASYMMETRIC BACKGROUND.

3.5.1. C₆D₆ spectra at various positions in the Experimental Area.

The ambient background in the experimental area was studied versus TOF in a more systematic way by placing the detectors at symmetric positions, 70 cm to the left and right of the neutron beam line, directly in front of the entrance wall and in the middle of the experimental area. These measurements were carried out without any sample in the beam and we recall that all measurements were performed with the beam tube under vacuum.

The resulting spectra in Figure 3-18 are arranged in the order of the corresponding detector positions with respect to the neutron beam. There are clear differences observed, in particular with respect to the structure between 100 eV and 10 keV (TOF smaller than 1 ms), which appears most pronounced on the right side close to the entrance wall of the experimental area (spectrum at lower left). The fact that this feature is much weaker for the other positions would support the picture that penetrating particles from the spallation target may create secondary neutrons preferentially on the right side of the entrance wall, which is less well shielded. The capture γ-rays from these neutrons would then dominate the ambient background

in the experimental area. The numbers in the insets, which represent the integral spectra, also reflect this enhancement.
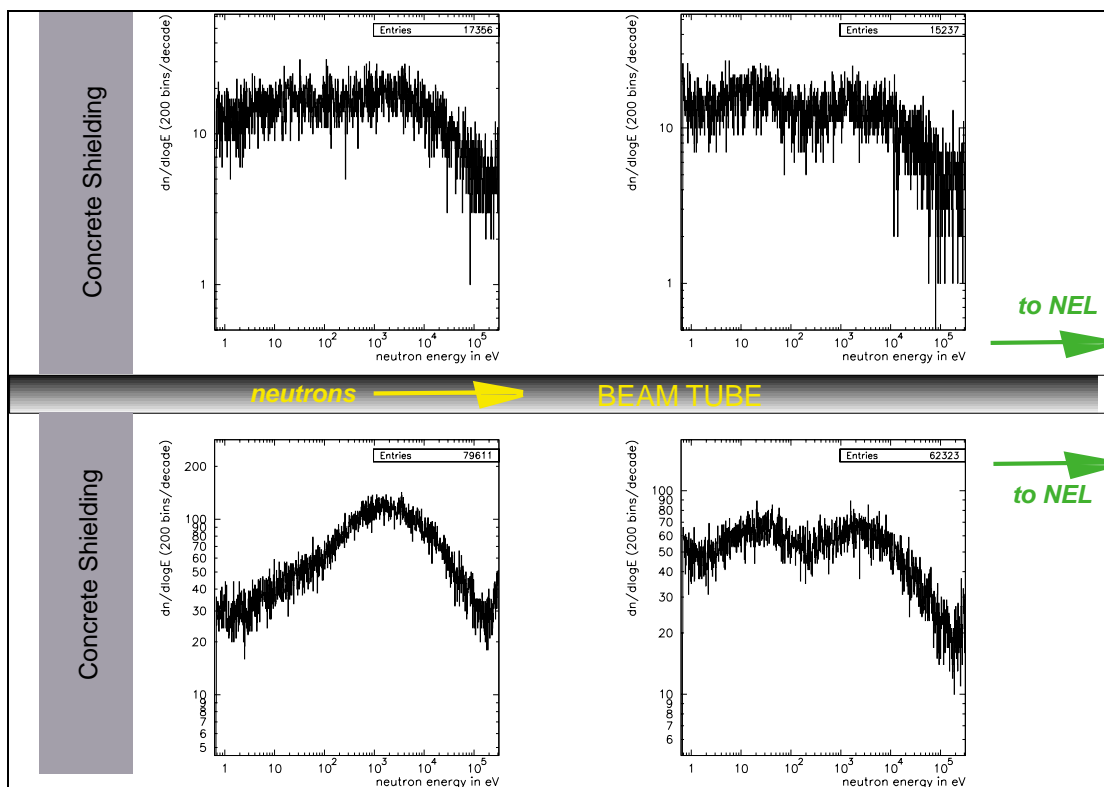

Figure 3-18: Background spectra taken at various points inside the experimental area normalised to equal number of protons. The arrangement of the spectra reflects the corresponding detector positions with respect to the neutron beam. Note the strong left / right asymmetry and the fact that the broad structure between 100 eV and 10 keV (TOF<1 ms) appears most pronounced on the right side close to the entrance wall.

The measurements of ^{197}Au(n,γ) capture events with the C_6D_6 detectors have strongly indicated the presence of an ambient background between one and two orders of magnitude higher compared to the results of Monte Carlo simulations. The main characteristics of this background can be summarised as:

- The measured background extends from several tens of microseconds to 15 ms after the arrival of the proton beam, corresponding to the neutron energy range from thermal to ~ 100 keV.

- The background exhibits a time distribution composed of two exponentials with decay times of approximately 160 μs and 1.8 ms (Figure 3-16).

- The background shows a strong dependence from the position inside the experimental area (Figure 3-18) with the right-hand side in the neutron beam direction being more enhanced.

- The spectra obtained with various samples having negligible capture cross sections show hardly a difference to the spectrum taken with no sample (Figure 3-17), providing evidence that the measured background does not originate from the material inside the neutron beam.

- From our measurements it is difficult to accommodate this background to secondary interactions of the beam with the second collimator, the vacuum TOF tube, and the neutron escape line.

From the above characteristics strongly indicating the ambient nature of the measured background, there is mainly one kind of contribution possible, i.e. neutrons leaking through the concrete shielding walls into the experimental area.

3.5.2. The "prompt" and "fast" component of the background – Measurements with BC–702, TLD and TED detectors.

The high-energy background has been investigated with several techniques including the BC702 and TLD detectors, sensitive both to photons and charged particles, the BC702 being in addition sensitive also to low energy neutrons, as well as the CR-39 fast neutron integral detectors.

This high-energy background would imply the presence of a very early component related to the "flash" following the PS pulse, including photons, charged particles and fast neutrons.
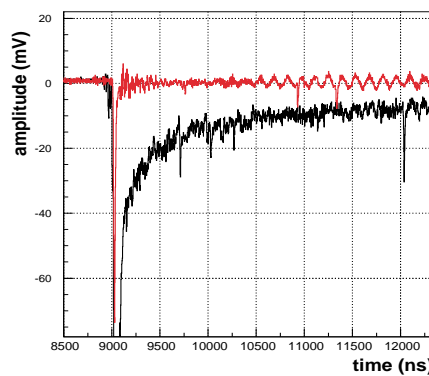
Figure 3-19: BC702 signals immediately after the "flash" measured at symmetric detector positions 1 m left (*red*) and right (*black*) from the "sample exchanger". Note that the time scale does not correspond to the time-of-flight.

In order to reveal such an early component, we have mapped the radiation of the secondary area and the experimental area with the BC702 detector, with the TLD-^{7}Li detectors being sensitive mainly to photons and charged particles, and with the CR-39 TED detectors being sensitive to neutrons above ~ 1 MeV.

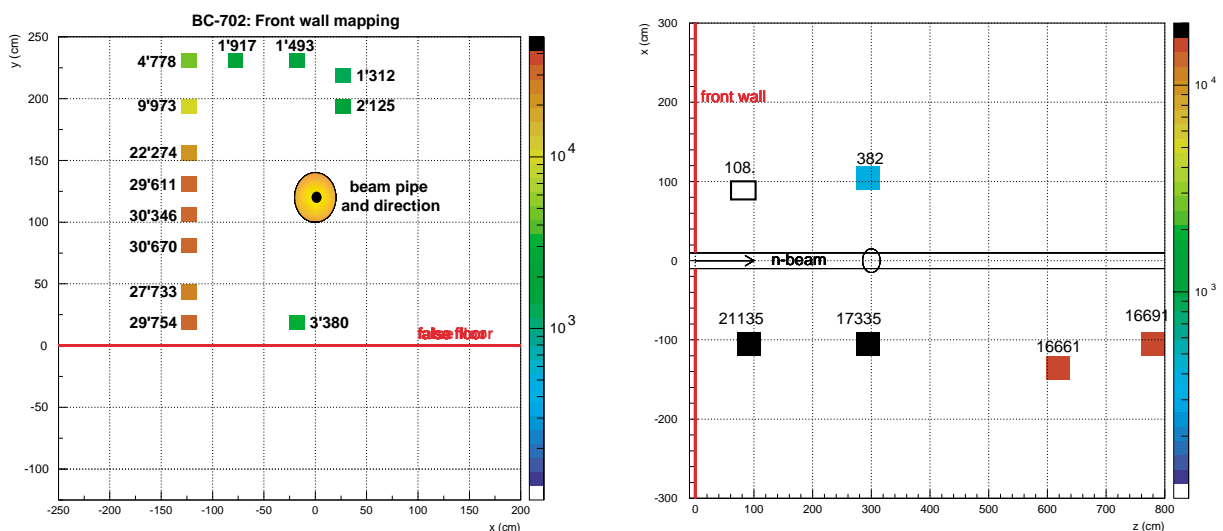**Figure 3-20:** Mapping of the front shielding wall inside the experimental area (*left*) and along the experimental area (top view, *right*).

The form of the BC702 signals corresponding to the symmetric detector positions 1 m left and right from the "sample exchanger" taken immediately after the "flash" (Figure 3-19) show a significant background component for the right position in respect to the beam direction. The charge of the BC702 signal integrated from 150 ns to 15.6 µs represents a measure of this early background component. The spatial distribution of this integrated charge inside the experimental area is shown in Figure 3-20 and indicates that the radiation level on the right side is higher by a factor of ten compared to the left side.

Using TLD-^{7}Li crystals the TIS group [16] has performed supporting integral measurements and the mapping of the experimental area has shown equivalent results to those of the BC702, as illustrated in the left panel of Figure 3-21.
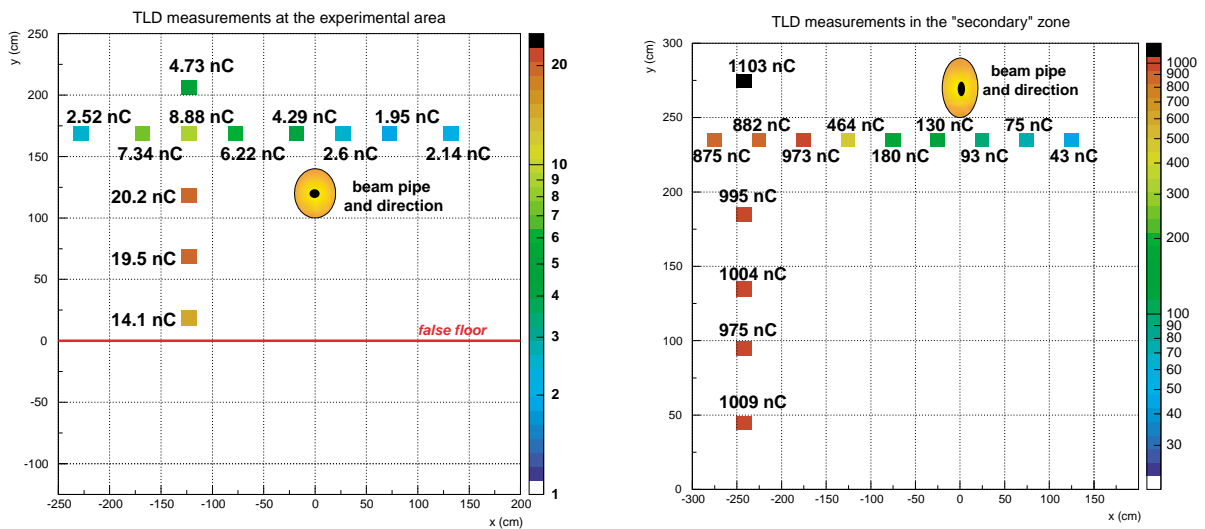
Figure 3-21: Mapping of the entrance walls of the experimental area (*left*) and of the "secondary area" before the sweeping magnet (*right*) with TLD detectors.
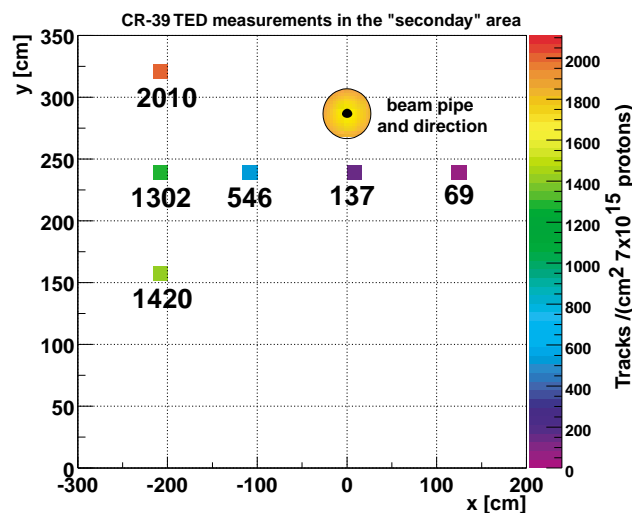
Figure 3-22: Mapping the fast neutron fluence at the entrance wall of the "secondary area" before the sweeping magnet with the CR-39 TED detectors.

In order to better understand the origin of this huge asymmetry of the background component at early times, we performed the equivalent mapping at the entrance wall of the "secondary area" situated upstream of the sweeping magnet. These measurements confirm the asymmetry of the background and indicate an increase of the asymmetry in the "secondary

area" by a factor of five as compared to the same measurements in the experimental area (Figure 3-21).

Furthermore, we have used CR-39 TED detectors showing a response exclusively to neutrons with energies above 1 MeV for mapping the fast neutron fluence at the entrance wall of the "secondary area" before the sweeping magnet. These integral measurements [17] of the fast neutron component confirmed the same level of asymmetry measured with the TLD detectors (Figure 3-22). Similar sensors at the entrance wall of the experimental area indicated the same asymmetry but at the sensitivity limit (20 tracks / cm^2 / 7×10^{15} protons).

4. RESULTS FROM MONTE CARLO SIMULATIONS.

4.1. THE "PROMPT" AND "FAST" BACKGROUND COMPONENT.

A special simulation was performed [18] to find possible weak points in the shielding of the TOF tunnel. For this task the full geometry of the TT2A tunnel was modelled in detail, conformable to the technical drawings and civil engineering plans and including the objects existing in the tunnel, like neutron tube, reductions, supports, shielding, collimators, but not the imperfections in the homogeneity of the concrete walls, in particular at the entrance of the experimental area. The FLUKA program tracks all the objects lying in the given direction and provides various quantities, like distance traversed in each material, mass, number of interaction lengths, etc.

Figure 4-1 shows the minimum of surface mass density projected at the measuring station. The minimum density of 1400 g/cm^2 at the left side of the plot corresponds to only 5.2 m of concrete. The maximum surface density of the order of 20 kg/cm^2 is found at the top of the tunnel.
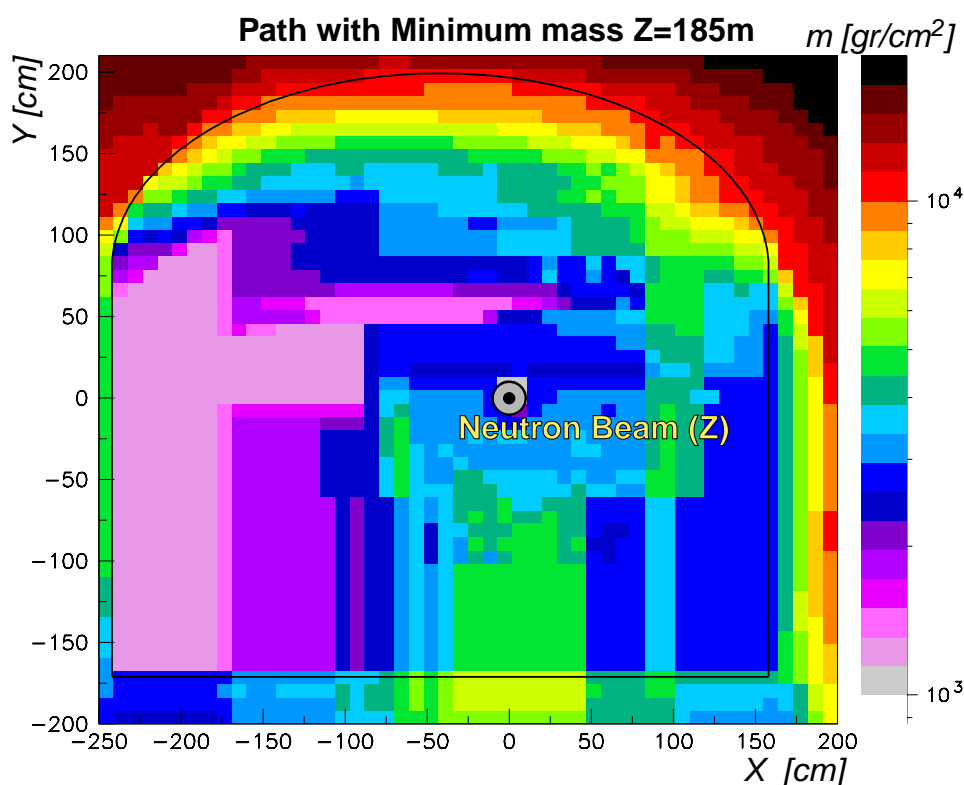
Figure 4-1: Trajectories with minimum surface density (g/cm^2) projected at the middle of the measuring station Z=185 m. The neutron beam is directed towards the observer.

The simulations show that fifty percent of the 20 GeV protons are not stopped in the spallation target, but hit the surrounding shielding and the walls of the tunnel resulting in a highly extended source of neutrons, which practically illuminates the whole tunnel (Figure 4-2). This fact in conjunction with the inhomogeneous shielding of the experimental area, in particular the weak areas at the right side of the beam, allows fast neutrons, charged particles and possibly photons to penetrate and to enter the experimental area, which acts as a cavity for

these neutrons. Such charged particles and photons would appear at the experimental area "promptly" following the PS bunch and would create the prompt background component measured with the BC702 and TLD detectors (3.5.2) and its asymmetric spatial distribution.
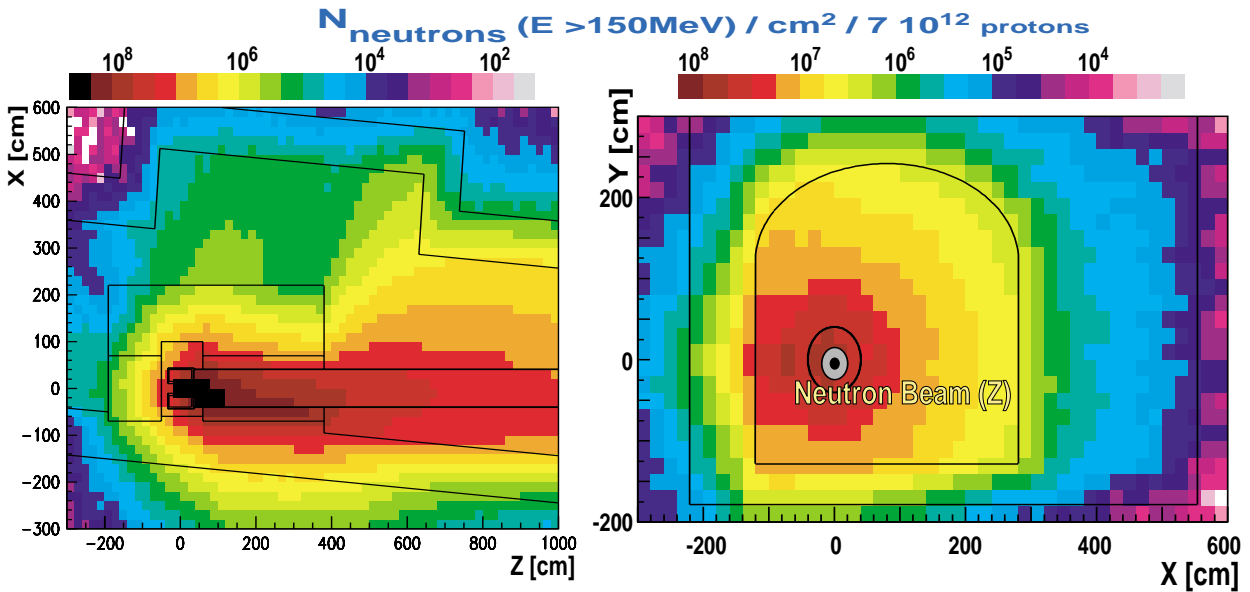
Figure 4-2: The fluence of fast neutrons (> 150 MeV) in the vicinity of the spallation target. The extension of the neutron source is shown in the right panel, which illustrates clearly that a substantial part of the fast flux is produced outside the Pb target preferentially on the right side of the tunnel.

In particular for the case of the charged particles, the long decay path of charged kaons and pions would imply an even more extended source of such prompt background. Extensive Monte Carlo calculations revealed the presence of a huge muon fluence of 10 to 100 $\mu/cm^2/7\times10^{12}$ protons entering the experimental area with an average energy of ~1 GeV (Figure 4-3). These muons can explain the measured prompt background, which is prohibitive for operating a crystal calorimeter of BaF_2.

Figure 4-3: Muons with a fluence of 10-100 $\mu/cm^2/7\times10^{12}$ protons enter preferentially on the right side of the experimental area in the direction of the beam (*left*). Their energy spectrum peaks at 1 GeV (right).

4.2. THE "LOW ENERGY" BACKGROUND COMPONENT.

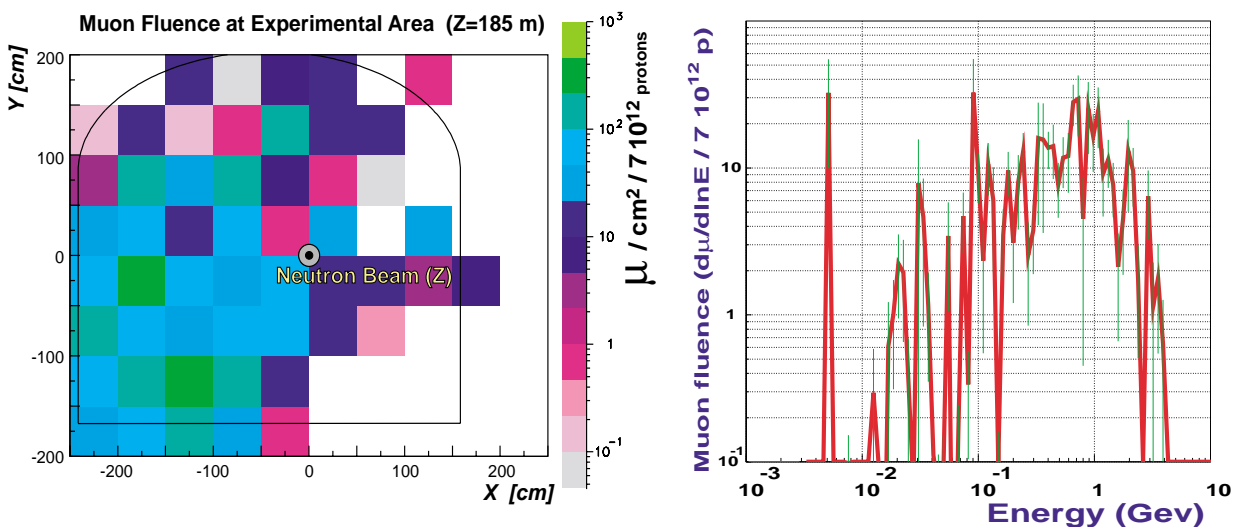We explore the possibility that the observed "low energy" background is due to photons produced by residual neutron captures in the experimental area during long time intervals (several ms). These neutrons arise from fast spallation neutrons produced outside of the lead target, which arrive at very short times, less than $50\,\mu s$ after the γ-flash. This chapter summarises the result of several high statistics MCNPX Monte Carlo simulations, performed in order to reveal the physics involved in these processes [19].

In the Monte Carlo simulation the experimental area and the neutron escape line (NEL) have been implemented with all the detail as shown in Figure 4-4.
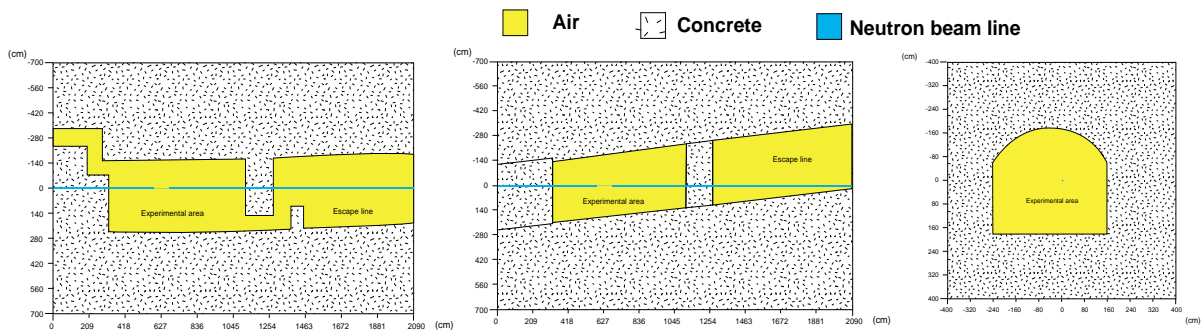
Figure 4-4: Top view (*left*), the side view (*middle*) and the front view (*right*) of the simulated experimental area

The fast neutrons reaching the environment of the n_TOF experimental area were studied (Figure 4-5) in two ways:

SOURCE 1: Neutrons with energies between 20 and 200 MeV, uniformly distributed in energy and surface density, are hitting the side wall (plane at Y=220 cm) of the n_TOF experimental area at an angle of 5° with respect to the neutron beam (green area in Figure 4-5).

SOURCE 2: Neutrons with energies between 20 and 200 MeV, uniformly distributed in energy and surface density, are hitting the entrance wall (plane at Z=0 cm) of the n_TOF experimental area (red area in Figure 4-5).
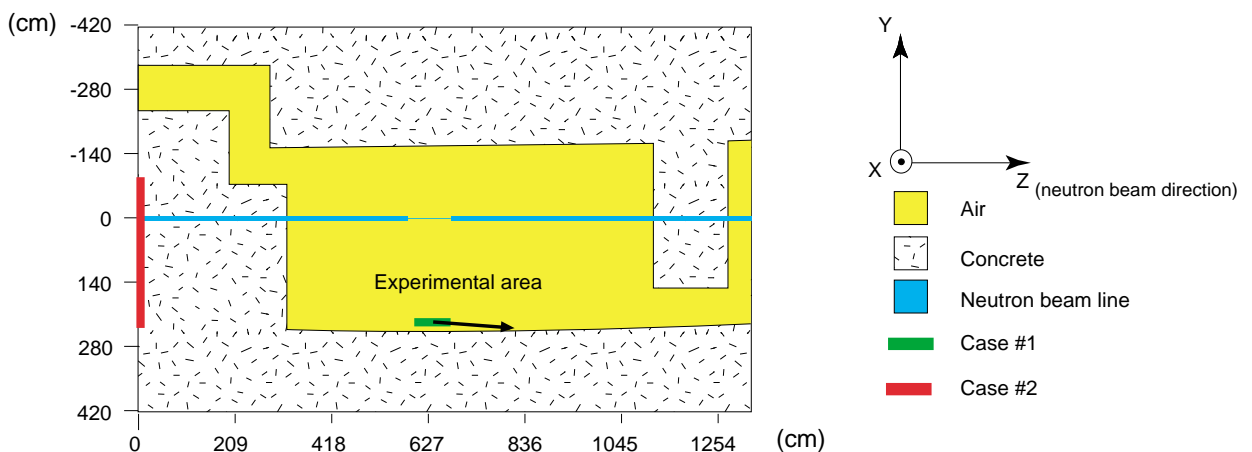
Figure 4-5: Position of the modelled neutron sources. In "case #1" (green) the neutrons hit the concrete wall with an angle θ=5° with respect to the neutron beam. In "case #2" (red) the neutrons are parallel to the Z-axis within a cone of 5°.

To follow the resulting gamma background we placed ten virtual detector volumes inside

the experimental area as indicated in Figure 4-6. In order to render the statistics of the Monte Carlo simulation more efficient, we assumed these detectors to have large solid angles. The detectors placed inside the concrete floor and the ceiling are not shown in Figure 4-6.
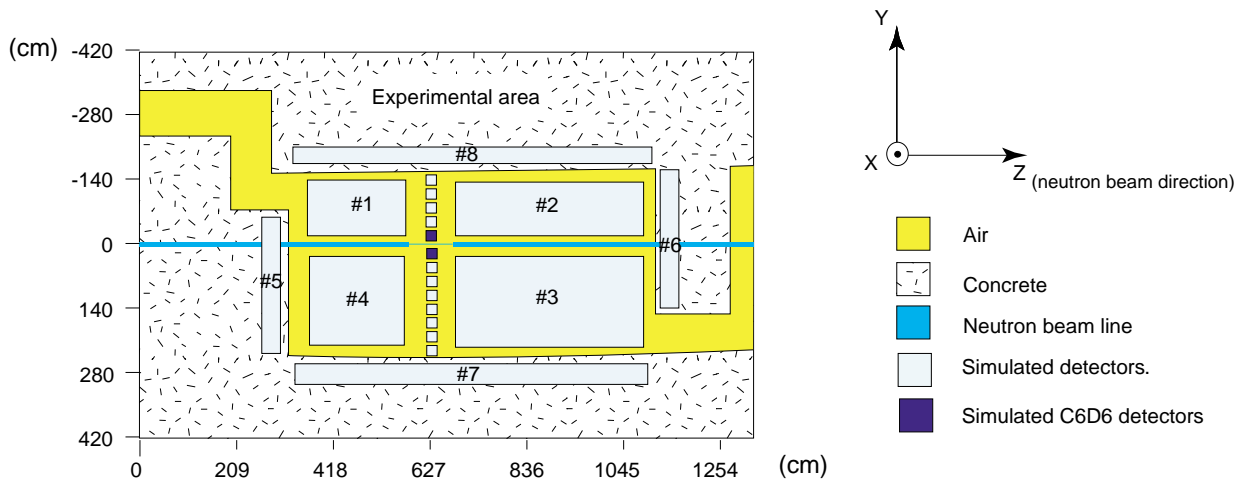
**Figure 4-6:** The position of the simulated virtual detectors inside the experimental area

For both neutron sources, the simulated time distributions of the capture photons crossing the active volumes 1 – 4 show the same double exponential decay behaviour (Figure 4-7) as the experimental data (Figure 3-16). The two exponential decay constants are 190 µs and 1.9 ms, close to the values derived from the experimental data. The corresponding energy spectra are illustrated in Figure 4-8 for detector #3 (SOURCE 1) and detector #1 (SOURCE 2).
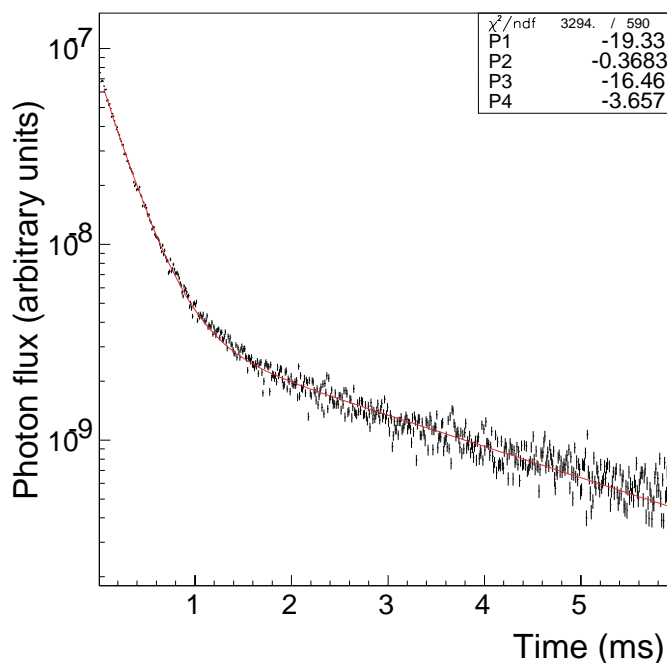
Figure 4-7: Simulated time distribution of the background photons due to interaction of fast neutrons in the walls of the experimental area, illustrated by detector #3 and "*SOURCE 1*".

Following the time history of the neutrons being moderated inside the concrete walls of the experimental area, Figure 4-9 shows that all neutrons are thermalised within a few hundred

microseconds after the proton pulse and that after this time capture events inside the concrete walls take place mainly at thermal energies. The MC simulation shows the predominance of the capture in hydrogen and silicon.
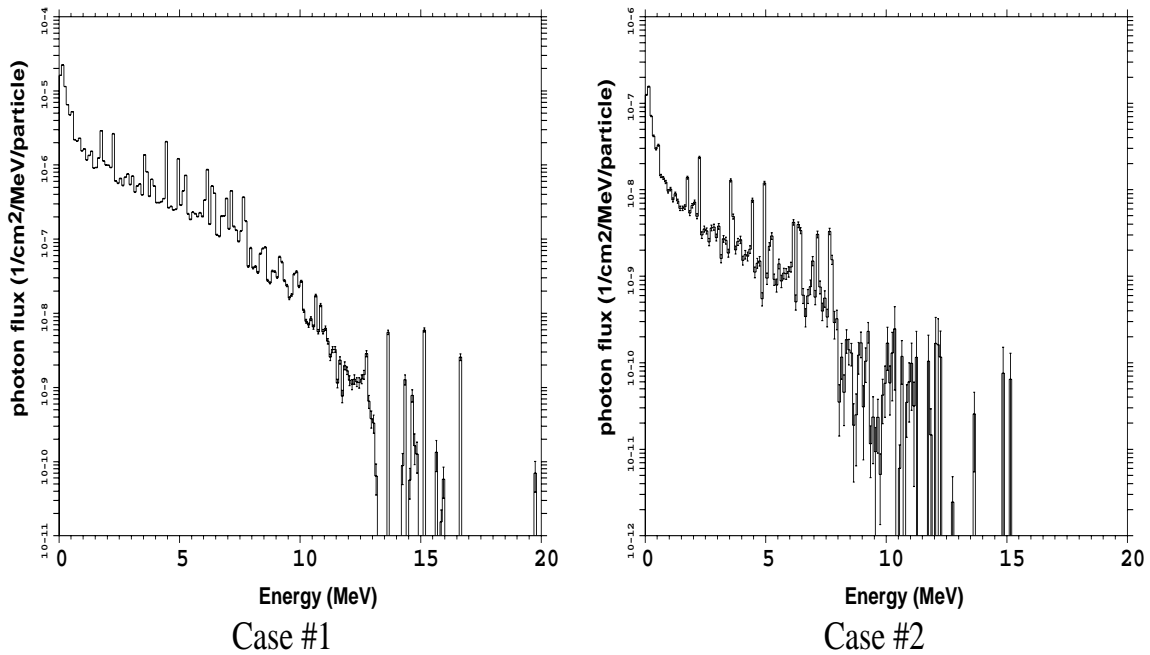
Figure 4-8: Energy distribution of the background photons for the two simulated sources, illustrated by detector #3 and #1 for "*SOURCE 1*" and "*SOURCE 2*" respectively.
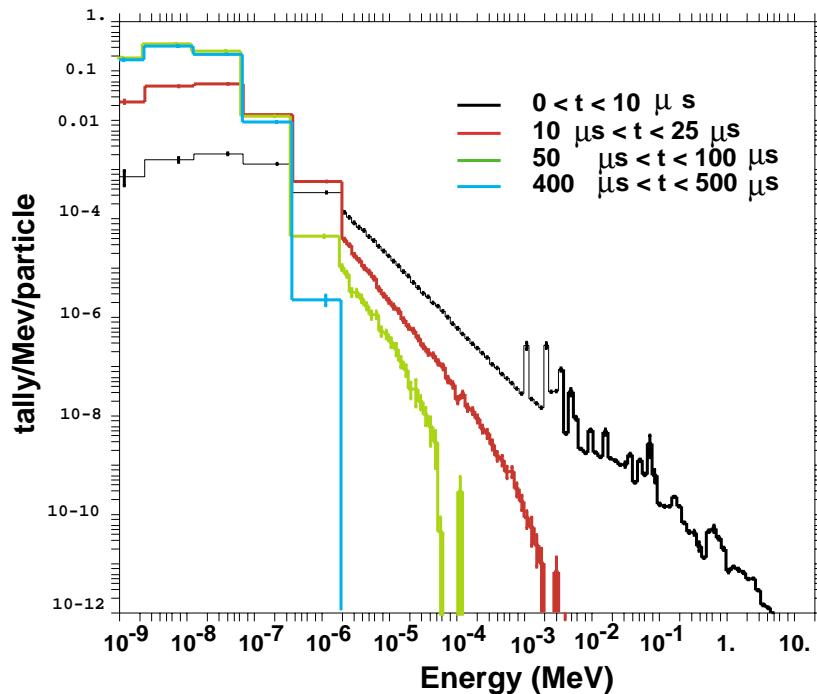
Figure 4-9: The capture rates inside the concrete walls of the experimental area as function of the neutron energy and for different time intervals for the simulation model "*SOURCE 1*". (The results are similar for the model "*SOURCE 2*").

The MC simulations corresponding to both sources show a substantial enhancement of approximately factor four, of the fast component (~200 μs) in the detectors close to the impact

area of the high-energy neutrons. This corresponds to the observed enhancement of the C6D6 background at keV energies in the lower left panel of Figure 3-18, assuming that the high-energy neutrons collide mainly with the right side of the entrance wall and the right-hand side walls of the experimental area. The difference in photon flux of the different detectors decreases as time increases, reaching very similar values for times close to 5 ms, according to the MC simulations

In order to understand the time constants of the simulated background photons, two additional studies have been performed. In the first one, an isotropic thermal (maxwellian distribution with kT=0.02 eV) neutron source is placed inside a concrete sphere of 30 m radius. The resulting decay constant is approximately 290 µs, both for the neutron and the photon fluxes. This time corresponds to the time required for thermal neutrons to cover a mean absorption length inside the medium (~80 cm) and it is compatible with the first, short decay time, component observed in the experimental data and simulations.
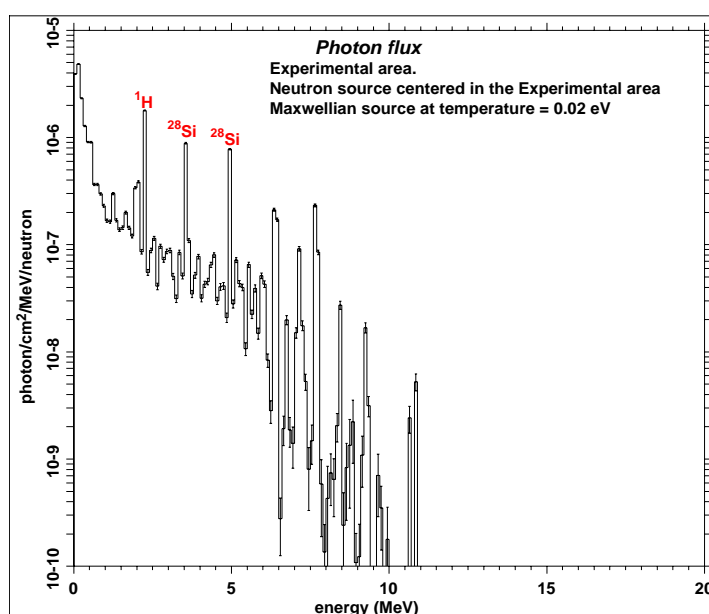
**Figure 4-10:** Energy spectrum of the photon flux produced by an instantaneous thermal neutron source placed in the centre of the n-TOF experimental area.

The second simulation assumes a thermal neutron source (kT=0.02 eV) in the centre of the experimental area. In this case the decay constant, both for the neutron and the photon fluxes, is approximately 2.9 ms, compatible with the second, long decay component observed in the experimental data. This corresponds to the time required for thermal neutrons to reach the walls of the experimental area. Since the probability for elastic scattering for thermal neutrons in concrete is 50 times larger than the capture probability, these neutrons can easily elastically scatter from wall to wall before being absorbed, resulting in the long decay component. This travelling implies longer (ms) time intervals.

Figure 4-10 shows the energy spectrum of the photon flux in the experimental area produced by this neutron source. It exhibits the same shape as in the previous full simulations of the experimental area with the high-energy neutron source. It should be noted that the spectrum of Figure 4-10 shows peaks which can be assigned to neutron captures on hydrogen and silicon, whereas the spectra simulated for the fast neutrons (Figure 4-8) exhibit additional contribution due to inelastic interactions at higher energies.

4.2.1. Summary and Conclusions.

Simulations of the neutron and photon background in the n_TOF experimental area produced by high-energy neutrons hitting the walls showed that the observed background in the C_6D_6 measurements could be attributed to the following mechanisms:

- A prompt background component in the neutron energy range above 1 MeV is due to γ-rays from inelastic scattering as well as to proton recoils in the scintillator.

- The high-energy neutrons are quickly thermalised (~100 μs) in the concrete walls and partially directly captured within 200 μs, dominating the background between 100 eV and 100 keV. A second, later component, which appears below 100 eV, could be due to scattering of these thermal neutrons across the experimental area where they are captured with a corresponding delay. Capture of these low-energy neutrons in the walls (and in any other material inside the experimental area) generates a photon flux that persists for several milliseconds after the arrival of the high-energy neutrons. The photon energy spectrum reaches more than 10 MeV and exhibits features of the predominant capture reactions on H, Si, K, Ca and Fe.

Yielding very similar time and energy distributions compared to the background measured with the C_6D_6 detectors, the above mechanisms may indeed be identified as the source of this background. However, this hypothesis must yet be confirmed by a quantitative evaluation of the neutron source strength produced outside the lead target, so that the simulated photon background can be directly compared with the experimental information.

4.3. MITIGATION OF THE BACKGROUND FROM THE EXTENDED SPALLATION SOURCE.

In the original n_TOF tube design, a very thick concrete wall was placed after the first reduction of the tube diameter (from 80 to 60 cm) at approximately 70 m from the lead target, closing completely the tunnel (sliding doors were proposed to enable the access along the tunnel). These walls could have made a significant reduction on the background due to neutrons and other particles produced outside the lead target, which travel through the right hand side of the n_TOF tunnel towards the experimental area. The exact position of this shielding is not relevant for this application, but the closer to the lead target the larger the expected reduction factor on the background.

Results from recent simulations with simplistic geometrical descriptions of n_TOF tunnel [13] show that by introducing a 3.2 m concrete wall at 10 m distance from the lead target would reduce the neutron flux at the entrance to the primary area by an average factor of ~50'000 (for a neutron energy spectrum similar to the spectrum of the flux at the entrance of the n_TOF vacuum pipe), with reduction factors slightly larger for the low energy neutrons (< 1 MeV) and smaller for higher energies (> 20 MeV). From this background reduction a factor of about 500 is obtained immediately after the wall, while the remaining factor 100 results from the dispersion on the neutron direction (originally parallel in the simulated source) by scattering. This second factor can be much smaller depending on the direction distribution of the neutrons reaching the shielding. The wall has to cover the complete cross section of the tunnel, but not necessary by a single wall. In this way the access along the tunnel would not be obstructed. Different parts of the transverse section can be covered at different distances along

the tunnel, as far as there is sufficient overlap between the covered areas and the distances of all the walls to the spallation area are still short (long distance to the experimental area).

Despite the promising results of these simulations, and because of the difficulties to make further interventions in the n_TOF tunnel, large safety margins should be taken on the design of these shielding walls. A design similar to the first collimator, with ~1 m iron (to disperse high energy neutrons) followed by more than 3m concrete should be considered as the first starting point for this shielding.

Finally it should be mentioned that, although there is little evidence concerning the influence of the polarity of the sweeping magnet on the observed background, the original design for shielding the deflected charge particles at the right hand side of the tunnel should be ultimately constructed.

5. THE DATA ANALYSIS.

5.1. CAPTURE MEASUREMENTS.

5.1.1. The Pulse Height Weighting Technique.

In the first two years of the n_TOF experiment the capture cross sections of several isotopes of interest for astrophysics and nuclear waste transmutation will be measured by using C_6D_6 photon detectors and the Pulse Height Weighting (PHW) technique. The PHW technique is based on, a) the use of low efficiency detectors (i.e. the C_6D_6 liquid scintillation detectors), such that only one γ-ray of the capture cascade is detected at a time, and b) the introduction of a weighting function for the energy deposited in the detector, which guarantees that the efficiency is proportional to the gamma-ray energy. In this way the cascade detection efficiency becomes proportional to the known cascade energy and independent of the multiplicity. This PHW is obtained from a set of detector response functions for different gamma-ray energies. The accuracy of the weighting function depends thus on the accuracy with which the gamma response functions could be determined.

In a previous study [20], we have shown that the detector response depends not only on the active detector volume, but is also very sensitive to the surrounding passive materials and in particular to the investigated sample itself. The determination of the γ-response functions can only be performed by means of accurate Monte Carlo simulations, taking into account the surrounding materials and the sample geometry. The precision of the obtained weighting function has to be verified by capture measurements on well-known resonances with different decay patterns (cascade energy and multiplicity) and using samples of various sizes. In this way the systematic effects of the PHW on the extracted cross sections will be diminished. In particular, the 1.15 keV resonance in ^{56}Fe, the 5.2 eV resonance in ^{109}Ag, and the 4.9 eV resonance in ^{197}Au are well suited for this purpose. These measurements have been part of the nTOF-2 experimental programme [1].

5.1.2. The Data Taking

During the week of June 4 to 11 a high intensity proton beam was available at the n_TOF spallation target consisting of 4 or even 5 bunches per PS supercycle. In spite of the unreasonable background level, it was decided to perform preliminary measurements on the PHW determination as a general check of the performance of our experimental set-up.

Two C_6D_6 detectors manufactured by Bicron with an active volume of 612 ml were placed at 90° with respect to the neutron beam direction very close to the "sample exchanger". The combined detection efficiency of both detectors was about 4 %. Figure 5-1 shows a view of the experimental arrangement. Two sets of samples were measured. One set had a sample diameter of 20 mm (smaller than the neutron beam size), and consisted of a 1.5 mm thick ^{nat}Fe sample and 0.2 mm thick ^{nat}Ag sample. The other set had a sample diameter of 45 mm (larger than the neutron beam size), and consisted of a 0.5 mm thick ^{nat}Fe sample and 0.1 mm thick ^{197}Au sample.

A total of more than 2.8×10^4 bunches with an average of 7.2×10^{12} protons were dedicated to measure the 1.5 mm Fe sample, and a total of nearly 4.4×10^4 bunches with an average of

6.8×10^{12} protons were dedicated to the 0.5 mm Fe sample measurement. This allowed to collect over 3×10^4 counts in the respective peaks corresponding to the 1.15 keV resonance. In the case of the Ag and Au samples about 1.6×10^3 proton bunches were enough to collect over 3×10^5 counts in the saturated peaks corresponding to the 5.2 eV and the 4.9 eV resonances, respectively.
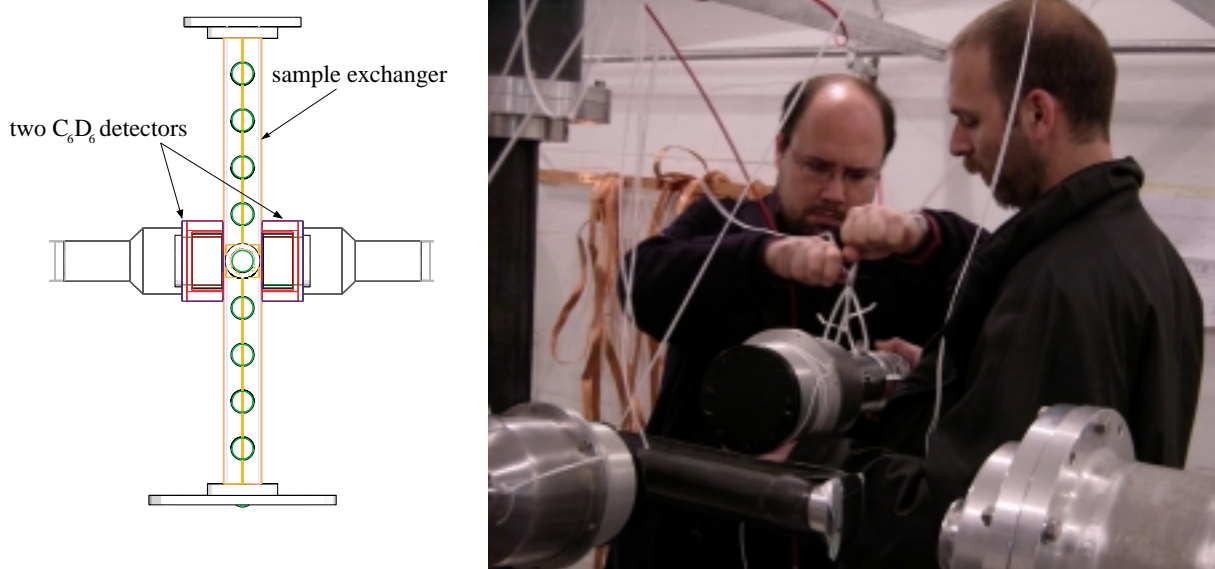

Figure 5-1: Schematic view of the experimental set-up with the two C_6D_6 detectors and the sample exchanger.

The photomultiplier anode pulses were digitised in steps of 2 ns with a FADC threshold of about 80 keV. The recorded waveforms for every proton bunch were stored at the CDR system for off-line analysis, yielding the relevant parameters as Time-Of-Flight (TOF), baseline, amplitude, pulse integral charge, time-of-flight, etc., which are then stored in the DST files. From these DST files convenient histograms, n-tuples, etc., are created to allow easy data handling.

5.1.3. Analysis, Monte Carlo simulations and results

The analysing routine searches for peaks in the zero suppressed flash ADC data and extracts the following quantities:

Amplitude:	Maximum height of the peak.
Baseline:	Averaged baseline for some channels before the peak.
Baseline variation:	Standard deviation of the baseline.
Charge:	Integral of the signal for first 16 ns.
Total charge:	Total charge of the peak.
TOF:	Time-of-flight determined by 30% of signal amplitude.
Pile up:	Indication flag for pile up [21].

The application of the PHW technique requires an accurate calibration of the energy deposited in the detector. The width of the detector resolution, assumed to be of gaussian shape, has to be experimentally determined in order to convolute the simulated response distributions. Both procedures were accomplished by matching the GEANT4 simulated detector response to the measured response for the ^{137}Cs and ^{60}Co calibration sources. Comparison of the simulated and measured spectra in Figure 5-2 shows that an instrumental width of the form $\sigma = 3 \cdot E$ allows

to reproduce the data adequately.
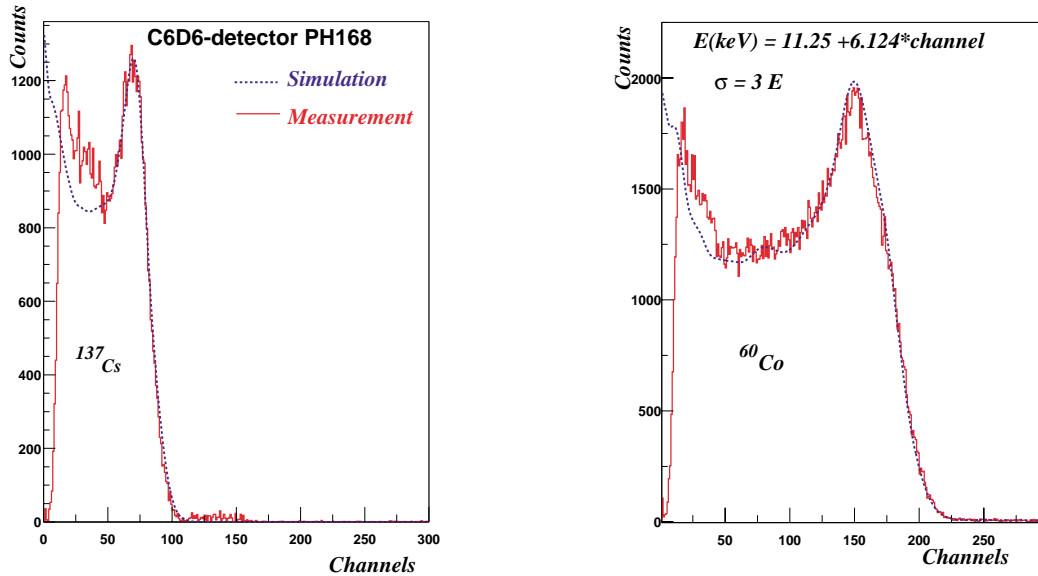
Figure 5-2: Energy and width calibration for one of the C_6D_6 detectors.

The geometry and materials of the experimental set-up (Figure 5-1) were carefully implemented in the GEANT4 simulations. The largest uncertainty in these simulations arises from the composition of the carbon fibre material of the "sample exchanger" and the vacuum chamber. A present simplification corresponds to the uniform distribution of the photons within the sample, which will be replaced, by the actual neutron beam profile distribution measured with the Micromega detectors.
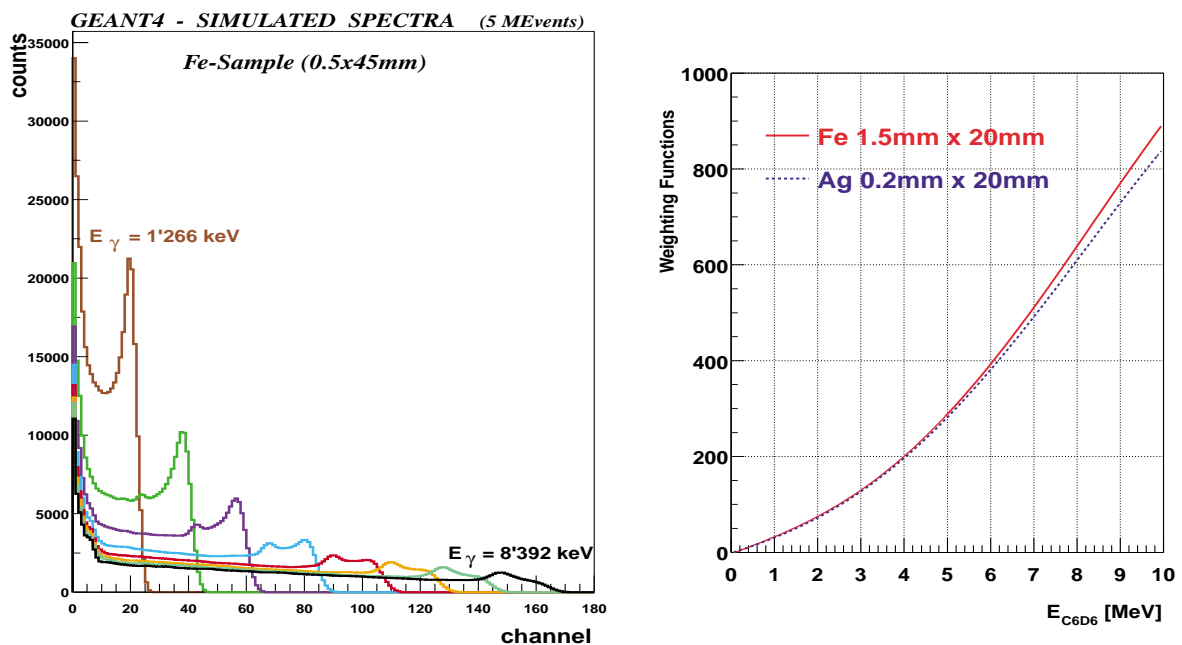
Figure 5-3: Example of the simulated gamma-ray response functions and of the deduced weighting functions.

Presently only eight photon energies between 1.26 MeV and 8.39 MeV have been simulated for each of the four samples considered. From the simulated response distributions (Figure 5-3) the weighting functions were parameterised as a fourth degree polynomial and are

obtained by the least squares method. In Figure 5-3 the PHW obtained for the small diameter Fe and Ag samples are also shown. It was demonstrated [22] that the MC uncertainty in determining the PHW is negligible in the capture measurements.

The determination of the C_6D_6 energy calibration and of the weighting functions allows to obtain the "weighted" capture spectra by processing the DST files. These spectra have then been analysed using the resonance analysis codes SAMMY [23]. In this analysis proper consideration has to be given to another important parameter of the neutron beam, namely the TOF resolution function.
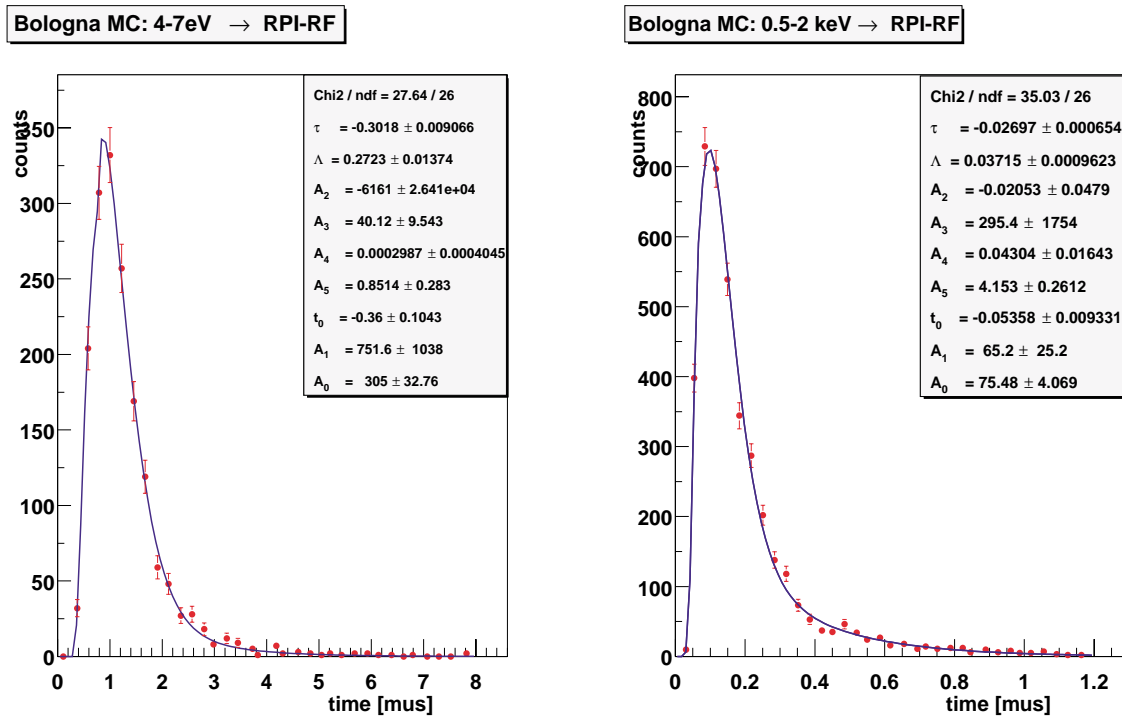

Figure 5-4: Result of the MC simulation for the target resolution function (red dots) and the corresponding fit for two neutron energies [25].

The Resolution Function (RF) describes the distribution of neutron time-of-flight leading to captures at a given resonance energy. At low neutron energies thermal Doppler broadening dominates, but in the keV region the resolution is mainly affected by the properties of the spallation target. This component is characterised by a long tail extending to large times, reflecting the different production-moderation histories of neutrons of a given energy.

In order to parameterise the RF in a form that can be handled by SAMMY we have analysed the results obtained from a Monte Carlo simulation of the spallation process [24,25]. The data available for neutrons of about 5 eV and 1.15 keV were fitted with the so-called RPI resolution function [23] and are plotted in Figure 5-4.

Figure 5-5 shows the weighted capture spectra in the region of the investigated resonances in ^{109}Ag and ^{56}Fe, measured with the small diameter (20 mm) samples and the fits obtained with the SAMMY programme. The well–known parameters of these resonances were kept fixed in the fit with the exception of the resonance energy, thus allowing a check of the neutron energy and TOF relation.

Fitted parameters were the global yield normalisation factor and the shape of the background, which at this stage was assumed to be constant. In the case of the 1.5 mm Fe

sample the multiple scattering contribution to the spectrum is clearly visible to the right of the resonance peak. This corresponds essentially to neutrons of higher energy, which after an elastic collision loose enough energy to match the resonance energy. This process is included in the SAMMY fit shown in Figure 5-5, leading to a very good reproduction of that part of the spectrum. Note also the rather good fit of the low energy tail of the resonance, which is only possible with the inclusion of the resolution function of the Pb target discussed before, thus confirming the information on this important parameter of the neutron beam. A more detailed RF study extending to higher energies will be performed in the future.
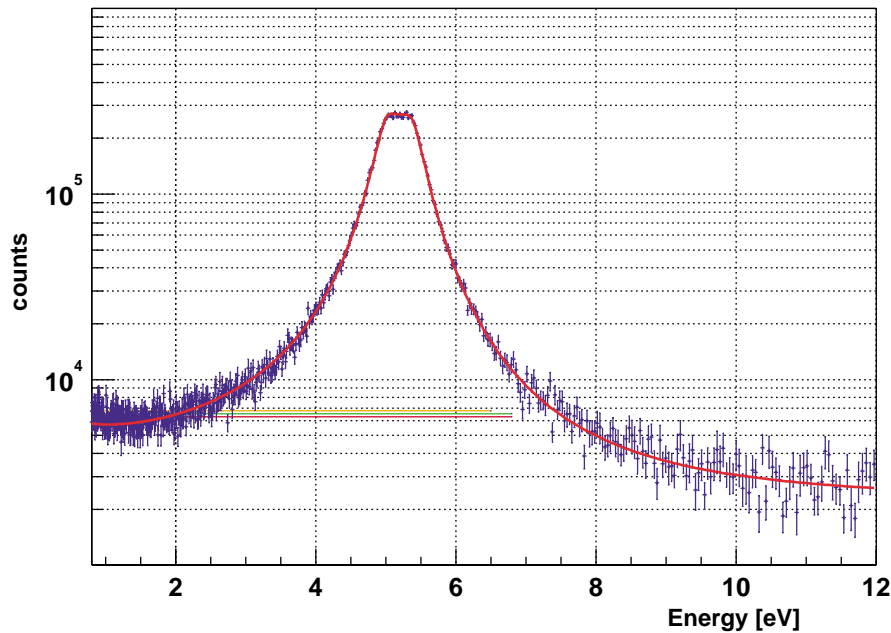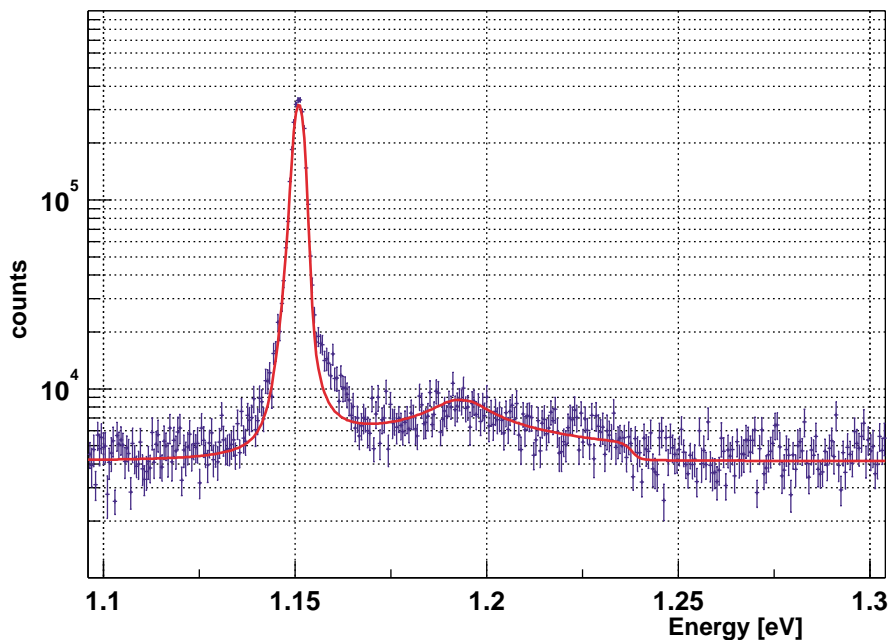

Figure 5-5: Weighted spectra and SAMMY fit for the Ag and the Fe resonance peaks.

In general a very good fit is achieved for both resonance peaks. The only remarkable

discrepancy appears at the right tail of the Fe peak. The origin of this feature, which may due to a background resonance, is under investigation. The accuracy of the weighting functions will be deduced from the consistency of the normalisation factors for both resonance peaks, which is at this stage outside of the purpose of this preliminary analysis. On the other hand, from the uncertainties and correlation of the fitted parameters - normalisation and background - it can be concluded that the required precision can be attained assuming similar statistics also for the future data.

5.2. CAPTURE MEASUREMENTS WITH THE C_6D_6 DETECTORS.

During the period (April 28 until June 11, 2001) of this report, six C_6D_6 detectors (four from BICRON and two from FZK) have been installed in the experimental area, but only two C_6D_6 detectors, one from FZK and one from BICRON with a modified photomultiplier base were actually used. These two C_6D_6 detectors were mounted at an angle of 90° with respect to the beam direction and at a distance of 5 cm from the centre of the sample (Figure 5-1).

5.2.1. Signal amplitudes.

Figure 5-6 (*left*) shows a histogram of the pulse height distribution for run 1758 taken with a ^{60}Co source in front of the detector. The cut at channel 5 corresponds to a γ-ray energy of about 70 keV.
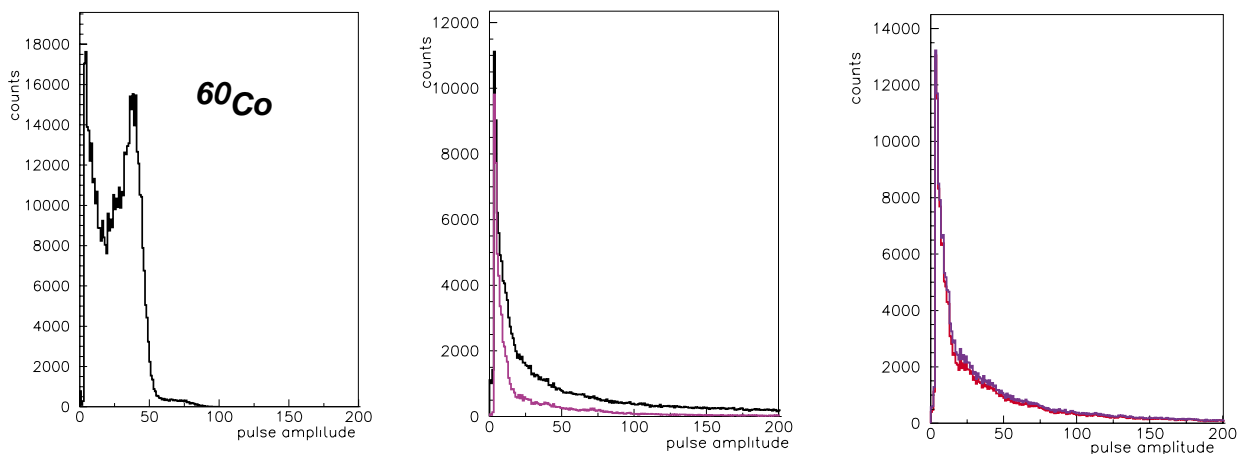
Figure 5-6: Pulse height spectrum taken with a ^{60}Co source (*left*). Pulse height spectrum taken in a n_TOF background run without sample (*middle*). Pulse height spectrum taken with a 1 mm thick gold sample (*right*).

The corresponding spectrum for run 1762, which was the background run without sample, is plotted as black line in Figure 5-6 (*middle*). Neglecting events just after the gamma flash (TOF<10 μs) yields the blue line, the reduction being due to the fact that most events in the background run originate immediately after the gamma flash. Figure 5-6 (*right*) shows the pulse height distribution with a 1 mm thick gold sample in the beam (run 1718). Applying the same TOF cut as described before (blue line) has little influence, since most of the events in the gold sample occur at later times (large resonance at E_n=4.9 eV).

While the photomultiplier base seems to recover immediately after the γ-flash (Figure 5-7), the baseline may exhibit instabilities induced by the γ-flash.
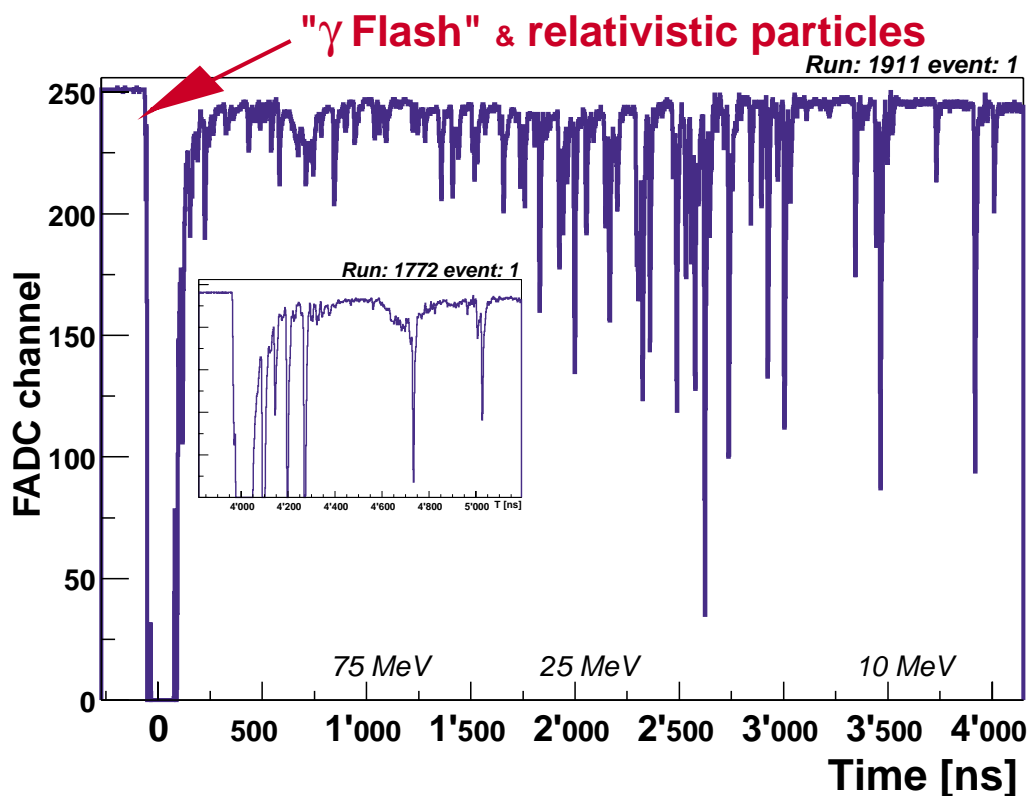
Figure 5-7: Two typical histories of the C_6D_6 signals immediately after the γ-flash.

However, shortly after the γ-flash these instabilities disappear, which means that the baseline remains well defined in the TOF range of interest for capture experiments, corresponding to neutron energies below 1 MeV, i.e. after the 16 μs following the γ-flash. This result is demonstrated in Figure 5-8 which shows the total background as a function of neutron energy (black line) together with a cut allowing only for events with baseline fluctuations of less than 1σ (blue line).
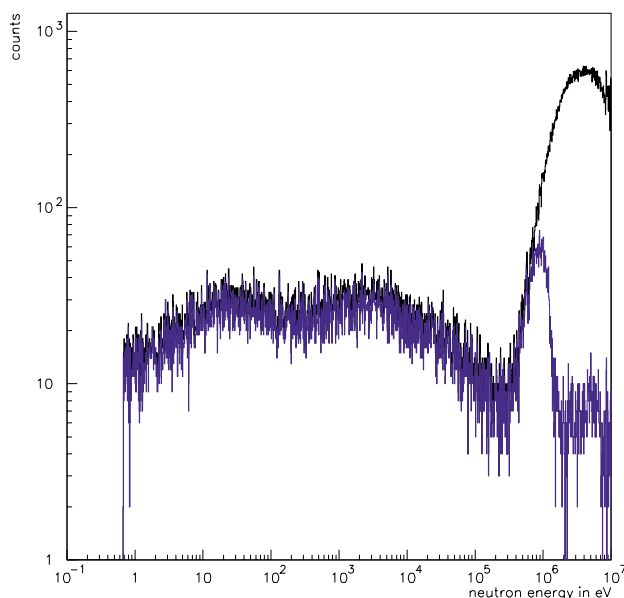
Figure 5-8: Background run without sample (black). Restriction to signals with undisturbed baseline (blue) illustrates that baseline fluctuations are correlated with the intense background at short flight times.

The integral over the signal (technically denoted as total charge) corresponds to the deposited energy in the detector and represents another relevant information that can be deduced from the raw data. In this mode saturation is smoothed out. Figure 5-9 shows the histograms of this variable for the runs discussed before. Again, a cut in TOF (TOF<10 µs) was applied for Figure 5-9 (blue lines) to illustrate the influence of the gamma flash.

Figure 5-9: Integrated signals from the n_TOF background run without sample (*left*) and with the gold sample (*right*). Events in the neutron energy range below 1 MeV (blue) differ from the full spectrum.
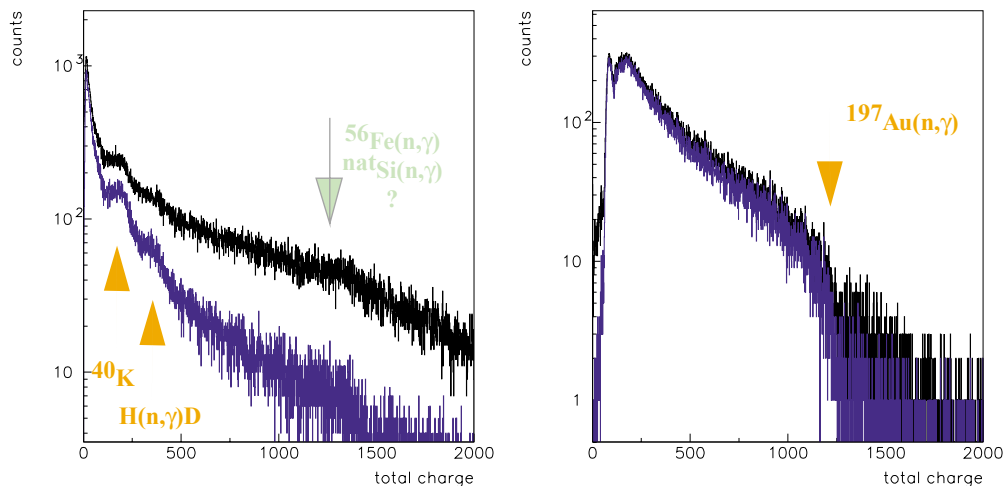
The background spectra in the left panel of Figure 5-9 are the experimental counterparts of the simulated data shown in Figures Figure 4-8 and Figure 4-10. The features due to the ^{40}K line as well as the γ-rays from neutron captures on hydrogen can be clearly identified.

It should be noted that the background spectrum (Figure 5-6 and Figure 5-9) extends to much higher gamma energies than the spectrum taken with the gold sample, which is essentially confined to the range below 6.6 MeV corresponding to the binding energy of the captured neutron. Even with a cut for flight times greater than 19 µs (equivalent to a neutron energy of 500 keV) this background contains a sizeable component at high energies, which may be a hint that a considerable part of this background could be due to capture of ambient neutrons in the experimental area.

In the runs with the gold sample as well as in the background run the fraction of pile-up events is of the order of 2 to 4 percent. Since most of these events occur immediately after the γ-flash when the count rate is very high, its impact for the energy range of interest for capture measurements is negligibly small.

In view of the count rate and baseline oscillations problems at short TOF outlined above, any further capture analyses are restricted to neutron energies below 1 MeV, where the C_6D_6 detectors are operating under clean conditions.

5.2.2. Background measurements

The analyses presented in this section are dealing with various background sources and their effect on the n_TOF measurement program for neutron capture cross sections. In particular, the cuts were applied on the measured data in order to exclude events with negative or small total charge, mostly caused by noise and signals affected by baseline variations and by the γ-flash [26].

GOLD SAMPLE AND RELATED BACKGROUND

The background spectrum versus time of flight measured without sample in the beam is shown in Figure 3-16 on a neutron energy scale after rebinning and normalisation to the intensity of a single proton pulse.

Additional measurements were performed on two different gold samples, one with 20 mm diameter and 1 mm thickness (sample mass = 5.9 g) and one with 45 mm diameter and 0.1 mm thickness. Figure 5-10 (*left*) shows the measured spectrum for the 1 mm thick sample (red) compared to the expected spectrum constructed from the evaluated reaction rate (blue). In Figure 5-10 (*right*) the measured background spectrum without sample (Figure 5-8) has been added to the expected spectrum.
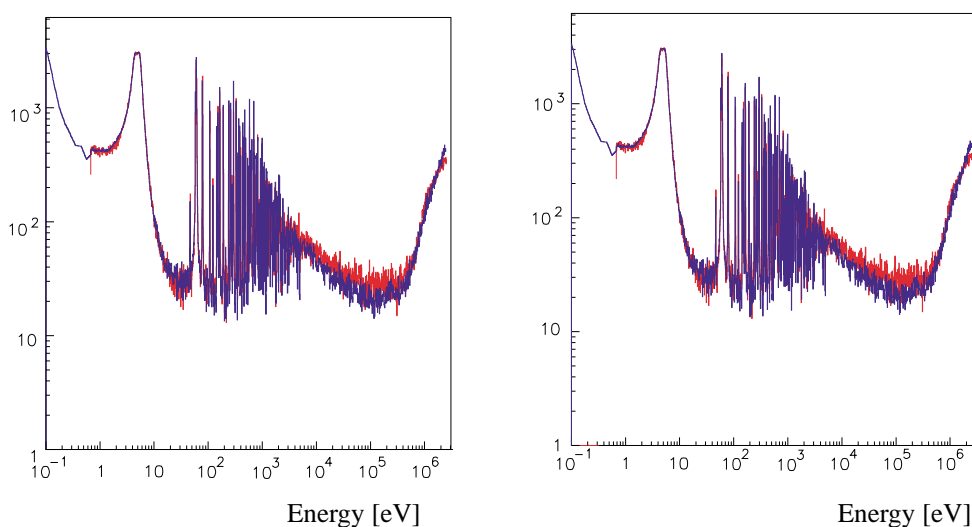

Figure 5-10: Experimental spectrum from a 1 mm thick gold sample (red) compared to the expected effect constructed from the cross section and the simulated flux (blue). The spectra are normalised via the strong resonance at 4.9 eV (*left*). Same as the left spectrum, but in this case the measured background (Figure 5-8) has been added to the expected spectrum (*right*).

Obviously, summation of the expected capture yield and the background measured without sample is in fair agreement. This means, however, that the effect of sample-scattered neutrons is not the dominant background contribution, although the simulations predicted this component to dominate the ambient background.

On the expanded scale of Figure 3-8, the background situation for the 0.1 mm thin gold sample is illustrated in more detail. While there are comparably small differences between the hypothetical spectrum based on the evaluated cross section (black) and the predicted spectrum including the simulated backgrounds (blue), the present situation (red) is far from being satisfactory. The measured background between resonances obviously exceeds the simulated background (including the effect of sample scattered neutrons) by almost two orders of magnitude. This excessive background has the most severe consequences for the approved cross section measurements TOF-03 and TOF-04, where the expected signal/background ratios are much smaller than for the example of Figure 3-8.

The dominance of the ambient background over the sample-related background represents a strong contradiction to the situation obtained in detailed Monte Carlo simulations based on the original concept for the n_TOF neutron beam line.

LEAD AND CARBON SCATTERING SAMPLES

This severe problem has been investigated in more detail by using carbon and lead samples. A 6.5 mm thick C and a 1 mm thick Pb sample were used to study the background due to neutron scattering in the sample. The Monte Carlo simulations suggested that this component should dominate the overall background seen by the C_6D_6 detectors even for small samples. Therefore, a massive effect was anticipated for the comparably thick samples chosen. The results of the TOF measurements on the C and Pb samples are compared in Figure 5-11.
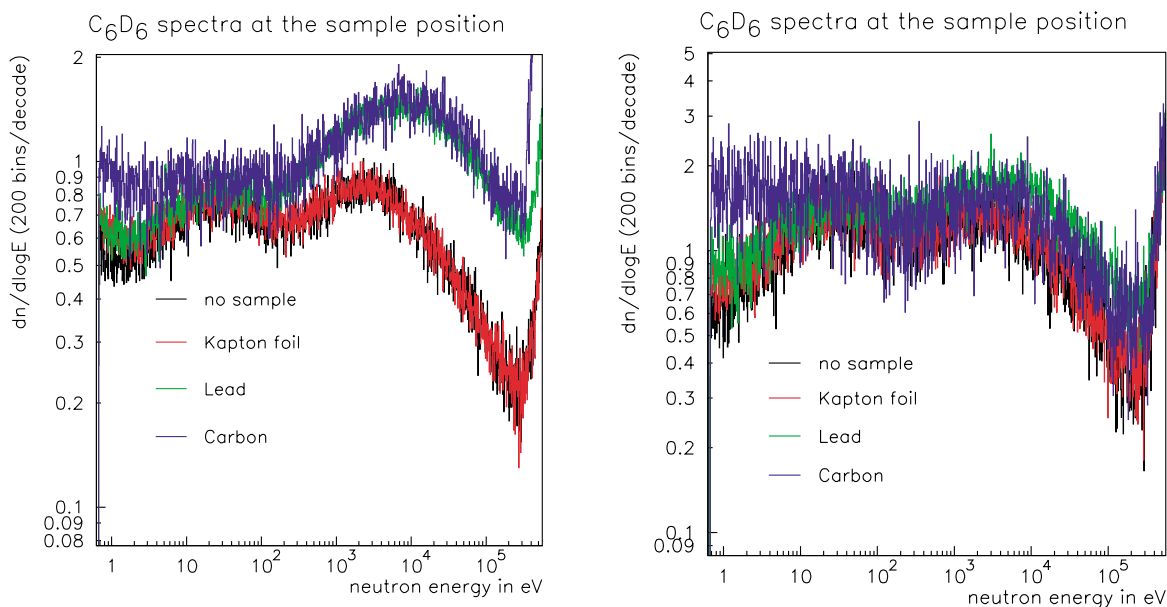

Figure 5-11: Comparison of measured background spectra with and without scattering samples (*left*). Same as the left spectrum after application of pulse height weighting (*right*). Even for the massive scattering samples used, the ambient background is by far dominant.

Figure 5-11 (*left*) shows the measured spectra for no sample (black), a thin Kapton foil (red), a 1 mm thick Pb (green) sample and a 6.3 mm thick carbon sample (blue). Figure 5-11 (*right*) displays the experimental spectra after application of a linear weighting function to approximate the situation expected in later measurements of (n,γ) cross sections. This operation, which gives less weight to low-energy γ-rays, indicates that part of the spectrum must be comparably soft. This was also demonstrated by putting a 5 cm thick lead shield around the detector as demonstrated in Figure 5-12. In any case, the background seems to show at least two components, the soft part being sensitive to pulse-height weighting and a hard component, which is little affected by the weighting, and looks to be independent of the presence of any sample on the beam.

In contrast to the expected effect after application of the weighting function, the spectra obtained with the carbon (blue in Figure 5-11) and Pb samples (green) show no significant difference compared to the spectra taken without any sample (black) or with only a very thin Kapton foil in the beam (red). This provides additional strong evidence that the present background is much too high.

The spectrum taken with the lead sample shows another interesting feature. The zoom on the low energy part of this spectrum in Figure 5-13 shows a small resonance at 4.9 eV. This effect could originate from neutrons scattered in the lead sample but captured in a gold sample,

which was mounted on a neighbouring position of the sample changer at a distance of 10 cm. The comparison with the corresponding resonance in the gold spectrum of Figure 5-10 shows that the probability for this cross talk can be significant and has to be considered in later experiments by leaving enough space between samples with large scattering probabilities. Note that this effect was never observed in spectra taken without sample (see also Figure 3-13).
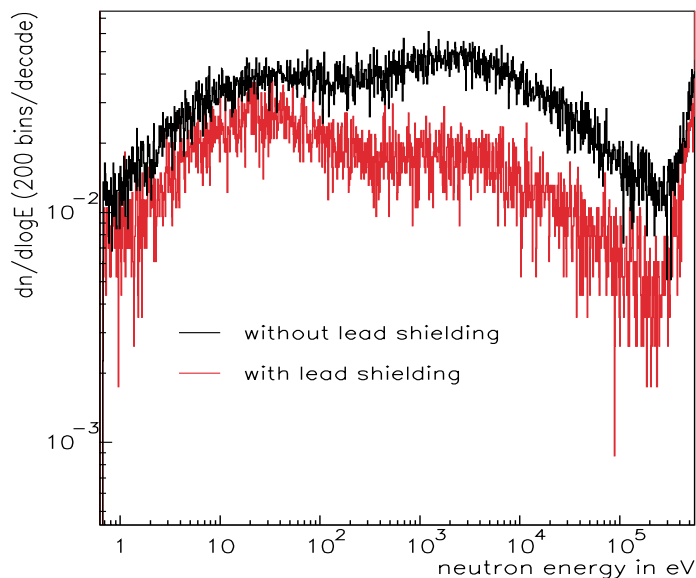
Figure 5-12: Measured background with and without 5 cm lead around the detector.
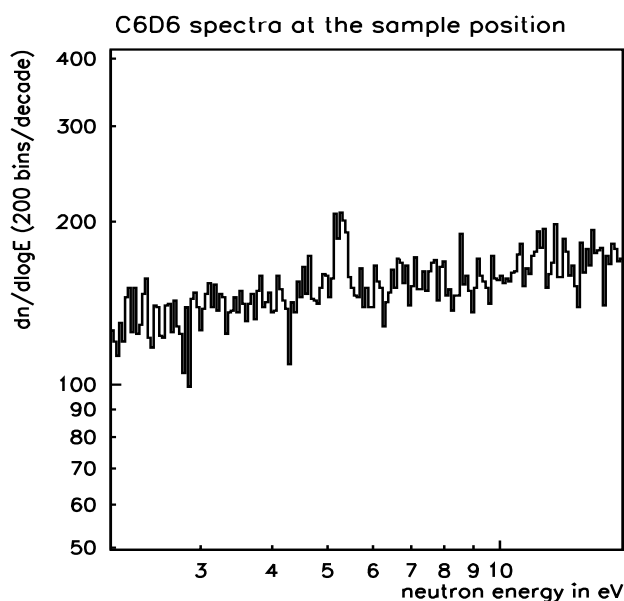
Figure 5-13: Background spectrum taken with the Pb sample showing the 4.9 eV resonance from the gold sample, which was mounted on the neighbouring position of the sample ladder.

5.2.3. Comparison to other neutron facilities.

We have compared our 100 μm Au sample measurement with the 50 μm Au sample measurement [10] performed at GELINA. In the eV region the background of the n_TOF measurements is comparable (10-20% higher) to the GELINA background, but in the keV

region the n_TOF background is 8 times larger.

The TOF spectrum of a similar gold sample taken with the Oak Ridge set-up [11] of two C_6D_6 detectors could also be used for comparison. Figure 5-14 shows zoomed parts of the TOF spectra from Oak Ridge (black) and their n_TOF counterparts (red). Obviously, there is excellent agreement in the resonance positions, thus confirming that data acquisition and analysis are working properly. Since the resolution at these energies is still determined by Doppler broadening the resonance widths are in perfect agreement. The superior resolution of the n_TOF data starts to show up only at higher energies but can not be demonstrated at the gold spectra since in this case the level density is so high that the resonances overlap already before this energy regime is reached.

The second interesting aspect concerns the background level. Note that the sample used at n_TOF was twice as thick as in the Oak Ridge measurement. For a fair comparison, the n_TOF background spectrum should hence be multiplied by this factor of two.
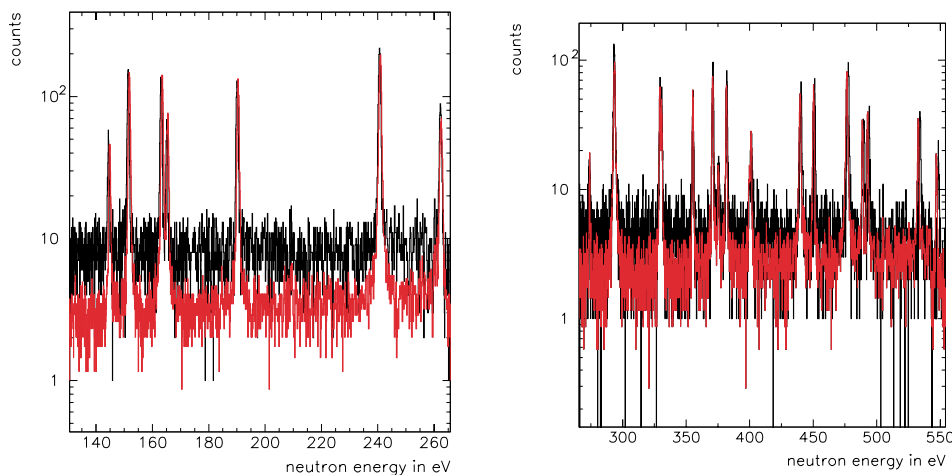
Figure 5-14: Different sections of a gold spectrum measured at n_TOF (red) compared to a corresponding spectrum taken at ORELA (black). Since the sample thickness differed, the n_TOF background has to be multiplied by a factor of two.

5.2.4. Conclusions from the capture measurements using C_6D_6 detectors.

The present results of the C_6D_6 measurements of the first n_TOF campaign were carried out with particular emphasis on background problems. The results can be summarised in the following points:

- Under the actual experimental conditions the C_6D_6 detectors are working well as expected. They exhibit the clear signal shapes on a clean baseline necessary for application of the pulse height weighting technique and for achieving good TOF resolution.
- Backgrounds are still a crucial problem. The information collected in a series of measurements indicates that backgrounds are about 50 times larger than expected from simulations. Possible additional background mechanisms have been discussed and have been be verified by further simulations (see chapter 4). Although n_TOF should have a clear advantage with respect to the background due to its unique combination of a 4 times longer flight path and a 50 times lower duty cycle, comparison with existing facilities yields in fact only similar conditions.
- The resolution in neutron energy is as anticipated, but the superior performance of n_TOF will be more obvious at higher energies, where suited examples have yet to be illustrated.

5.3. FISSION MEASUREMENTS.

The **P**arallel **P**late **A**valanche **C**ounters (PPAC) built at IPN-Orsay have been used in detecting the neutron induced fission reaction on the isotopes ^{235}U, ^{238}U and ^{209}Bi. All twelve constructed detectors fully equipped with preamplifiers, delay lines and electronics, are operational, as well as their gas regulation system complying with CERN's safety regulations. The aluminium support designed to hold the detectors and the samples has already been employed. A new less cumbersome aluminium chamber with significantly less material has been designed and is presently under construction.

For the period of this report only five detectors and three samples have been used, i.e. ^{235,238}U and ^{209}Bi with surfaces of 1.7 cm^2 and 10 cm^2 and a thickness of 100μg/cm^2 and 300 μg/cm^2 respectively. We applied 550 V between the electrodes and maintained the pressure of the isobutane gas at 6.6 mbar. The detectors were connected to 25 channels of the ACQIRIS 500 Ms/s FADC system.

The anode signals were analysed using a peak extraction method to obtain the proper parameters, e.g. the arrival time and the amplitude of the signals. The peak position corresponding to the arrival time was determined by a cubic fit of the signal form and by considering a threshold of 100 mV. Since the information on the exact time of a fission event provided by the cathode signals is essential for the fission programme, we are developing a more sophisticated method of signal analysis, which is presently tested.

Fission leads to two simultaneously emitted fragments, which are detected by the two anode planes of a PPAC detector within a time interval of 3 ns. The results presented in this report are obtained by analysing the anode signals only. In the future the improved localisation of the fission tracks by means of the delay line technique will allow extracting the angle between the fission product trajectory and the target symmetry axis. The corresponding signals have been found as expected, i.e. anode signals of 10 ns width and 300 mV average amplitude, and the respective cathode signals of 30 ns width and 150 mV amplitude. By setting the coincidence window to 3 ns, we can eliminate the cross-talk between detectors, i.e. the observed events can unambiguously assigned to each sample.
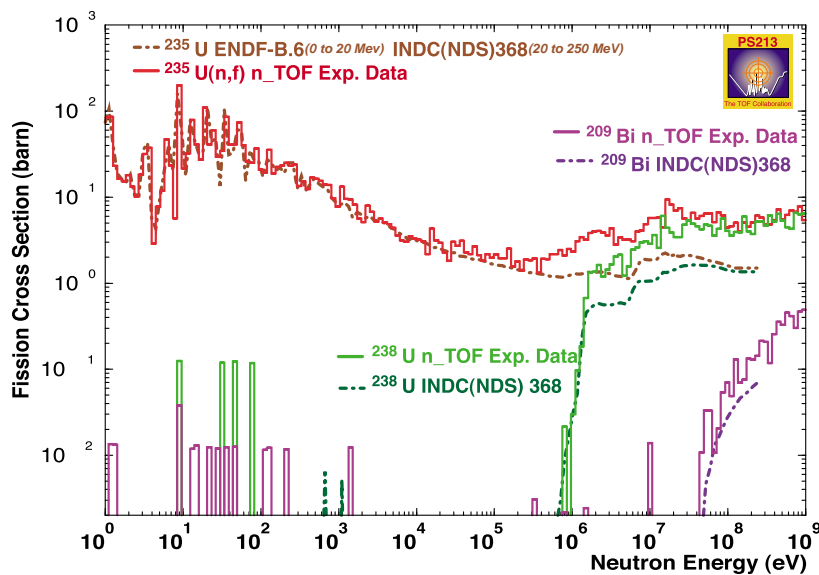

Figure 5-15: Comparison between experimental data for ^{235}U, ^{238}U and ^{209}Bi with evaluated cross sections.

5.3.1. Preliminary Results.

Preliminary fission cross sections between 1 eV and 1 GeV were calculated using the neutron flux from the Technical Report [2], the dimension of the collimators and the number of atoms per sample.

As shown in Figure 5-15 the fission thresholds of ^{238}U at 1 MeV and of ^{209}Bi at 30 MeV were correctly reproduced. These experimental results were compared to the ENDF-B6 database between 0 and 20 MeV and to INDC database at higher energies. While there is good agreement at low energies, we observed discrepancies above 100 keV. One of the possible explanations for this difference could be an energy dependence of the beam shape, which shows up in the simulations and in measurements with the Micromega detector.

In order to check the quality of the measurement at low energies, the ^{235}U counting rate is shown in Figure 5-16 as a function of energy between 8 eV and 20 eV. The achieved energy resolution is excellent, but needs to be confirmed at higher energies where the influence of Doppler broadening is less important. The peak-to-valley ratio seems to be larger in the experimental data, which would confirm the expected good resolution at n_TOF as well.
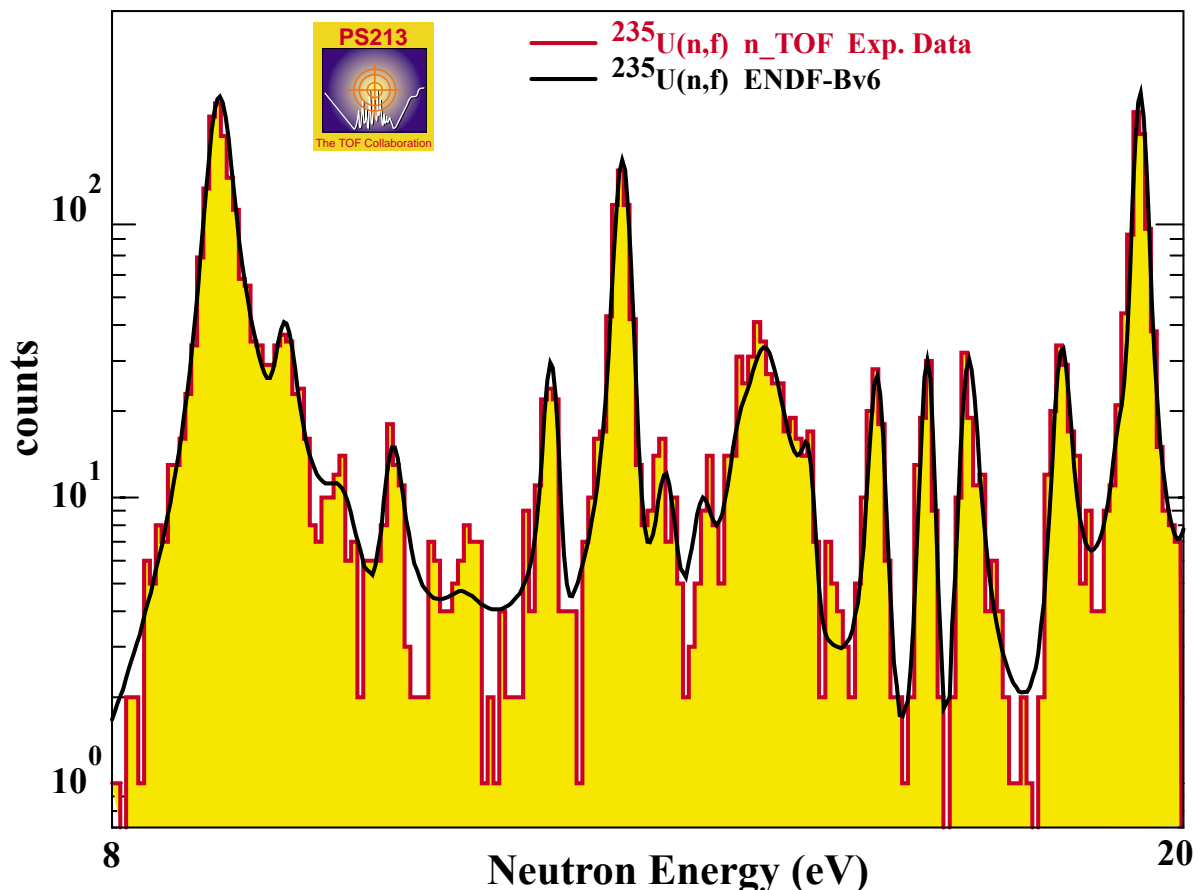

Figure 5-16: The measured fission yield of ^{235}U compared to evaluated data in the energy range from 8 to 20 eV. Note the logarithmic energy scale.

5.3.2. Preliminary Evaluatution of the Neutron Flux.

We have evaluated the neutron flux under the assumption that the adopted cross sections from the data bases ENDF/B-6 and INDC between thermal energies and 200 MeV are correct.

The results, presented in Figure 5-17, are given per cm^2 since the uranium targets were smaller than the beam size.
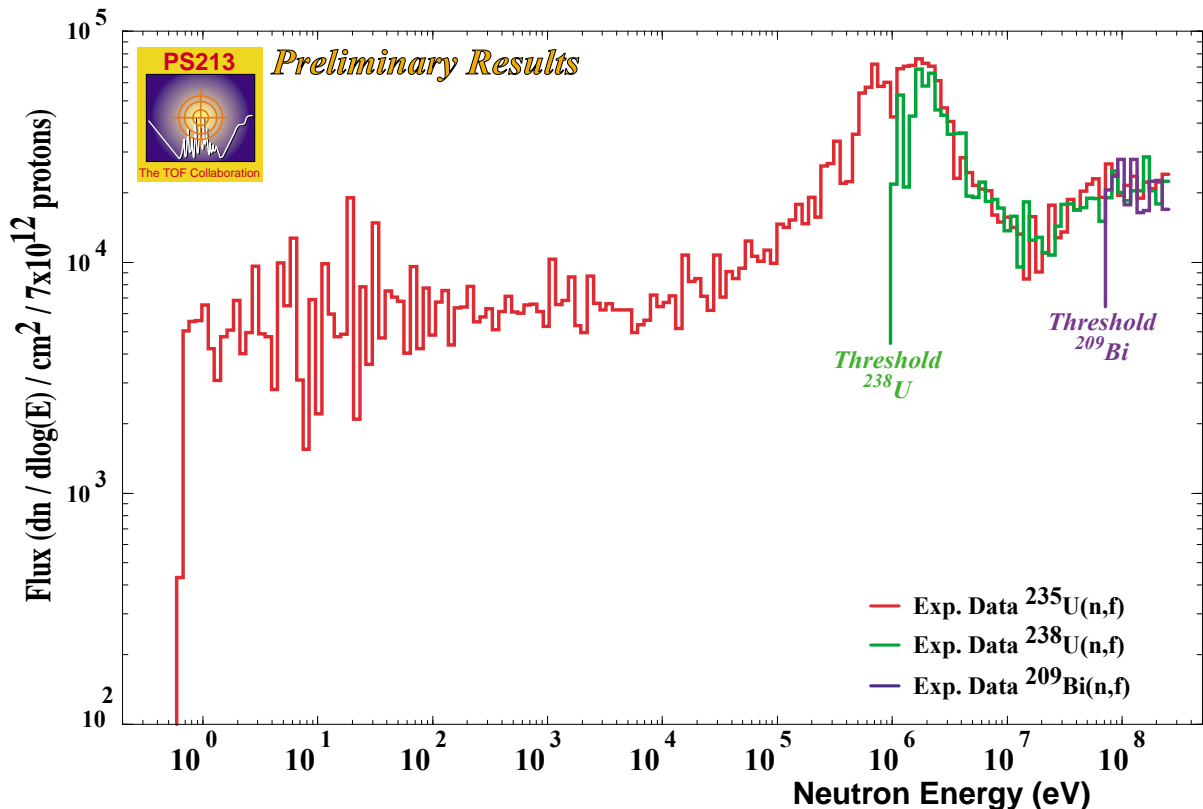
Figure 5-17: Neutron flux measurement from 1 eV to 400 MeV based on the fission data taken with PPACs and using ^{235}U, ^{238}U and ^{209}Bi samples.

5.3.3. Conclusion

This preliminary analysis illustrates the excellent performance of the PPACs during the test period at n_TOF: superb time resolution, negligible backgrounds, and reliable operation over the total neutron energy range from 1 eV up to 400 MeV.

Further improvements concerning the position information by a more detailed extraction method are presently being prepared and will allow identifying fission events more precisely. The analysis of the run without target is to be completed and we also will elaborate a beam profile from the data taken with the ^{209}Bi sample, which was larger than the beam.

In summary, we find that the PPACs are ready to start fission cross section measurements with targets relevant for the thorium cycle. Compared to the test runs performed so far we expect to improve the count rates by a factor 100. This can be achieved by using a larger beam diameter of 8 cm and by investigating six samples of 300 µg/cm^2 thickness simultaneously.

6. DETECTION OF THE Ar, Kr AND Xe PRIMARY SCINTILLATION LIGHT WITH NOVEL PHOTOSENSITIVE GASEOUS DETECTORS.

6.1. INTRODUCTION

The detection of primary scintillation light in combination with the charge or the emission of secondary scintillation is an efficient technique to separate particles and photons in large mass **T**ime **P**rojection **C**hamber (TPC) detectors filled with noble gases, condensed or not. This technique allowing a powerful neutron and photon separation represents a major improvement of the liquid noble gas calorimeter prototype to be tested in the n_TOF experiment. Moreover, the detection of this scintillation light permits to precisely determine the time of arrival of each event, the so-called "t=0" of the event.

This method is based on the simultaneous measurement of ionisation and direct scintillation light from the noble gas. While electrons and photons produce roughly the same number of ionisation electrons and scintillation photons, recoils from heavy particles are strongly suppressed by columnar recombination, while scintillation persists though at somewhat lower level. Therefore recoil events will be characterised by scintillation with essentially no associated primary ionisation.

The most important challenge of a liquid Ar/Xe TPC is the detection and processing of both signals, the primary scintillation and the charge signal produced by drifting primary electrons on a system of wire electrodes immersed in the liquid. The charge multiplication around these electrodes was extensively investigated [27].

Instead of the charge signals, the secondary scintillation light can also be used, which is generated in the region of strong electric fields inside the liquid or outside in the case of the double-phase detectors, where a gas layer is interposed between the liquid phase and the detection devices. In such detectors the ionisation electrons have been actually extracted from liquid into gas with the help of an appropriate electric field (>1 kV/cm) and multiplied in the gas by a wire. In this way, even a few electrons, produced in the liquid, once extracted in the gas, can be detected unambiguously. In particular the luminescence light produced by the electron multiplication process near the wire is detected as additional light, but arriving after a delay because of the drift time in the liquid and in the gas. Single pulses recorded by the photosensitive detector constitute the signature of neutron recoils in the calorimeter module and double pulses represent events due to photon interactions.

The advantage of this approach is that it gives a powerful method for particle separation, because the ratio of these two signals depends on energy and other characteristics of the particles or photons [28]. Earlier, expensive photomultipliers (PMT) with VUV transparent windows were mostly used for the detection of the primary scintillation light [27,28,29].

The first step towards the construction of this liquid Ar or Xe calorimeter module was to demonstrate that costly photomultipliers could be replaced by cheap novel photosensitive gaseous detectors, e.g. wire counters, GEM[9] or glass capillary tubes coupled with CsI photocathodes. We named this device gaseous photomultiplier or GPM. They have similar quantum efficiency as vacuum PMTs, but in contrast to them they are cheap, compact, can be

---

[9] **G**as **E**lectron **M**ultiplier.

manufactured with large sensitive area, are position sensitive and insensitive to magnetic fields. GPM with CsI and other solid photocathodes show advantages with respect to ordinary photosensitive gaseous detectors due to their good time resolution and the possibility to work at low temperatures [30,31].

We performed systematic measurements with Ar, Kr and Xe gas at pressures in the range of 1 to 50 atm as well as some preliminary measurements with liquid Xe and liquid Ar. With the gaseous detectors we succeeded to detect scintillation light produced by 22 keV X-rays with an efficiency close to 100%. We also detected the scintillation light produced by beta particles depositing 5 keV energy with an efficiency close to 25%.

The successful detection of scintillation light from 22 keV γ's opens new experimental possibilities not only in neutron experiments, but also in neutrino experiments and WIMP searches through nuclear recoil emission.

The experimental setup was a scintillation chamber separated by VUV transparent windows from the GPM and the PMT as sketched in Figure 6-1. For some measurements the separation window between the chamber and the GPM has been removed. Radioactive ^{241}Am, ^{109}Cd or ^{60}Sr sources could be placed inside and a ^{57}Co source outside the scintillation chamber. The scintillation chamber could handle highly purified noble gases, i.e. Ar, Kr or Xe, at pressures up to 50 atm or in liquid phase.

Three different types of GPM were used [32,33,34,35,36]: a single wire counter coupled to a CsI photocathode, double GEM and capillary tubes operating in tandem [33], and a combination of GEM and capillary detector, named as optimised GMP.
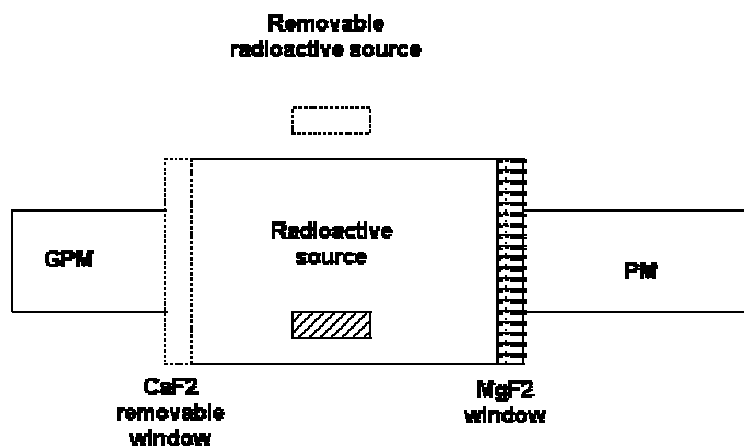
Figure 6-1: Schematic drawing of the experimental setup.

6.2. DETECTORS WITH WINDOWS, OPERATING IN QUENCHED GASES.

6.2.1. Results with single wire counters.

The GPM quantum efficiency was determined by detecting the primary gas scintillation of alpha particles from an ^{241}Am source. The detector was calibrated with photons from a ^{55}Fe source [32,33], each X-ray photon producing ~220 primary electrons inside the GPM. The scintillation light of the alpha particles released from the CsI photocathode approximately 200, 100 and 20 primary electrons for the case of Xe, Kr (Figure 6-2) and Ar, respectively. The deduced CsI quantum efficiency amounts to ~20% at 175 nm. The detection probability for the

22 keV X–rays of the Cd source was measured to ~100% in Xe, ~50% in Kr and ~10% in Ar.

In order to estimate the detection efficiency for the scintillation light produced by minimum ionising particles we used the beta radiation from a ^{90}Sr source. Typical signals and the pulse height distribution are shown in Figure 6-3. The estimated detection efficiency for minimum ionising particles is ~25%.
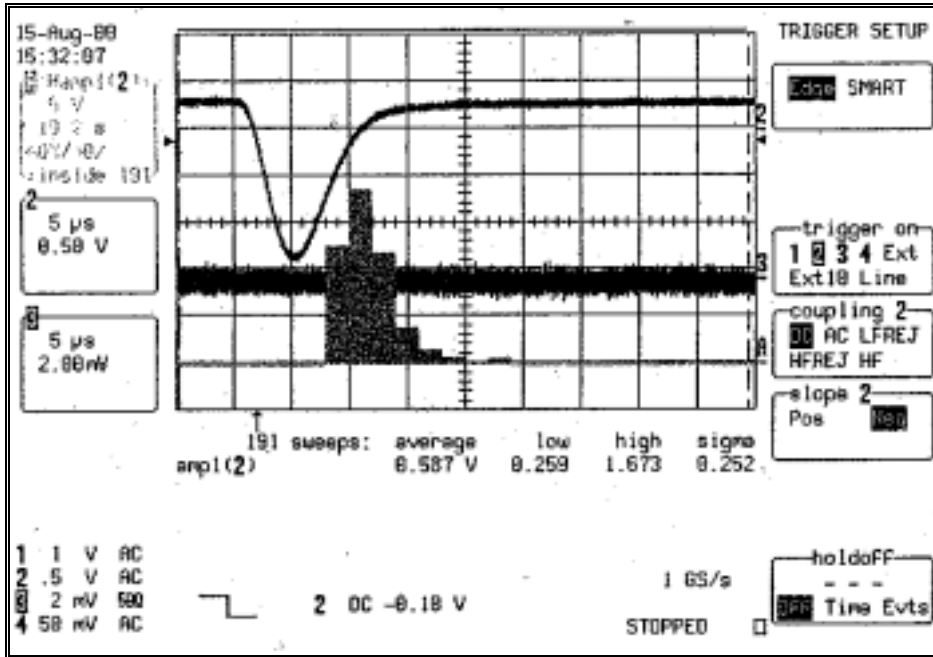
Figure 6-2: Oscilloscope photograph of the signals from the GPM (the upper beam) and the PMT (the middle beam) in the case of the detection a primary scintillation light produced by 22 keV X–rays in Kr at a pressure of 1 atm. A pulse-height spectrum is also shown (the lowest beam).

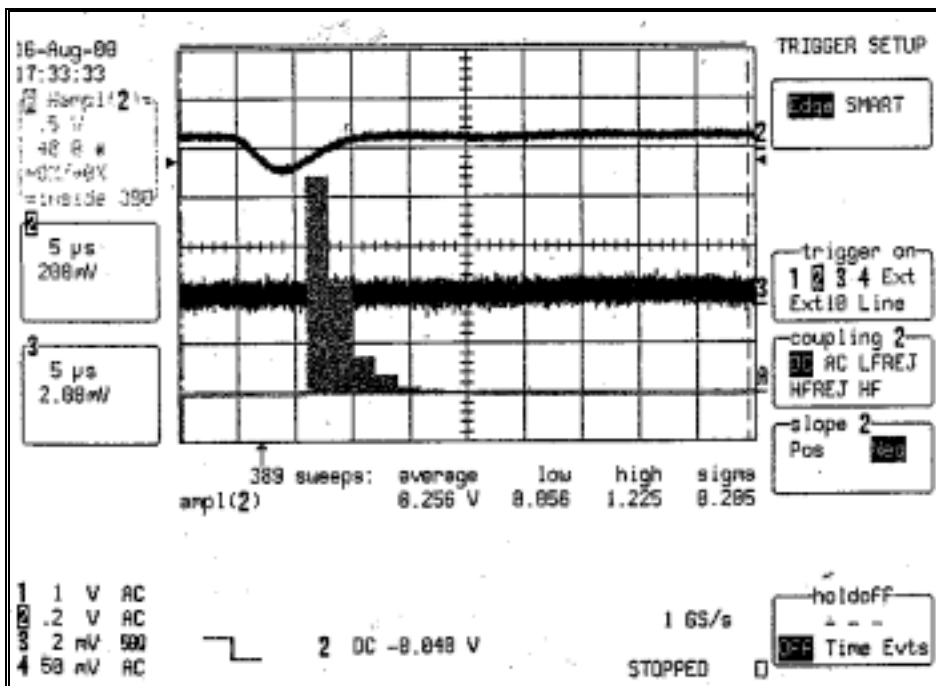**Figure 6-3:** Oscilloscope photograph of the signals from the GPM and the PMT in the case of the detection of the primary scintillation light produced by beta particle with 5 keV energy deposited in the Xe, at 1 atm.

Figure 6-4 shows the intensity of the primary scintillation light as a function of the Xe density. For the case of liquid Xe, the signal drops by only a factor of two as compared to the gaseous Xe at 1 atm.
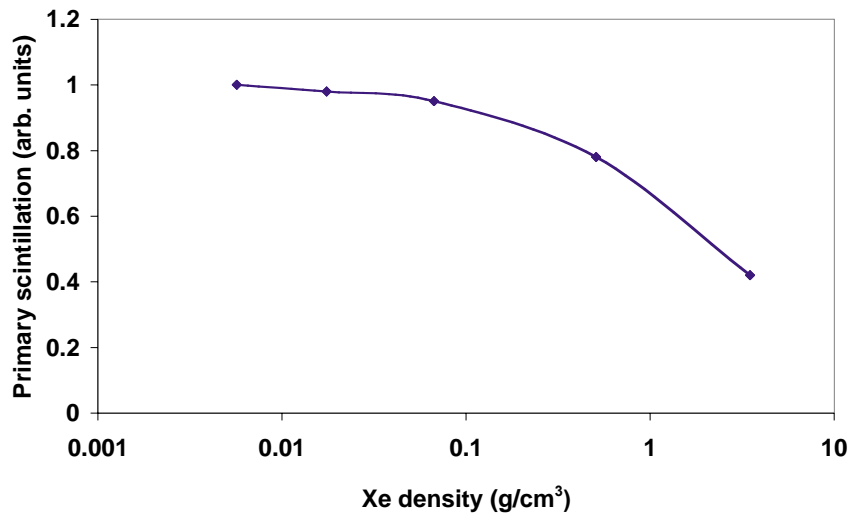
Figure 6-4: The intensity of the primary scintillation light (produced by 30 keV photons) as a function of the Xe density. Note that in the case of liquid xenon a 60 keV source was used.

6.2.2. Results with GEM and capillaries

Intense efforts by several groups are presently underway for developing micropattern detectors in combination with solid photocathodes [37,38].

The operation of double GEM and double capillary plates, combined with a CsI photocathode, has been tested [33]. The obtained results for the primary scintillation light produced by α's indicated that the total gain of the micropattern detectors was lower by an order of magnitude (Figure 6-5) and the detection efficiency by a factor of 3-4 [34] compared with the single wire counter.

Figure 6-5: Gain of double-step GEM operating at 1 atm (P10 gas) without CsI coating (*blue*) and with CsI coating (*red*).

Therefore, in the case of a detector configuration with window, the micropattern detectors do not offer any advantage compared to single-wire counter, especially for applications in TPCs where there is no need for extremely high position resolution.

6.3. *WINDOWLESS DETECTORS OPERATING IN PURE NOBLE GASES.*

In order to increase the detection sensitivity, the TPC should operate in the charge multiplication mode. Charge multiplication in pure nob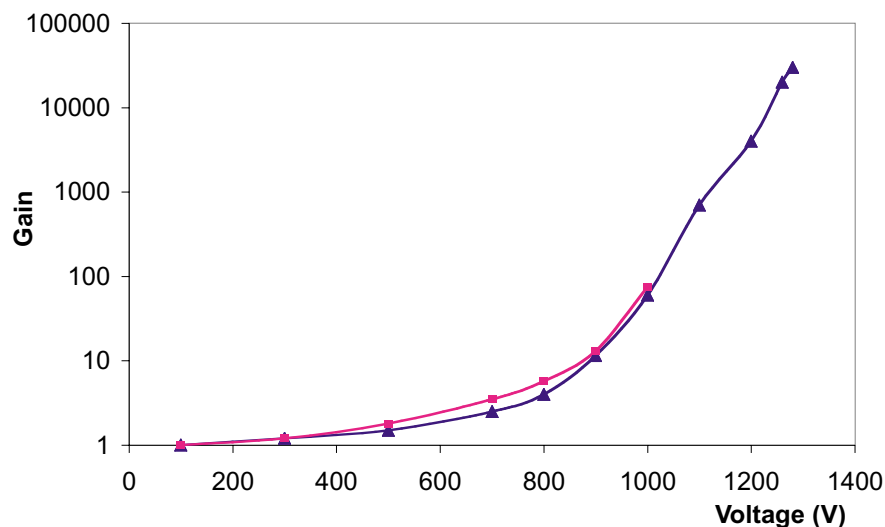le liquids or gases is difficult and therefore the use of secondary scintillation light was suggested. This secondary scintillation light is produced in the vicinity of the electrodes in both the liquid and the gas phase. For the detection of primary or secondary scintillation light in the case of double-phase detectors, it would be convenient to use windowless detectors. In this application the micropattern detectors may have advantages because they can operate in pure noble gases, since the photon feedback is geometrically blocked.

6.3.1. Windowless GEM and capillary tubes

The obtained results are summarised as follows:
- All detectors worked in pure noble gases, however two or more steps of multiplication were required for achieving gains above 10^3 [34], making thus the detection system too complicated.
- Due to the constraint on the maximum allowed total charge in the avalanche before a break-down appears [35], the dynamic range of the multistep configuration is restricted and the TPC has a reduced sensitivity.
- The detection efficiency of the windowless GPM was measured with the primary scintillation produced with alphas. In Ar, the detection efficiency was 2-2.5 less than the detection efficiency of a single wire counter. However in Xe and Kr it was lower even by a factor of 8-15. The single wire counter is superior in gain, efficiency and maximum achievable gain.

6.3.2. Tests of optimised GPM

From reference [36] it follows that several thin micropattern detectors operating in tandem are equivalent in maximum achievable gain to one detector with a thick avalanche gap. This is why we developed and extensively tested an optimised GPM design with a combination of capillary tubes and GEM.

The use a windowless optimised GPM for detection of primary and secondary scintillation light has been studied. Figure 6-6 shows the pulses from an optimised GPM and a PMT produced by the scintillation light of 122 keV γ-rays. The detection efficiency was found to be 15 times lower as compared to a single wire counter.

6.4. *CONCLUSIONS.*

6.4.1. Detectors with window.

This work has demonstrated that GPMs could successfully detect the scintillation light from noble gases. The best option seems to be a single–wire counter. These detectors are very

simple and cheap. They are sensitive to single photoelectrons and at the same time practically have no "dark current" or "spurious" pulses (typical for PMT).

We succeeded to detect the scintillation light produced by alphas, 60 keV and 22 keV X–rays with an efficiency close to 100%. Since the detected signals were at the level of single electrons, no energy resolution was obtained for 22 keV X–rays. With a larger solid angle or by using reflective coating in the scintillation chamber, better results are expected. The scintillation light produced by beta radiation releasing in the detector 5 keV energy has been detected with an efficiency of ~25%.

Figure 6-6: Signals from the optimised GMP and PM produced by scintillation light from Xe at 2.5 atm by 122 keV γ-rays.

The fact that the primary scintillation light does not drop significantly with pressure represents an important result, which allows to detect primary scintillation also in high pressure detectors, similar to that used in liquid noble gases.

Our measurements demonstrated the superiority of GPM with respect to PMT, i.e. the GPM has the same quantum efficiency of the PMT, but no noise pulses or after-pulses. Therefore the use of GPM in a "high rate" application, e.g. at n_TOF, is particularly suited.

6.4.2. Windowless detectors.

In the case of Ar the total efficiency of the windowless GPM can be close to the total efficiency of the single wire counter with window. However, in the case of Kr and Xe the efficiency of the optimised GPM was lower than the single wire detector with window. Using larger sensitive areas could compensate this reduction in efficiency.

For the first time the scintillation light from Ar, Kr and Xe was detected with a GPM. This may open a possibility for simple and cheap readout of high pressure or liquid noble gas scintillation detectors. Advantages of GPMs compared to PMTs are: low cost, large area, insensitivity to magnetic fields, as well as very simple and compact designs. This novel technique can be applied not only in some important physics experiments, like WIMPS searches, neutrino and neutron detectors, but also in medicine and industry to improve the time and position resolution of various detectors.

7. STARTING–UP WITH THE NUCLEAR DATA EVALUATION.

7.1. INTRODUCTION

This activity aims at providing the measured n_TOF cross sections to the international data banks and to make them accessible to the user as soon as possible. To reach this goal the following tasks are subject of this sector:

Standard evaluations and modelling procedures of part of the measured cross sections;

Development of improved evaluation and modelling procedures on a microscopic basis to allow more reliable inter- and extrapolations;

Link to international databases (NEA/OECD, IAEA) providing measured cross sections in appropriate form for inclusion in the world-wide data files as early as possible.

As already outlined previously [2], a n_TOF theory group has been set up which includes members of the n_TOF collaboration as well as external expert teams. In the n_TOF Theory Group meeting in Bologna in June 2000, several open challenging scientific questions have been identified which should be considered in order to allow for more reliable inter- and extrapolation of not available or not measurable quantities as:

- Consistent analysis of overlapping resonances;
- Level densities at high excitations;
- Improved description of fission;
- Onset of pre-compound reactions (especially for capture reactions);
- Improvements of multi-step direct reaction theory.

7.2. ACTIVITIES

In the period up to May 2001 the following activities have been performed:

a) Co-operation with International Data Centres;

b) Establish a Nuclear Data, ND, evaluation network, named Onet–ND, coordinated by the IPPE at Obninsk;

c) Development of evaluation and modelling procedures;

d) Installation of the STAPRE ND evaluation codes at the n_TOF computers by Onet–ND;

e) Evaluation of ^{233}Pa in the energy range up to about 25 MeV; draft evaluation of ^{232}Th.

7.2.1. Co-operation with International Data Centres.

Further co-operation with the NEA/OECD and the JEFF-project has been mutually agreed. The concept of the n_TOF project and the outline of the measurement programme have been presented at the measurements specialist meeting in Aix-en-Provence (15.5.2001) which was jointly organised by NEA, GEDEON and the JEFF project. Triggered by this meeting a new working group within the JEFF project has been set up which aims at a reconsideration of the high priority list taking into account the potential of the n_TOF experimental capacity.

A workshop on the code SAMMY was organised by NEA (March 9-13, 2001) which was attended by several members of the n_TOF collaboration.

Close contacts have also been established with the nuclear data section at IAEA in Vienna, interested in the n_TOF data. Specifically, the members of IAEA asked for a fast transfer of the measured cross section data into the EXFOR format in order to include them into the data files soon after release by the n_TOF collaboration.

7.2.2. The "Onet–ND" network for ND evaluation.

In the framework of the n_TOF project a network mobilising the expertise of the Obninsk, Dubna, Kiev and Minsk Institutes, involved since decades in the evaluation and modelling of Nuclear Data, has been created under the name "Onet–ND" having as main node the IPPE Institute. The "Onet–ND" network is partner of the n_TOF Collaboration, but its internal co-ordination lies under the responsibility of Prof. A. Goverdovski [41].

In respect to the n_TOF project a first activity of the "Onet–ND" network was to re-evaluate the existing data for ^{233}Pa relevant to the Thorium fuel cycles (see also section 7.2.5 below).

7.2.3. Development of evaluation and modelling procedures

More detailed planning of the evaluation and the modelling procedures has been started with emphasis on the flow of data and their treatment, as displayed in Figure 7-1. Experimental data should be transferred into EXFOR format and included into the data bank. These data will be used for new n_TOF related evaluations and offered to the international nuclear data banks for inclusion in the evaluated data files. Since the experimental data with all their experimental characteristics are also available in EXFOR format to the international community further international evaluators might perform evaluations as well.
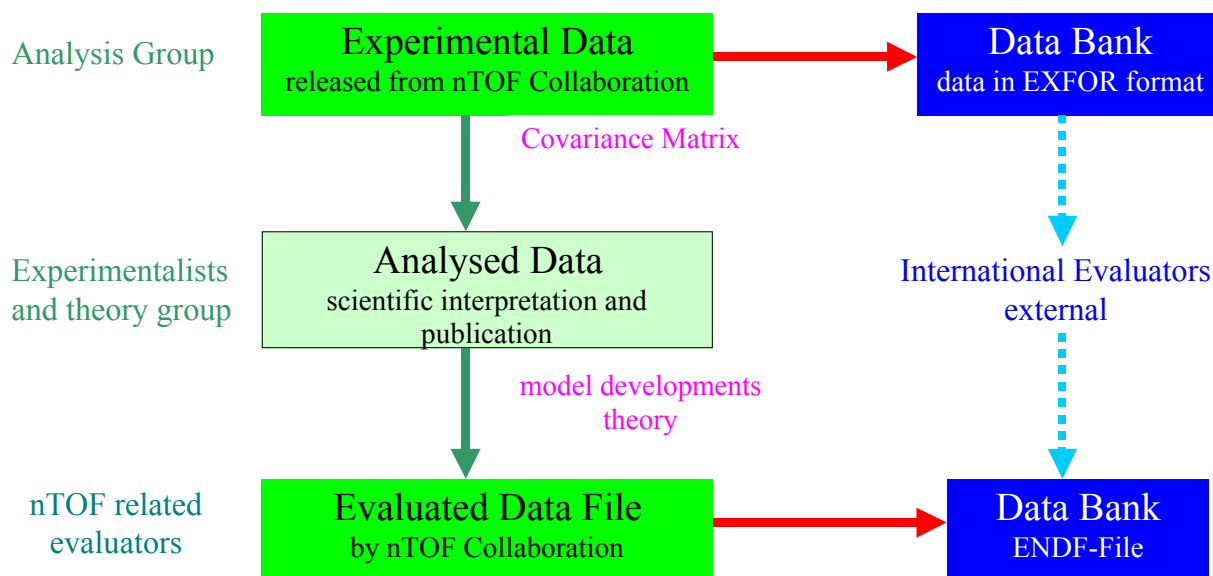
Figure 7-1: Scheme of the nuclear data treatment.

Standard procedures and established codes will be used in the evaluation. At energies beyond 20 MeV consistent modelling and evaluation procedures are under development and are subject of discussions in a specific working group in the JEFF project. Members of the n_TOF project will join this effort. For modelling nuclear reactions we will apply both code systems currently under development, i.e. the TALYS-code and the EMPIRE-code. Both codes have similar features; differences occur at higher energies.

An essential point is the time scheduling of the evaluations. Since the schedule strongly depends on the finalisation of the measurements any planning can only be very preliminary. In order to avoid duplications we will start the evaluation of an isotope in general only after finishing all corresponding measurements within the n_TOF project. Considering the envisaged isotopes and the current measurement planning one clearly sees that the main working load on evaluation will be in the last year of the project. This fact will be independent on the detailed sequence of the measurements.

7.2.4. Installation of the STAPRE ND evaluation codes at n_TOF computers.

The ONet-ND has installed [40] the STAPRE computer code system containing:

The STAPRE statistical model code calculating the reaction cross-sections.

The Libraries for the input parameters, i.e. LDPL-97 containing the level density parameters for more than 2'000 nuclei, BN_MOL for the binding energies, BARRIER for the two humped fission barriers and LIB_TL containing the transmission coefficients of neutrons, protons and alphas for the case of 200 nuclei calculated with the optical model.

The INPUT and OBRAB service codes preparing the input data files for the STAPRE format and for reprocessing the STAPRE output.

The STAPRE code [42] was created for the calculation of reaction cross sections induced by various particles including fission assuming sequential evaporation. A statistical model in the Hauser-Feshbach-Moldauer formalism [43,44] describes each step of the evaporation taking into account total angular momentum and parity conservation. For the first reaction product the opportunity of pre-equilibrium decay is also taken into account. For a specified sequence of emitted particles (up to seven) the capture cross section, the energy spectra of all emitted particles and γ's, and the fission cross section are calculated for all nuclei involved in the sequence.

The initial user-defined data require the definition of the target nucleus, the reaction type and the energy range of the projectile. The INPUT code is automatically created and tested by using the data files: LDP – the parameters of level densities, SEDL- the discrete levels characteristics, BARRIER – the doubled humped fission barriers, GRD – the parameters of giant dipole resonances and B_n_MOL – the particle binding energy for neutrons, protons and alpha-particles. The result of the STAPRE code is a file containing the reaction cross sections as a function of the projectile energy. The service program OBRAB provides additional opportunities for testing and normalisation and is used for processing of this file. The present version includes specific additions for calculating the fission cross sections up to 200 MeV neutron energy.

Calculation of the level density are performed either by the «back shifted» Fermi-gas model [45] or by the generalised superfluid model (GSM). The installed version [46] includes the collective vibrational and rotational effects introduced into the level density formulas by an energy depending enhancement with damping effect at the higher energies, the shell effects of the level density parameters and the pair correlation (superfluid type) of the nucleons.

The expert group under the IAEA co-ordinated research programme [47] provides the large number of input data required by the code. These data are the level density of the exited nuclei, the characteristics of discrete levels (energy, spin and parity), the fission barriers, the particle binding energies, the parameters of optical potentials, etc. The experimental information on the

characteristics of discrete levels is presently available for approximately 85'000 discrete levels of 2'800 nuclei. For the installed version of the STAPRE code the LDP file contains level density parameters within the framework of the generalised model of a superfluid nucleus and the SEDL file contains the characteristics of discrete levels for 2'800 nuclei.

For testing and commissioning the whole installation, calculations of fission probabilities for the Pa isotopes were performed and predictions for the ^{233}Pa(n,f) cross section were made for the neutron energy range between 1 and 10 MeV.

7.2.5. Evaluation of ^{233}Pa in the energy range up to about 25 MeV.

In the first period an evaluation of the isotope ^{233}Pa has been performed by the n_TOF IPPE-Obninsk network of evaluators, Onet–ND. The data of this isotope are important for a reliable study of the Thorium cycle. Although no measurements on ^{233}Pa are planned within n_TOF an update of the evaluated data file was in the spirit of the project. As you can see from the scheme in Figure 7-2 new capture, photon production and fission product data have been included in the evaluation.
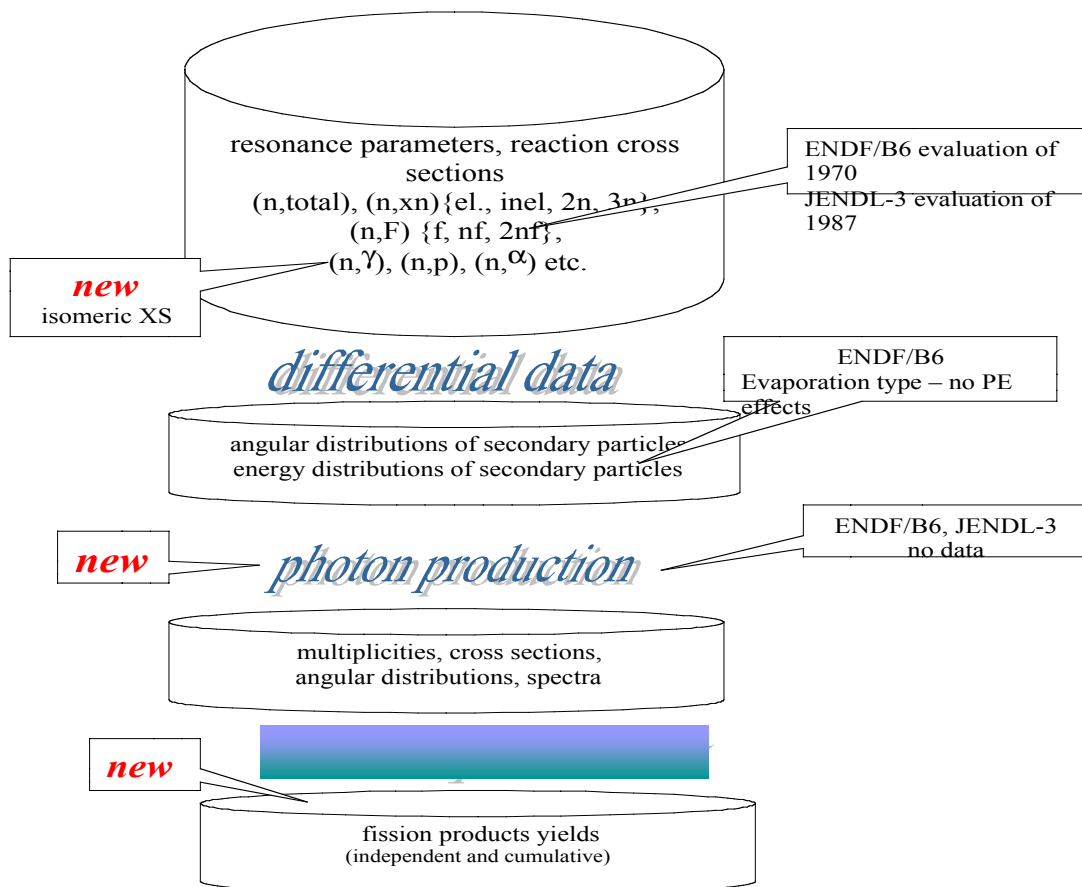

Figure 7-2: Experimental data entering the evaluation of ^{233}Pa.

A complete evaluated file has been compiled and physical tests with FYZCON and PHYHE codes have been performed. In Figure 7-3 the new evaluation [40] is illustrated at the example of the capture cross section.

In addition a first draft evaluation has been performed for ^{232}Th by V. Maslov. The evaluation includes total, fission, capture, (n,xn) and inelastic cross sections in the energy range between 4 keV and 20 MeV. The evaluation differs in several observables from ENDF/B-VI,

JEF2.2, BROND. The evaluation provides a reference for the new data taken at n_TOF during the next year.
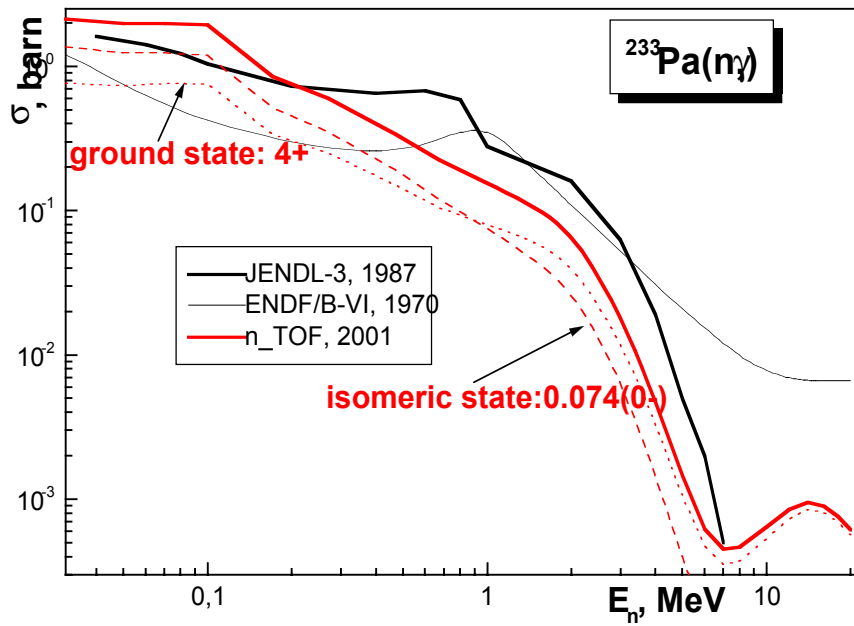

Figure 7-3: The n_TOF calculated ^{233}Pa(n,γ) capture cross sections, evaluated by "Onet–ND". Note the large differences compared to previous less sophisticated evaluations.

8. REFERENCES

1 The n_TOF Collaboration, "Determination of the neutron fluence, the beam characteristics and the backgrounds at the CERN-PS TOF Facility", CERN/INTC 2000-016; INTC/P123, nTOF-02-Experiment.

2 The n_TOF Collaboration, "n_TOF Technical Report", CERN/INTC 2000-018, 3 November 2000.

3 The n_TOF Collaboration, "The importance of ^{22}Ne(α,n)^{25}Mg as s-process neutron source and the s-process thermometer^{151}Sm", CERN/INTC 2000-017; INTC/P124, nTOF-03-Experiment.

4 The n_TOF Collaboration, "The Re/Os clock revised", CERN/INTC 2000-020; INTC/P125, nTOF-04-Experiment.

5 H. Wendler et al., "The n_TOF General Data Flow", n_TOF Note 200502, May 2000.

6 D. Cano-Ott et al., "The n_TOF data access package", n_TOF Note 210402, April 2000.

7 R. Plag et al., "Upgrade of the n_TOF on-line software package", n_TOF Note 210404, April 2001.

8 M. Heil et al., "Preliminary Analysis of the first C_6D_6 Data", n_TOF Note 210504, May 2001.

9 T. Papaevangelou et al., "Simulation of the response of C_6D_6 detector for a carbon and a lead sample", n_TOF Note 210601, June 2001.

10 Provided to the n_TOF Collaboration by courtesy of Frank Gunsing (CEA).

11 Provided to the n_TOF Collaboration by courtesy of Klaus Guber (Oak Ridge).

12 V. Vlachoudis et al., "MC simulation of the Neutron TOF Facility at CERN", Monte Carlo Conference – Lisbon2000, 25-28 Sept. 2000, Lisbon, Portugal.

13 E. Gonzalez et al., "Workpackage 4: Design and Beam Characteristics", 1st Progress Meeting of the EC programme n_TOF-ND-ADS, 6 July 2000, CERN.

14 C. Lamboudis et al., "Integral profile of the n_TOF neutron beam measured with TED detectors",n_TOF Note 210506, May 2001.

15 V. Vlachoudis, "Various Background components", 10th n_TOF Collaboration Meeting, CERN, 4-5 July 2001.

16 The n_TOF Collaboration like to thank Dr. D. Müller from the TIS Division, CERN.

17 C. Lamboudis et al., "The fast neutron fluence upstream and inside the n_TOF Experimental area",n_TOF Note 21058, May 2001.

18 V. Vlachoudis, "Particle trajectories with minimum mass along the n_TOF tunnel",n_TOF Note 210606, June 2001.

19 D. Cano-Ott et al., "Monte Carlo simulations of the photon and neutron background in the n_TOF experimental area produced by a high energy neutron source hitting its walls " n_TOF Note 210702, July 2001.

20 J.L. Tain et al., "Monte Carlo simulation of the response of a C_6D_6 total energy detector for neutron capture studies", IFIC Preprint 2000-11and n_TOF Note 210608, June 2001.

21 T. Papaevangelou et al.,"Fast analysis algorithm for the C_6D_6 detectors", n_TOF Analysis Meeting, CERN, 25 May 2001 and n_TOF Note 210611, June 2001.

22 J.L. Tain et al., "Accuracy of the pulse height weighting technique for capture cross-section measurements", to be presented at ND2001, October 7-12, Tsukuba, Japan.

23 N.M. Larsson, "SAMMY: Multilevel R-matrix fits to neutron data using Bayes equations", ORNL/TM-9179, Oak Ridge NL, 2000.

24 C. Rubbia et al, "A high resolution Spallation driven Facility at the CERN-PS to measure neutron cross sections in the interval from 1 eV to 250 MeV", CERN/LHC/98-02 (EET) and Add.1, 1998.

25 C. Coceva et al., "Neutron flux and resolution function", n_TOF Preprint, 2000.

26 M. Heil et al., "Measurements with C_6D_6 detectors during the nTOF-02 campaign", n_TOF Note 210706, July 2001.

27 D. Cline et al., Asropart. Phys. 12 2000 373; R. Periale, Tesi di laurea in Fisica-INFN e Universita'di Torino, Italy 1998; A.J.P.L.Policarpo et al., Nucl. Instr and Meth in Phys.Res. A365 (1995) 568.

28 F. Arneodo et al., "Scintillation efficiency of nuclear recoil in LXe", to be appear in Nucl. Instr and Meth in Phys.Res. A, 2000.

29 C. Bolozdynia et al., Nucl. Instr and Meth in Phys.Res. A385 (1997) 225.

30 V. Peskov, Journ. Appl. Spectr. 48 (1988) 316.

31 V. Peskov "Gaseous detectors with solid photocathodes", CERN Yellow report 97-06 (1997) 48.

32 L. Periale et al., "First observation of the primary scintillation light from Ar, Kr and Xe with GPM", n_TOF Note 200803, August 2000.

33 L. Periale et al., "Observation of a primary scintillation light produced by X-rays and MIP in noble gases with GPM" n_TOF Note 201007, October 2000.

34 L. Periale "Study of the scintillation light from high pressure Xe", n_TOF Note 210208, February 2001.

35 L. Periale "Study of windowless micropattern detectors for LAr TPC application", n_TOF Note 210214, February 2001.

36 V. Peskov et al., "The study and optimization of new micropattern detectors for high rate applications" submitted to IEEE Nucl. Science.

37 Sharma "Gaseous micropattern detectors in Astrophysics, Radiology and Plasma Physics" to be published in IEEE Nucl. Science, 2000.

38 V. Peskov et al., Nucl. Instr and Meth in Phys.Res. A433 (1999) 492.

39 D. Cline et al., "Measurements of scintillation amplification in Xe detector with CsI luminescence plate", Presented at the 4th Int. Symp. on Sources and Dark Matter in the Universe - 2000 Marina del Rey, CA, USA.

40 O.T. Grudzevich, "The installation and operation of the STAPRE code calculating nuclear reaction cross sections", n_TOF Note 210104, January 2001.

41 A.A. Goverdovski, private communication, January 2001.

42 M. Uhl and B. Strohmaier, Report IRK 76/01, Vienna. 1976; Addena, Sept. 1976.

43 W. Hauser and H.Feshbach, Phys. Rev. 87 (1952) p.366.

44 P.A. Moldauer, Phys. Rev. 135 (1964) p.642.

45 W. E. Dilg, Nucl. Phys. A217 (1973) p.269.

46 O.T. Grudzevich et al., Proceedings in Int. Conf. On Nuclear Data for Science and Technology, 1988, Mito, Japan, p.1221.

47 "Handbook for calculations of nuclear reaction data", IAEA-TECDOC-1034, Vienna, 1998.

48 O.T. Grudzevich, "The evaluation of ^{233}Pa(n,γ) cross section by the "Onet-ND" group", n_TOF Note 210802, May 2001.